

ALMA MATER STUDIORUM UNIVERSITÀ DI BOLOGNA DEPARTMENT OF PHYSICS AND ASTRONOMY SECOND CYCLE DEGREE IN SCIENCE OF CLIMATE Academic Year 2024-2025

Seasonal predictability of compounded variable renewable energy droughts in Europe using the German Climate Forecast System

Supervisor: Student:

Dr. Salvatore Pascale

Beatrice Ciancarella

Alma Mater Studiorum Università di Bologna

Co-supervisors:

Dr. Leonard Borchert, Dr. Marlene Klockmann

Universität Hamburg

Abstract

Variable Renewable Energy (VRE) droughts — prolonged periods of low renewable energy availability — pose a significant threat to the stability and resilience of Europe energy grid, as renewable energy sources expand to meet climate targets. While the climatology and synoptic drivers of these events are well-documented, their seasonal predictability remains largely unexplored. This thesis assesses the German Climate Forecast System (GCFS) version 2.2 prediction skill for compounded wind and solar VRE droughts across Europe. We develop novel operational indices for solar, wind and compounded energy production, from surface solar radiation and wind speed, weighted by national energy capacities. Validation of the compounded index against documented events confirms its utility in identifying real-world energy shortfalls. This research bridges a critical gap in VRE drought predictability, despite the current lack of model bias correction and sensitivity tests on drought thresholds. Future work should resolve these limitations and explore ensemble subsampling and advanced statistical methods that leverage teleconnection patterns like the North Atlantic Oscillation (NAO) to enhance predictive skill. Our analysis reveals that the GCFS's skill in predicting the local frequency of VRE droughts is spatially heterogeneous. Furthermore, the predictability of compounded droughts is not a direct function of its individual components, revealing complex, non-additive dynamics. However, we demonstrate that the model provides significant and reliable skill in forecasting the spatial extent of droughts when aggregated over larger regions. Anomaly correlation coefficients (ACC) reach 0.59 for Central Europe and 0.65 for Southern Europe. This research confirms the potential of operational seasonal forecasting models to provide actionable prediction skill on large-scale VRE droughts, which is crucial for strategic energy planning, grid management and risk mitigation.

Contents

1	Intr	Introduction							
	1.1	The potential of seasonal forecasts	1						
	1.2	Research questions	3						
	1.3	Variable Renewable Energy (VRE) shortages	3						
		1.3.1 Literature review	3						
		1.3.2 VRE drought definition	6						
	1.4	Bridging the Gap: scope and thesis outline	8						
2	Data	and methodology	11						
	2.1	Data	11						
		2.1.1 Reanalysis	11						
		2.1.2 German Climate Forecasting System (GCFS)	12						
		2.1.3 Energy capacities	12						
	2.2	Definition of VRE droughts	14						
		2.2.1 Methodologies in literature	15						
		2.2.2 Wind velocity extrapolation	16						
		2.2.3 Operational definition	18						
	2.3	Frequency, persistence and spatial extent of VRE droughts	20						
3	VRI	VRE droughts predictability and index validation 22							
	3.1	Evaluation of the GCFS	22						
		3.1.1 Primary climatological fields	22						
		3.1.2 Energy production metrics	24						
	3.2	VRE drought characterisation	25						
		3.2.1 Individual sources mix	25						
		3.2.2 Persistence of VRE droughts	26						
		3.2.3 Spatial extent of VRE droughts	27						
	3.3	VRE droughts prediction skill	3(
		3.3.1 Individual drivers							

	3.4	Valida	tion of the compounded VRE drought definition	33					
4	Dyn	amics a	and challenges of VRE availability	38					
	4.1	Predic	tability of VRE droughts	38					
		4.1.1	Assessing the predictability of compounded and individual energy sources	40					
		4.1.2	Role of model biases	40					
		4.1.3	VRE droughts extent and ensemble spread	43					
5	Conclusions								
	5.1 Summary of methodology and key findings								
	5.2	Contri	bution to the seasonal predictability of VRE droughts	49					
	5.3	Limita	ations and future research outlook	50					
A	Data and methodology								
	A.1	Germa	an Climate Forecast System 2.2	52					
	A.2	VRE o	droughts persistence bound	53					
В	Results								
	B.1	Prima	ry field biases	56					
	B.2	VRE o	droughts characterisation	57					
	B.3	VRE o	droughts prediction skill	58					
	B.4	Valida	tion of VRE droughts metrics	64					
C GCFS large-scale circulation patterns									
Ac	know	ledgme	ents	68					
Bi	Bibliography								

Chapter 1

Introduction

Is it possible to predict, months in advance, periods when both wind and solar energy generation are low across large regions of Europe? As global temperatures continue to rise and the transition toward sustainable energy accelerates (IPCC 2023b), European countries are increasingly dependent on renewable sources, such as wind and solar power. During periods of low resource availability, in the absence of reliable energy storage, the system must rely on alternative sources. However, when the energy system relies heavily on renewables, simultaneous scarcity of two or more resources poses a risk of energy shortages. The term Variable Renewable Energy (VRE) shortage indicates these prolonged periods of extremely low resource availability or energy supply of a single or multiple VRE technologies (Kittel et al. 2024). Given the financial and societal impact of VRE shortages and the expansion of VRE technologies in the energy production share, it is likely that the demand of seasonal climate prediction services for the energy sector is going to increase (Bett et al. 2022).

This thesis addresses the anticipated future demand for improved predictions of coincident low wind and solar generation events at seasonal time scales. It focuses on the European region with the objective of assessing the seasonal predictability of such events by leveraging historical hindcasts and reanalysis datasets.

1.1 The potential of seasonal forecasts

At the core of this investigation is the use of a seasonal forecasting system. These models provide ensembles of predictions for the coming months, offering a potential window into future large-scale energy availability.

Seasonal forecasts aim at predicting the average conditions of the climate system over periods ranging from one month to a year ahead. Unlike weather forecasts, they are not primarily determined by the initial conditions of the system (*initial value problem*). Unlike longer multi-decadal to centennial projections, they do not derive predictability primarily from forcing scenarios and do not begin at the pre-industrial equilibrium state (*forced boundary conditions problem*). Seasonal forecasts require both initial and boundary conditions, they rely on the predictability provided by

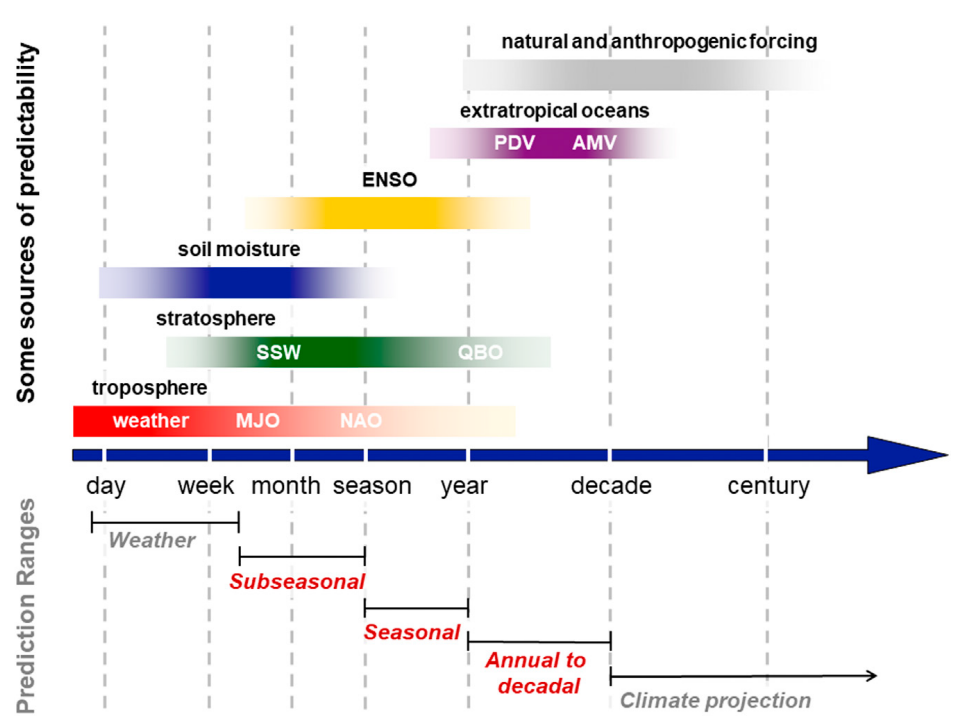


Figure 1: Schematic depiction of (bottom) temporal ranges and (top) sources of predictability for weather and climate prediction (Merryfield et al. 2020). The acronyms define: Madden Julian Oscillation (MJO), Sadden Stratospheric Warming (SSW), North Atlantic Oscillation (NAO), Quasi-Biennial Oscillation (QBO), El Niño–Southern Oscillation (ENSO), Pacific Decadal Variability (PDV) and Atlantic Multidecadal Variability (AMV).

slower-varying components of the Earth system and by teleconnections (Yuan et al. 2018; Wang et al. 2021). The initialisation of these boundary conditions (such as sea surface temperatures, sea ice concentration and soil moisture) is crucial, as their evolution modulates atmospheric processes on sub-seasonal to decadal timescales (Merryfield et al. 2020).

Seasonal forecast systems are typically based on complex coupled ocean-atmosphere-land general circulation models (GCMs), as also used in climate projections. GCMs are initialised with the best available estimate of the current state of the climate system, often derived from reanalysis data, like ERA5 (Hersbach et al. 2017) and are then run forward in time. To account for the chaotic nature of the atmosphere (Lorenz 1963; Charney 1966), an ensemble approach is used, where multiple simulations (ensemble members) are performed with slightly perturbed initial conditions. The ensemble mean is then analysed to identify the predictable signal beyond the noise.

Despite their utility, seasonal forecasting models face several limitations, with fair but not excellent skill scores (White et al. 2017). Their horizontal resolution, often around $100 \ Km$, is too coarse to explicitly resolve many mesoscale to local processes, which are instead represented through parametrisations. This can lead to errors in simulating regional phenomena, such as oro-

graphically influenced winds or local cloud cover (Merryfield et al. 2020), the latter being particularly critical for accurately representing solar irradiance and thus solar energy droughts.

Several operational seasonal forecast systems exist, such as the ECMWF's SEAS5 (Johnson et al. 2019), the UK Met Office's GloSea (MacLachlan et al. 2015) and the German Climate Forecast System (GCFS) (Penabad 2025). In this study, we employ the GCFS, version 2.2, which is a collaborative effort of German institutions and it is based on the high-resolution MPI-ESM-HR model.

1.2 Research questions

This work addresses a clear gap in the literature: studies on the climatology and synoptic signatures of VRE shortages exist (Kittel et al. 2024; Bett et al. 2013; Kaspar et al. 2019; Wiel et al. 2019a; Wiel et al. 2019b; Jerez et al. 2013a; Jerez et al. 2013b; Jerez et al. 2015; Mockert et al. 2023), but assessments of their seasonal predictability are limited (Lledó et al. 2022; Bett et al. 2022). This thesis' key research questions follow from the previous premises: Can the GCFS skilfully predict the frequency of compounded VRE shortages at a seasonal lead time? To address this seemingly straightforward question, several additional questions arise:

- 1. How does the predictability of compounded shortages relate to the predictability of its individual wind and solar components?
- 2. What are the main dynamical, methodological and model-based challenges that limit or improve this predictability?

By addressing these questions, this study provides a foundational framework for future research aimed at improving the reliability of seasonal VRE shortages forecasts.

1.3 Variable Renewable Energy (VRE) shortages

A review of the current literature on VRE droughts is presented, with a focus on previous seasonal predictability efforts. This is followed by a discussion on the complexities inherent in defining such events, which informs our methodological choices.

1.3.1 Literature review

The climatology of VRE shortages has been extensively analysed and the same holds true for studies examining their future projections under climate change scenarios. Long term trends of wind speed showed very little significant signals in Europe. Bett et al. 2013 analysed over 140 years of

data from the *Twentieth Century Reanalysis*. The significance and magnitude of the trends were so small that they questioned whether it was in any way relevant for wind energy applications (Bett et al. 2013). On the same note, Jerez et al. 2015 found small decreases of PV power generation under different representative concentration pathways (RCPs) scenarios, limited to Northern countries. Nevertheless, theirs findings proved climate change unlikely threatens PV generation in Europe. Lastly, Kaspar et al. 2019 found a decrease in the low extreme compounded shortage frequencies both over Germany and Europe. Although their work consisted of a relative climatological comparison based on simplified assumptions, it represents one more piece of evidence that trends on solar and wind VRE shortages related to climate change are rarely significant and, if anything, not yet alarming for the energy sector.

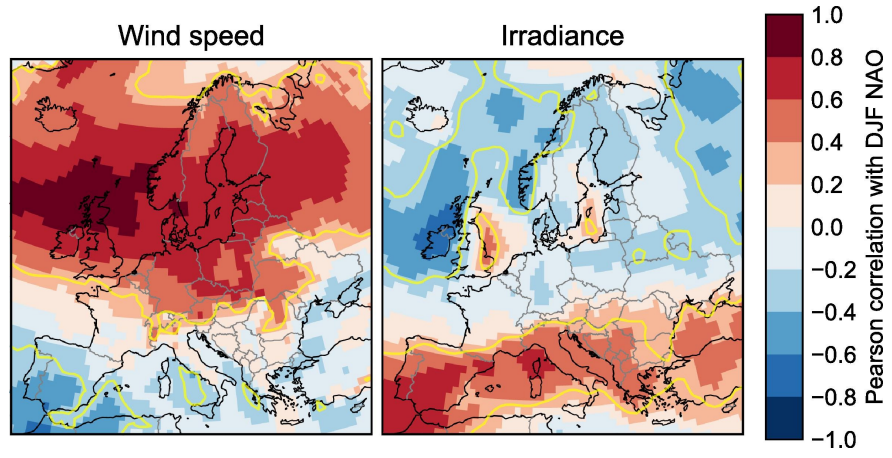


Figure 2: Maps showing the correlation between the DJF NAO index and 10m wind speed (left) and surface irradiance (right), based on ERA-Interim data for winters from 1979/1980 to 2015/2016 inclusive. Contour lines indicate the approximate threshold for statistical significance at the 5% level over a 37-year period. From Bett et al. 2022

Works on the links between synoptic weather patterns and VRE shortages are also found in literature (Wiel et al. 2019a; Wiel et al. 2019b; Bett et al. 2022; Lledó et al. 2022; Mockert et al. 2023; Jerez et al. 2013b). All agreed that the the North Atlantic Oscillation (NAO) has the strongest influence on the intensity and frequency of VRE shortages. In Southern Europe, a positive NAO index was correlated with irradiance, while showing variable wind speed (low and not-significant correlation coefficients) (Lledó et al. 2022; Bett et al. 2022). In Northern and Central Europe the negative NAO phase was linked with reduced wind speed due to the weaker pressure gradients and low solar irradiance due to higher cloud cover (Wiel et al. 2019a; Mockert et al. 2023). Blocking regimes influenced more Northern and Central Europe, while they did not have relevant impact in the Southern countries (Wiel et al. 2019a; Bett et al. 2022). The Scandinavian blocking highs were specifically linked with prolonged winter VRE shortages (Wiel et al. 2019a) and the

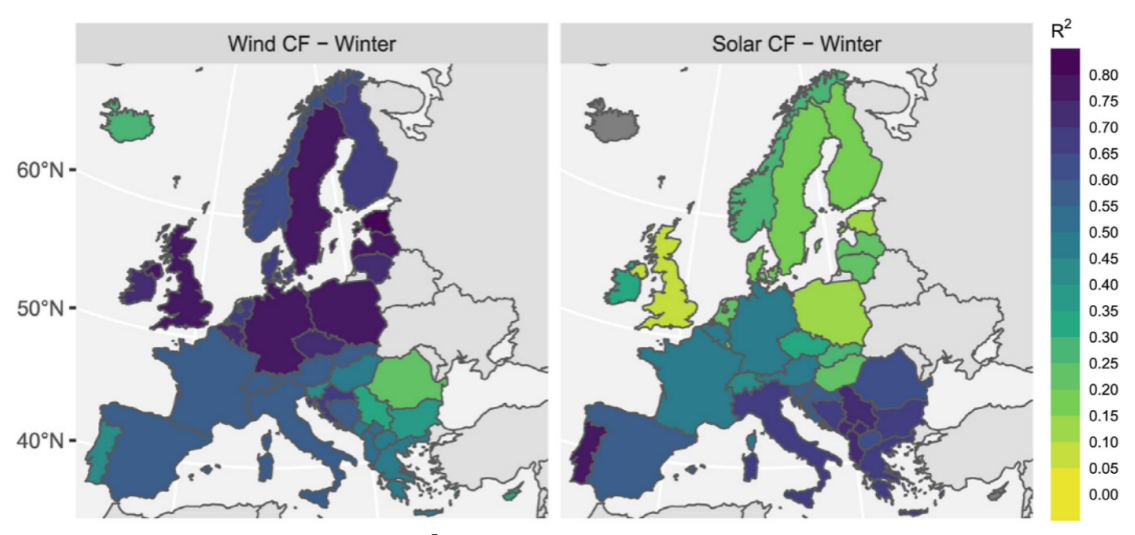


Figure 3: Determination coefficient, R^2 , of the multi-linear regression model for wind (left column) and solar (right column) capacity factors at country level in winter from Lledó et al. (Lledó et al. 2022).

East-Atlantic/Western-Russia (EA/WR) teleconnections were linked to solar shortages (Lledó et al. 2022). The NAO, especially in winter, along with the Scandinavian blocking pattern and the East Atlantic/Western Russia (EA/WR) pattern, are three of the four principal modes of variability in Europe during the DJF (December–January–February) season. These large-scale circulation patterns are known to exert a significant influence on the winter climate across the continent. Nonetheless, local factors, such as topography, mountain ranges (i.e., the Alps) and coastal influences, including land–sea breeze dynamics, play a crucial role in modulating the intensity of VRE shortages at regional and local scales (Mockert et al. 2023).

Forecast skill for VRE shortages predictions up to a 10-day lead time have been studied, whereas forecasts at longer timescales remain relatively rare. One notable exception is the work by Lledó et al. 2022, who focused on seasonal predictions by employing a bridging method that links VRE shortages with synoptic circulation pattern indices, including the NAO, EA/WR and Scandinavian Blocking. A multi-linear regressor was tested on wind and solar capacities forecasts at country level (Lledó et al. 2022). It represented up to 80% of the winter wind generation in some Northern countries and a moderately good fraction of the winter solar generation in Southern countries (Fig. 3) (Lledó et al. 2022). Another study by Bett et al. 2022 demonstrated that seasonal forecasts are moderately skillful in predicting seasonal mean irradiance and wind speed, although their skill tends to be spatially variable. Bett et al. 2022 claimed there is no need of introducing the complex non-linearities of VRE generation potentials, but acknowledged the limits of coarser time and spatial resolution and of not addressing the predictability of shortages frequency. They also

employed a linear regression method using synoptic patterns as predictors.

1.3.2 VRE drought definition

Variable renewable energy shortages have been discussed in the literature under various terms. In particular, the term *Dunkelflaute* (dark-and-dull) has gained popularity to describe compounded solar and wind shortages. However, as Kittel et al. 2024 noted, there is currently no consensus in the literature on a standard terminology for such shortage events. To contribute to the adoption of a consistent terminology, this study follows the terminology proposed by Kittel et al. 2024. Hereafter a compounded VRE drought (or simply compounded drought) is defined as the simultaneous occurrence of weak downward solar irradiance at the surface (*RSDS*) and weak wind speed (*U*) intensities which lead to low solar and wind power production; individual droughts indicate either solar or wind power shortages.

The operational definition of VRE droughts is as vast as the terminology because quantifying these events is highly complicated. Kittel et al. 2024 offered a comprehensive overview also of these definitions, on the different input data, methodological choices and parameter assumptions. Depending on the input data considered, they identified four types of VRE shortages: VRE droughts, VRE anomalies, positive residual load events and electricity system stress events. **VRE droughts** are periods of low resource availability affecting one or multiple VRE technologies, they are the focus of investigation in this thesis. For the identification of VRE droughts, multiple methods were described (Kittel et al. 2024):

- Constantly-Below-Threshold (CBT) selects consecutive time steps where VRE availability is constantly below a threshold;
- Mean-Below-Threshold (MBT) selects time steps where the moving average of VRE availability is below a threshold, the averaging interval can be fixed or variable;
- Sequent Peak Algorithm (SPA) selects the maximum cumulative energy deficit of an event, allowing for intermediate periods above the threshold.

In this thesis, we choose the CBT method due to its simplicity and straightforward implementation. Unlike the MBT and SPA methods, the CBT approach identifies two separate events when a brief period of higher resource availability occurs between two longer drought periods. This results in an underestimation of drought duration and overestimation of the event frequency. Nevertheless, we preferred the CBT method because the fixed MBT method results are highly sensitive on the chosen interval, the variable MBT is in general computationally expensive and the SPA might underestimates less extreme long droughts. All methods require the definition of a threshold, a time

window, or both; however, the CBT method only requires the selection of a threshold. Kittel et al. 2024 described the available threshold-selection methods:

- percentile-based threshold, a percentile of the availability distribution (followed in this thesis);
- absolute threshold, a fixed, arbitrary value;
- scaled threshold relative to the maximum aligns to a fraction of the peak availability (i.e., $0.05 \times max(x)$);
- scaled threshold relative to the mean aligns to a fraction of the mean availability (i.e., $0.1 \times \overline{x}$).

Kittel et al. 2024 recommended to avoid absolute thresholds that lead to biased results and warned the percentile-based method does not account for variations in the total annual energy output of different VRE technologies or systems. As we will explain in more detail in the methodology section (Chapter 2), this study develops an index to serve as a measure of resource availability. No assumption is made on the type of VRE technologies and, moreover, it is constructed in such a way that it smooths out extremely different energy generation potentials among regions. Therefore, the percentile-based method is preferred since it reflects the shape of the distribution and accounts for variability across regions. Nonetheless, Kittel et al. 2024 pointed out all methods introduce a sensitive choice of the percentile or the scaling fraction: too low captures true extremes but short events, too high captures prolonged periods of below-average availability rather than true droughts. The best practice is to follow a sensitivity test and develop the analysis on multiple percentile or fraction choices.

Adding to the complexity of the VRE drought quantification, the energy availability depends on VRE technologies which vary notably among VRE sources and infrastructures models (wind turbines and photovoltaic (PV) panels in this case). An analysis on compounded droughts requires the measures of the wind and solar VRE availabilities to be comparable, thus it is not possible to simply work on the irradiance intensities and wind velocities. When the analysis focuses on a single technology VRE drought, or if it is constrained at shorter time frames or smaller spatial domains, the problem does not occur. Otherwise, when analysing a portfolio of VRE technologies Kittel et al. 2024 suggested to build a composite time series combining the availability factors of the different VRE technologies. For example, an average of the technology-specific time series weighted on the corresponding technology share of the given region can be computed. This practice, while being very rigorous, is not feasible in this study, in fact, it requires the information on the technologies share and installed capacities at each location and time of the analysed domain. This thesis works

on historical datasets extending back to 1990 and aims at providing an assessment over all Europe, it is clearly quite difficult to follow such an heterogeneous load of information. In summary, this work tries to follow at best the directions illustrated by Kittel et al. 2024 in their recent and comprehensive work, when not possible, new solutions are designed and will be explained in Chapter 2.

1.4 Bridging the Gap: scope and thesis outline

We established the current knowledge on VRE shortages climatology and links with large-scale climate patterns, but we identified a gap in assessing their predictability. Studies on the actual predictability of VRE droughts on seasonal timescales in particular in dynamical forecasting system models remain unexplored. The need for such research is underscored by the critical importance of renewables for Europe's energy future.

The European Union, particularly under the framework of the European Green Deal, has set an ambitious target of achieving 45% renewable energy in its overall energy mix by 2030 (Ciucci 2024). According to the European Statistical Office (Eurostat), renewable sources accounted for the largest share of energy production in the EU in 2023, reaching 45% (Eurostat 2025). Of this, wind power contributed 17.6%, while solar power accounted for 9.3%. In terms of final gross energy consumption, renewables represented 25% (see Fig. 4).

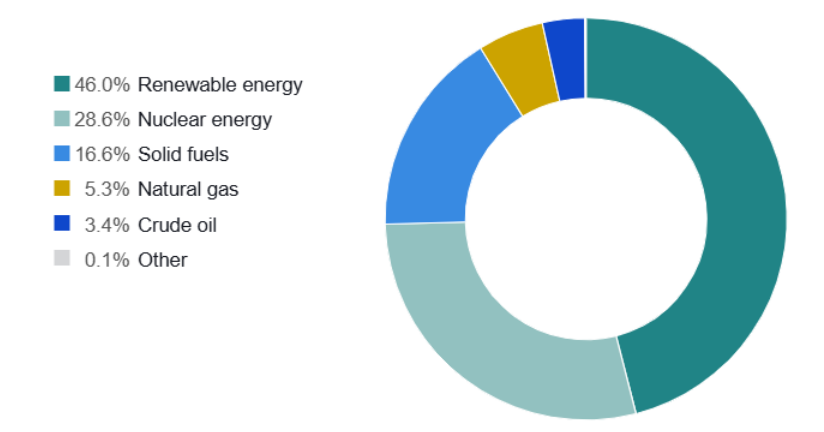


Figure 4: Share of energy production by source in 2023 in European Union, expressed in %. Source: Eurostat (Eurostat 2025).

Europe is not alone in its efforts to transition towards a more sustainable, low-carbon, energy system. Hassan et al. 2024 reviewed renewable energy growth trends over the past decade, across several global regions. They found a widespread increase in renewable energy capacity and technologies, driven largely by their potential to reduce greenhouse gas emissions. Nevertheless, the

benefits of the renewable energy transition extend beyond environmental impacts. These include reductions in energy costs (IPCC 2023b), improved energy access in remote areas and, from a societal perspective, more inclusive development approaches that have contributed to the advancement of human rights, gender equality and social justice (Hassan et al. 2024).

Despite the evident potential of renewable energy to address climate change issues and deliver broader societal benefits, resistance persists among the general public and policy makers. Financial feasibility, adverse environmental impacts and diminishing of land value are among the most common concerns (Susskind et al. 2022), but the biggest opposition is based on the *non-sustainability hypothesis*, as called by Albert 2022. The non-sustainability hypothesis is the view that renewable energy sources cannot fully replace fossil fuels for the residential, commercial, industrial and transportation energetic demands. VRE sources droughts are the physical phenomenon that gives this hypothesis its credibility. Such low-generation events are one manifestation of the claimed unreliability of renewables. Therefore, our ability to understand, predict and ultimately manage these droughts is key to disproving the hypothesis. Most of Integrated Assessment Models provide limited insight on VRE sources availability issue because their climate policy analysis on energy transition are constrained only by available financial investments and energy demand, while assuming an abundant and reliable supply of renewable energy resources (Capellán-Pérez et al. 2020). This gap in modelling approaches may contribute to the scepticism surrounding the feasibility of a fully renewable-based system.

In conclusion, given the increasingly significant financial and societal impacts of these events, reliable seasonal forecasts of VRE drought frequency are highly valuable. Predictions can inform strategic planning, optimize the use of backup generation and storage systems and help mitigate the risks associated with prolonged energy shortfalls (Denholm et al. 2011). Since many energy system models require detailed technological and infrastructural inputs, developing forecasting methods that do not depend on complex, site-specific energy models is advisable. We aim to address this gap by assessing the capability of the GCFS version 2.2 to predict the winter frequency of compounded (specifically, concurrent wind and solar) variable renewable energy droughts across Europe on seasonal timescales. To this end, we develop novel operational indices for solar (SEP), wind (WEP) and compounded (CEP) energy production. We leverage physical fields weighted by national energy capacities metrics. These indices, defined in Chapter 2, are generally applicable, independently of specific turbine or photovoltaic models. This methodology allows for a focus on the meteorological drivers of droughts and it relies on information that can be easily provided by dynamical forecasting system, while maintaining relevance to the energy sector.

Thesis outline

The structure of this thesis is as follows: Chapter 2 details the data (ERA5 reanalysis, GCFS hind-casts, Eurostat VRE capacities) and the methodology for defining VRE droughts, including the wind speed extrapolation and the threshold-based selection of events. In Chapter 3, we present the results, evaluating the GCFS's skill in predicting the frequency of these droughts. The analysis reveals that while the overall skill for inter-annual variability is low, there are spatially heterogeneous regions of significant predictability. In the discussion (Chapter 4), we provide a physical interpretation of these results and the limitation of the analysis. We discuss the role of model biases, the dynamics behind the events and the challenges posed by the complexity of compounded events. Finally, Chapter 5 summarizes the analysis results and relative interpretation and outlines future research directions.

Chapter 2

Data and methodology

2.1 Data

Since the objective of this work is to establish the predictability of compounded solar and wind VRE droughts, the seasonal forecasting model hindcasts and observations are compared. The seasonal forecasting model we use is the German Climate Forecast System (GCFS) version 2.2 (Fröhlich et al. 2021); as for the observations, an historical dataset is employed as reference, namely the fifth generation ECMWF reanalysis dataset ERA5 (Hersbach et al. 2017). The time range (from 1990 to 2024) and spatial domain (Europe¹) are selected for both datasets. Lastly, to give an estimate of a potential energy production value also a dataset for the energy capacity at country level is employed, provided by Eurostat statistics (Commission 2025). These datasets help defining three operational indices as a measure of the energy production: solar energy production (*SEP*), wind energy production (*WEP*) and the compounded solar and wind energy production (*CEP*). On these variables a thresholding method is applied to define individual and compounded VRE extreme low availability.

2.1.1 Reanalysis

The ECMWF atmospheric reanalysis data provided by the Copernicus Climate Change Service (C3S) are widely employed to represent observed historical weather conditions since 1940s because of their reliability, especially at synoptic level and over the Northern hemisphere (Soci et al. 2024). Reanalysis in general has been largely adopted to simulate also observed wind and solar power for its extensive coverage and availability (Li 2025). In addition, ERA5 is the dataset used for the atmospheric initialisation of the forecast model of the GCFS, assuring a fair comparison between the ERA5 and the hindcasts. By using the same initialization dataset (ERA5) for our evaluation, we ensure a consistent baseline. This avoids introducing biases or inconsistencies that could arise from comparing the GCFS hindcasts to a different observational dataset.

¹The region selected is $[71.5^{\circ}N, 29^{\circ}N]$ and $[31.5^{\circ}W, 45^{\circ}E]$

ERA5 fields are at a horizontal resolution of approximately $31 \times 31~Km$; all fields in the ERA5 dataset are calculated on the finer original grid and then coarsened using bilinear weights to match the model's grid at lower resolution (approximately $100 \times 100~Km$). The dataset combines historical observations and models estimates using advanced data assimilations systems. The following daily averaged fields are used in this thesis:

- surface solar radiation downwards (RSDS) $[J/m^2]$: the intensity of shortwave radiation at the Earth's surface, including both direct and diffuse solar radiation, thus the portion of the solar radiation neither back-reflected nor absorbed by clouds and aerosols. In sight of simulating the solar power, the fields units are converted to $[W/m^2]$;
- 10 m u and v component of the wind (u_{10}, v_{10}) [m/s]: the eastward and westward wind speed modules at 10 m above the surface;
- 100 m u and v component of the wind (u_{100}, v_{100}) [m/s]: the eastward and westward wind speed modules at 100 m above the surface.

2.1.2 German Climate Forecasting System (GCFS)

The GCFS is a collaborative effort of the Universität Hamburg, the Max Planck Institute for Meteorology and the Deutscher Wetterdienst. The forecast system provides hindcasts for the historical period 1990-2024 and it is based on the Max Planck Institute Earth system model (MPI-ESM-HR) (Müller et al. 2018) at a horizontal resolution of about $100 \times 100 \ Km$. The model is initialised in November of each year and run for 18 months. Each hindcast contains 30 ensemble members. This provides 2 predictions for each extended winter: one short lead forecast, spanning from November to March (first 5 months) and one long lead, spanning from October to March (months twelfth to seventeenth). Additional information about the GCFS 2.2 can be found in Appendix A.1.

The following fields are used in this thesis.

- Surface solar radiation downwards (RSDS) $[W/m^2]$: obtained from the subtraction of the surface upward shortwave radiation field from the surface net shortwave radiation field.
- 10 m u and v component of the wind (u_{10}, v_{10}) [m/s]: the eastward and westward wind speed modules at 10 m above the surface.
- 500 hPa geopotential height (Z500) [m]: used to derive the NAO index.

2.1.3 Energy capacities

The energy capacity is expressed in terms of annual Net Maximum Energy Capacity (*NMEC*), i.e., the total maximum electrical power that the full set of power plants in the country can produce un-

der normal operating conditions, minus (net) the electrical power used by the plants themselves to operate, expressed in megawatts. *NMEC*s are reported individually for each year for each country and broken down by renewable energy power source: wind, solar, hydrological. They represent

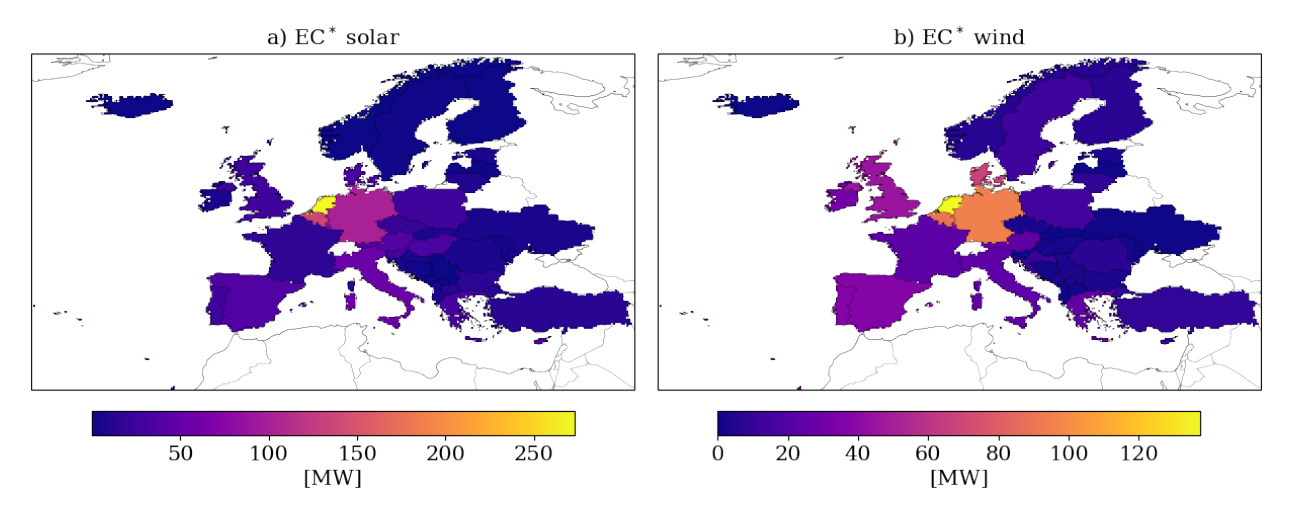


Figure 5: Most recent available data for nationwide a) solar and b) wind net maximum energy capacity (*NMEC*)normalised by area (measured in number of grid points).

the annual national highest *NMEC* or the national *NMEC* dated on the 31st of December of each year. The Eurostat dataset covers only certain European countries². Data are collected by the National Administrations competent for energy statistics and transmitted to Eurostat from the national authorities³ (Commission 2025). The most recent record of energy capacity for each country⁴ is chosen and considered as a constant for any time step although the analysis can be repeated with time-dependent datasets or updated parameters. Accordingly all the resulting energy potentials are computed assuming the latest net maximum energy capacities (*NMEC*) and normalised by the number of grid points in the country (henceforth indicated as EC^*). This field used in the subsequent calculation is shown here in Fig. 5.

The climatological analysis and the hindcasts assessments take into account only the extended boreal winter months from November to March (NDJFM). This choice is justified in view of the available studies on solar and wind power production seasonal climatology (Wiel et al. 2019a; Kas-

²Albania, Austria, Belgium, Bulgaria, Bosnia Herzegovina, Croatia, Czech Republic, Cyprus, Denmark, Estonia, Finland, France, Germany, Greece, Hungary, Iceland, Ireland, Italy, Kosovo, Luxemburg, Latvia, Lithuania, Macedonia, Moldova, Montenegro, Netherlands, Norway, Poland, Portugal, Romania, Serbia, Slovakia, Slovenia, Spain, Sweden, Turkey, Ukraine and United Kingdom.

³Depending on the country the providers can be: national statistical institutes, ministries, energy agencies or professional associations.

⁴2019 for the United Kingdom, 2020 for Ukraine and 2023 for the others countries.

par et al. 2019). As can be deduced from Fig. 6, over Europe wind and solar energy sources exhibit seasonal complementarity: reduced wind generation in warmer months is offset by increased solar generation (Kaspar et al. 2019; Kittel et al. 2025). Shortfalls still exists assuming that both sources are not everywhere available and that the solar energy annual cycle is slightly more pronounced due to the high daily variability of wind speed (Wiel et al. 2019a). The resulting extreme lows occur in general between October and March (Wiel et al. 2019a), hence the focus on extended winter. Because the hindcasts start in November, hereafter the period analysed is the period from the November 1st to March 31st, simply referred as winter.

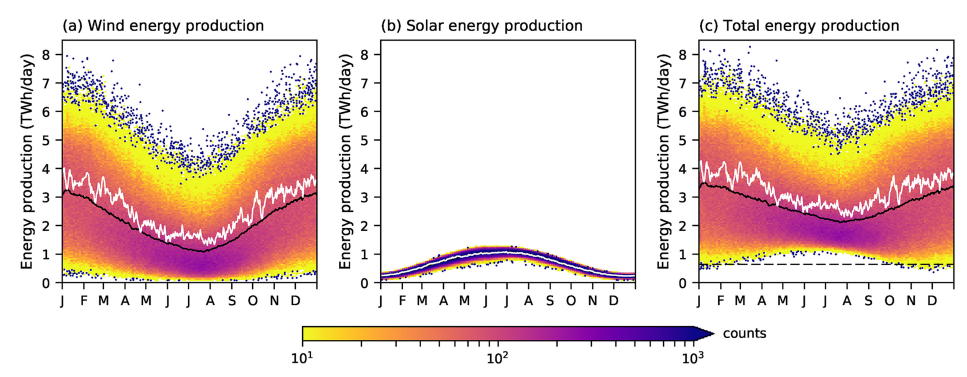


Figure 6: 2D histogram of (a) daily wind energy production, (b) daily solar energy production, (c) daily total energy production (TWh/day). The continuous black line shows the mean annual cycle. The threshold for 1-in-10 year high-impact events based on extreme low total energy production is indicated with a horizontal dashed line in (c) (Wiel et al. 2019a).

2.2 Definition of VRE droughts

As introduced in chapter 1 an extensive and reliable dataset of energetic variables is yet to be generated for a spatial domain covering homogeneously multiple countries. Firstly, this type of data is difficult to retrieve because of the heterogeneity of both infrastructures and spatial locations of the power plants. Moreover, the energy production ideal yield of a country represent sensitive information in specific circumstances and national authorities may not openly share the data. Secondly, the calculation of energetic variables and the selection methods used to define the compounded VRE drought events are quite challenging. The complex nature of these events entails a combination of attributes, foremost the temporal and spatial extents, which can significantly influence the identification of such droughts (Kittel et al. 2025). Depending on the study, shortfalls in the energy production were selected and then investigated only if they reached a spatial and temporal extent, large or long enough to actually affect the energy availability; no standardized values for these bounds exist to define the interesting occurrences. An agreement on a unique and official

definition is difficult to achieve also due to the different expertise interested in the investigation of VRE drought events, from economists to engineers and meteorologists. Furthermore, the climatological characteristics of the regions strongly influence the result. This study analyses weighted physical fields (radiation and wind speed) which benefits the generality of the results, instead of relying on specific energy power models and VRE technologies. But this choice also holds the downside of having to deal with particular local conditions (Pierro et al. 2022), deriving from the fields climatology. For example, for the chosen extended winter period, most of the northern latitudes experience persistently low solar radiation at the surface. The method that is defined here uses climatological weights. This ensures that the VRE generation indices reflect meaningful variations in energy potential, by emphasizing relative rather than absolute changes.

2.2.1 Methodologies in literature

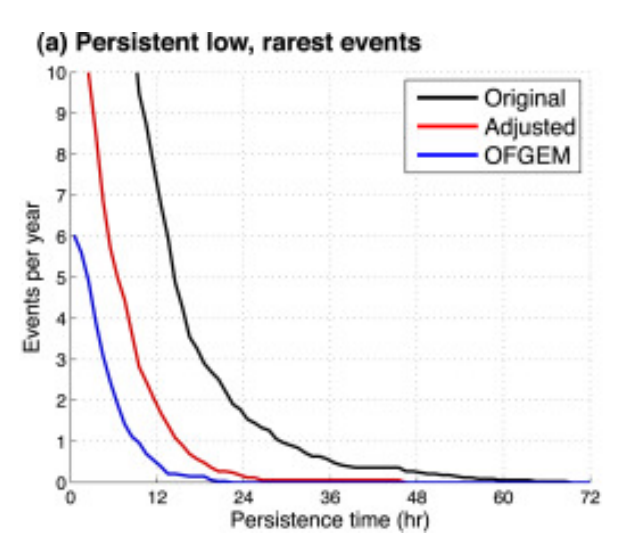


Figure 7: The mean frequency of the rarest extreme generation events from 1980 to 2012, as calculated using three different. Low generation events (capacity factor below 2.2%) (Cannon et al. 2015).

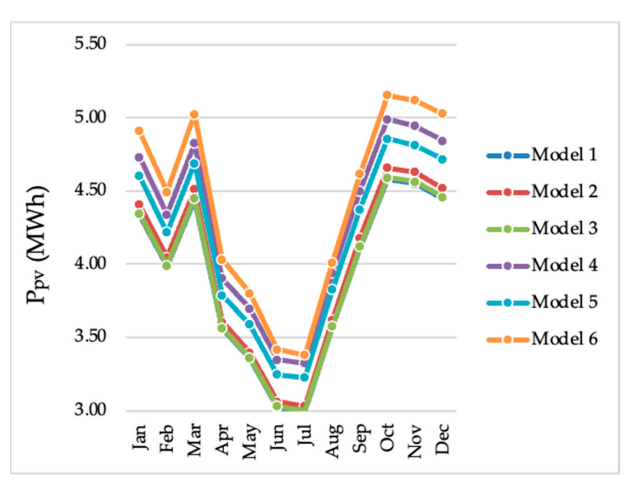


Figure 8: Solar power (P_{pv}) values per month for the PV production calculation models in the city of João Pessoa, PB, Brazil, between the years 1961 and 2021 for 100 Axitec AC 260P/156-60S PV modules (Araújo et al. 2024).

Energy production models, spatial and time extent limits and extremes selection methods defining VRE droughts in previous studies have been inconsistent (Kittel et al. 2024). Several studies worked with the power potential, which is the idealized amount of produced power given a certain intensity of the energy resource (in this case irradiance and wind speed) (Drücke et al. 2021; François et al. 2016). Computing both solar and wind power potential from irradiance and wind speed needs an empirical power model whose parameters depend on the energetic infrastructure. Thus, a specific or a synthetic photovoltaic (PV) panel model (Mavromatakis et al. 2010) and a turbine model must

be chosen among the available installed technologies. The potential is then weighted by the energy capacity for each area — the maximum output of electricity that a generator can produce under ideal conditions. For example, PV power depends on the area of the domain covered with PV panels and in fact this method should account for the exclusion zones — where infrastructure cannot be built — and neglect them from the potentials computation. Clearly, such method could be implemented at local scales, where detailed information of wind and solar electricity generation capacity and exclusion zones can be found and accounted for. At larger scales, though, the only viable approach is to make assumptions based on the most representative power models and average technologies installed. Besides, the sensitivity of the results on all the previous assumptions remains unstudied. There is a growing need of evidence on this matter, like the work of Cannon et al. 2015 on power curves: extreme low events occurrence turned to be sensitive to the power curves (one real and two synthetic curves were compared, Fig. 7) for the wind energy production. Also Araújo et al. 2024 studied PV power models: the discrepancy of PV power estimates found among different models were relevant (Fig. 8). Note how the estimates particularly spread during autumn and winter seasons, the focus period of this thesis investigation, even if the PV panel-dependable parameters used were the same for all models.

The other option, apparently simpler, is to compute a power potential index directly from the climatic variables (Gunderson et al. 2015). Therefore, we follow this option, leveraging the wind speed at hub height (although this parameter still requires an assumption), U_{hub} and the total downward solar irradiance at surface, $R_{surf}^{SW\downarrow}$ (or RSDS).

2.2.2 Wind velocity extrapolation

The wind speed at which wind turbines operate is the field at hub height. The hub height can span from 80 m up to 170 m depending on the turbine model, with taller turbines installed offshore. Even though technologies are continuously advancing and higher turbines are being built allowing greater rated powers (the amount of energy a facility is able to produce at best conditions), we assume a fixed hub height $H_{hub} = 100 \, m$, as for the majority of the works in literature (Cannon et al. 2015; Li et al. 2021).

As the GCFS model does not provide $100\ m$ height wind speed, those values are extrapolated from the $10\ m$ height wind speed values. Nonetheless this treatment is functional also in case the analysis should be repeated for different hub heights. For the extrapolation, previous studies have primarily employed either the log-profile or the power law (Kubik et al. 2011). The log-profile required the accessibility to many environmental variables, even in the simplified neutral atmospheric

stability-form (such as surface roughness, zero-plane displacement, shear velocity). Moreovere, for Gualtieri 2019 was more reliable in the lower part of the planetary boundary layer (around 10-20 m) than at higher altitudes. The wind power law appeared to be the best available option (Peterson et al. 1978) and the most common in literature (Drücke et al. 2021; François et al. 2016). The wind power law can be applied using a fixed exponent (usually $\sim 1/7$ at neutral stability conditions) or a variable one. Despite many papers in the literature used the 1/7 fixed exponent (Gualtieri 2019), the second performs better (see Fig. 9). Gualtieri 2019 pointed out that the variable exponent power

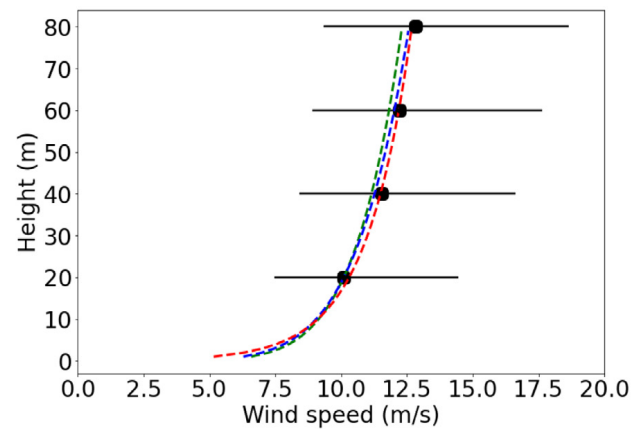


Figure 9: Vertical wind speed profiles from different adjustments to measurements during daylight for winter: the blue dashed line represents the profile estimated from the variable wind shear exponent of the power-law equation (adopted in this thesis); the green dashed line corresponds the profile estimated from the power-law considering $\alpha = 1/7$; the red dashed line represents the profile obtained using the log-law equation; the black solid markers represent the mean values from the measurements and error bars (Lopez-Villalobos et al. 2022).

law is the best recommended method — even compared to the log-profile, in absence of complementary data, like air temperature and relative humidity (Lopez-Villalobos et al. 2022).

Taking all the above points into account, we opt for the power law profile method. The reference ERA5 dataset provides both (u_{10}, v_{10}) and (u_{100}, v_{100}) wind speed fields, hence we use the historical reanalysis data for interpolating the exponent locally at each grid point $(\alpha(x,t))$. The interpolation is calculated along the time steps and then averaged over the focus period (winters from 1990/91 to 2023/24). After, we use the result in the analysis of both ERA5 and GCFS hindcasts for extrapolating the wind field at hub height. The method is summarised in the following formula:

$$U_{100}(t,x) = \sqrt{u_{10}^2(t,x) + v_{10}^2(t,x)} \times 10^{\alpha(x)} \qquad ; \tag{1}$$

where U_{100} represents the total wind speed module intensity at 100 m height, u_{10} and v_{10} respectively the zonal and meridional components of the wind speed at 10 m height. The fields are expressed as a function of space (x) (x indicating one grid point) or space and time (t). The ex-

trapolated wind at 100 m is used for both ERA5 and GCFS analysis so, if any error is introduced by the extrapolation, it affects equally the two results. The comparison between the original and extrapolated ERA5 U_{100} highlights the bias introduced by the extrapolation. It is mostly positive over Europe, between 0.0 and 0.4 m/s, with only few coastal regions and Mediterranean countries underestimating the velocities (Fig. 10). The magnitude of the bias is not severe, thus, we consider

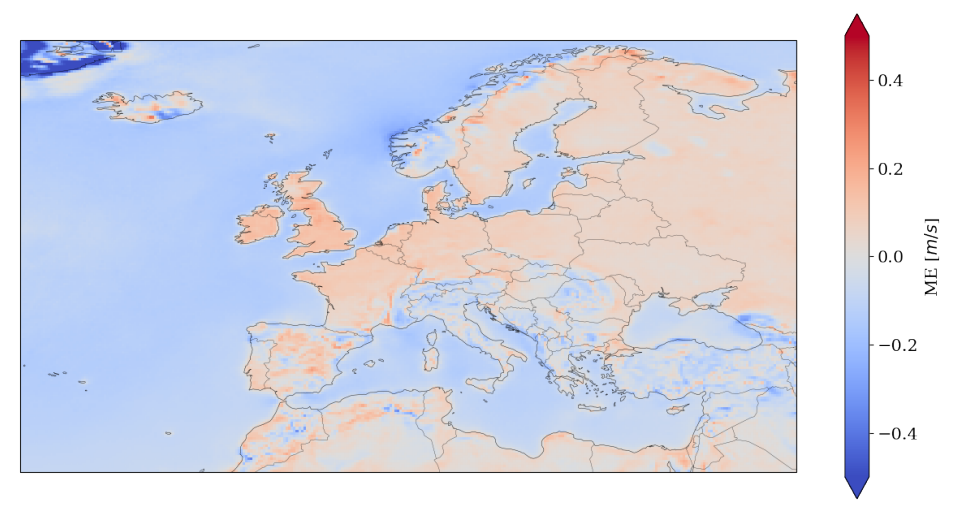


Figure 10: Mean error for the wind at 100 m height calculated as the difference between ERA5 original data and extrapolated with the power law.

the power law method accurate enough for the nature of our applications.

2.2.3 Operational definition

In this thesis, an index for the intensity of the compounded, solar and wind, energy production is developed, without opting for wind power curves or PV models, but weighting the physical fields by the country energy capacity. The raw physical fields are weighted assuming that countries prioritise installing the infrastructure where the physical energy source is the most intense. With these weights, irregular coverage of installations is approximately accounted for in absence of information about the exclusion zones. The weight, which we call source potential (γ) , is defined at each grid point, x, as the ratio between the grid point climatological mean $(\overline{R_{surf}^{SW\downarrow}}(x))$ and $\overline{U_{100}}(x)$ and the respective country, $c\ni x$, climatological mean $(\overline{R_{surf}^{SW\downarrow}}(c))$ and $\overline{U_{100}}(c)$ for surface radiation and $100\,m$ height wind speed.

$$\gamma_s(x) = \frac{\overline{R_{surf}^{SW\downarrow}}(x)}{\overline{R_{surf}^{SW\downarrow}}(c)} \quad , \quad \gamma_w(x) = \frac{\overline{U_{100}}(x)}{\overline{U_{100}}(c)} \quad ; \quad (2)$$

where the subscript letters s and w refer respectively to solar and wind. The definition of the solar (SEP^*) and wind (WEP^*) energy production follows:

$$SEP^*(t,x) = R_{surf}^{SW\downarrow}(t,x)\gamma_s(x)EC_s^*(c)$$
(3)

and

$$WEP^*(t,x) = U_{100}(t,x)\gamma_w(x)EC_w^*(c)$$
 ; (4)

where $R_{surf}^{SW\downarrow}(t,x)$ and $U_{100}(t,x)$ are the surface radiation at day t and grid point x. Given the definition of γ and EC^* , the product of these two terms, integrated over the country, returns the original *NMEC*. The compound-sourced energy production (*CEP*) is calculated as the weighted sum of the normalised solar and wind energy productions:

$$CEP(t,x) = \frac{SEP^*(t,x)}{\max_{x \in c} (SEP^*(t,x))} \omega_s(c) + \frac{WEP^*(t,x)}{\max_{x \in c} (WEP^*(t,x))} \omega_w(c) \qquad ; \tag{5}$$

with
$$\omega_{\{s,w\}}(c) = \frac{\text{NMEC}_{\{s,w\}}(c)}{\text{NMEC}_s(c) + \text{NMEC}_w(c)}$$
 (6)

The weight ω is there to not penalize countries that, usually for climatic reasons, install substantially more solar than wind plants or vice versa. The energy production indices SEP, WEP and CEP are computed from ERA5 dataset and GCFS hindcasts raw fields, together with the Eurostat dataset, following equations 3, 4 and 5. Hereafter, SEP and WEP refer to the normalised and omega-weighted SEP^* and WEP^* . Now, CEP can expressed straightforwardly as SEP + WEP and analysing if the compounded results behave additively from the individual sources is simpler.

Once the wind and solar power is obtained, we define a threshold that defines the drought extreme condition. As discussed in Chapter 1, one method is leveraging percentiles: we prefer this method a over fixed absolute threshold, since it always selects the same amount of most extreme events, it partly accounts for the difference among models and technologies (Cannon et al. 2015). In this thesis the threshold is set as the 15^{th} percentile of the distribution over the all grid points and time steps. Any day whose CEP(t,x) falls under the threshold is defined as a drought day; for the sake of this study droughts frequency is computed only for droughts with persistence between 1 day and 2 weeks. More than 14 consecutive drought days are simply justified by climatological reasons. For example, the Scandinavian countries during the selected winter months experience very low solar radiation during the day thus some areas where constantly under threshold for the chosen definition.

The operational definition described has multiple benefits, the estimation of the individual solar and wind energy production allows comparisons among countries and at the same time focuses on the physical fields rather than on the specifics of the technologies used. The end results are not actual real energy estimates like capacities or generation, but they represent a realistic measure of the intensity. This method is developed from scratch since most of the studies chose to follow some wind power curve and PV model; a direct comparison with other studies is therefore hindered. Focusing on the compounded *CEP* variable, the field has a less immediate interpretation than the individual *SEP* and *WEP*. Nevertheless, it respects the mix of installed wind and solar capacities, preventing to evaluate the extreme based only on the natural intensity rather than on the energetic magnitude associated to the natural source. Sorting out the droughts after tailoring the *CEP* to the national capacities through the normalisation accounts for lack of information on demands. Lastly, following Kittel et al. 2024 recommendation, the percentile method is applied directly to the metric of the compounded production. The two VRE sources are not treated separately, but their energy production is interwined and so are the weak extremes.

2.3 Frequency, persistence and spatial extent of VRE droughts

In view of the concerns of the energy market or of the stakeholders around the occurrence of the VRE droughts, the analysis and following predictability assessment focuses on the frequency of the events. The frequency is computed as an aggregated count of the drought days over a certain period (i.e., months or extended season); alternatively over a certain area (i.e., European macro-regions of Northern, Central and Southern Europe⁵ or all of Europe⁶). When spatially aggregated, the drought occurrence, referred to as "extent", is the count of grid points experiencing a drought, normalised over the total number of grid points in the region. Thus, the final value represents a percentage of the respective area under drought conditions.

To characterise the compounded VRE drought events their temporal persistence is also used as a measure of their intensity or temporal evolution. At each grid point two time series are constructed, a drought persistence index and a drought ordinal day index. In the first, each day is assigned a value corresponding to the number of consecutive drought days it belongs to; specifically, days without drought are coded as 0, while for each drought spell of length n, all days within that spell are coded as n. For example, a grid point experiencing a 4-day drought would record the following series: [..., 0, 4, 4, 4, 4, 0, ...]. This encoding captures the duration, providing a simple but effective persistence measure. Furthermore, since longer events represent more severe shortfalls of energy production, this index can also be interpreted as a measure of drought intensity. Secondly, the ordinal day time series tracks the order of each day within a drought spell. In this encoding,

⁵Reproducing the Europe domain subdivision used in the IPCC 6th assessment report (IPCC 2023a)

⁶Europe indicates here the group of European countries in the Eurostat dataset that have been analysed.

non-drought days are set to 0 and for each drought spell of length n, the respective n days are set to [1,2,...,n]. For example, a grid point experiencing a 4-day drought would record the following series: [...,0,1,2,3,4,0,...]. This representation does not quantify the event intensity directly but rather its temporal progression, allowing an analysis of how conditions evolve within a drought episode.

VRE droughts predictability and index validation

Following the data analysis described in Chapter 2, in this chapter we present the results and provides interpretations for the main features obtained in the seasonal forecast analysis. The physical interpretation and relevance of these results will be discussed in detail in the following chapter (Chapter 4).

3.1 Evaluation of the GCFS

As an initial step toward evaluating the skill and limitations of the GCFS hindcasts, an analysis of the raw meteorological fields used in this study is conducted. First, we assess the solar radiation and surface wind fields; secondly, we evaluate the operational energy potential indices both individually for wind and solar energy and as a combined (compounded) power index. While these fields do not directly indicate skill in forecasting variable renewable energy (VRE) drought events, their analysis is a necessary prerequisite for understanding the origins of predictive skill or lack thereof in the model's representation of VRE droughts.

3.1.1 Primary climatological fields

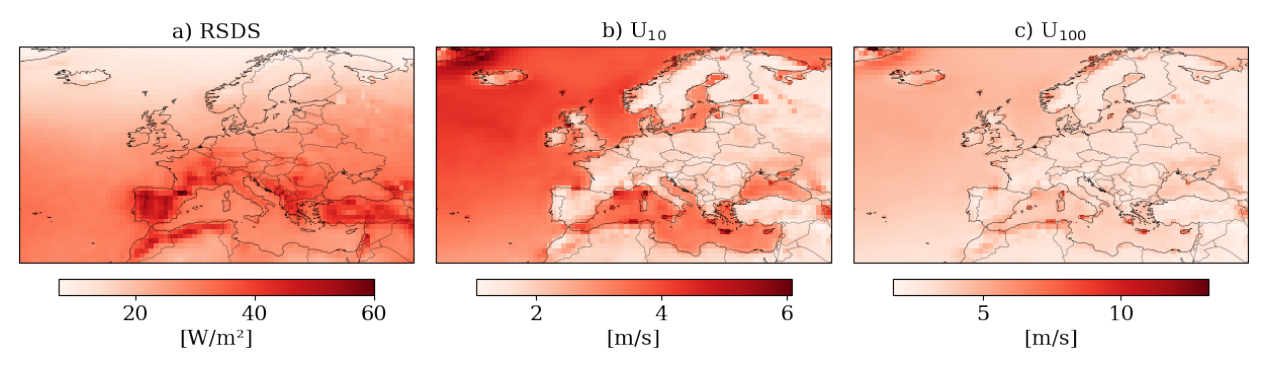


Figure 11: Root mean square error for a) shortwave downward radiation at surface, b) wind speed at 10 m height and c) wind speed at 100 m height. The RMSE is computed only for the extended winters (NDJFM) 1990/91 to 2023/24; we use the ensemble mean of the GCFS hindcasts for the evaluation.

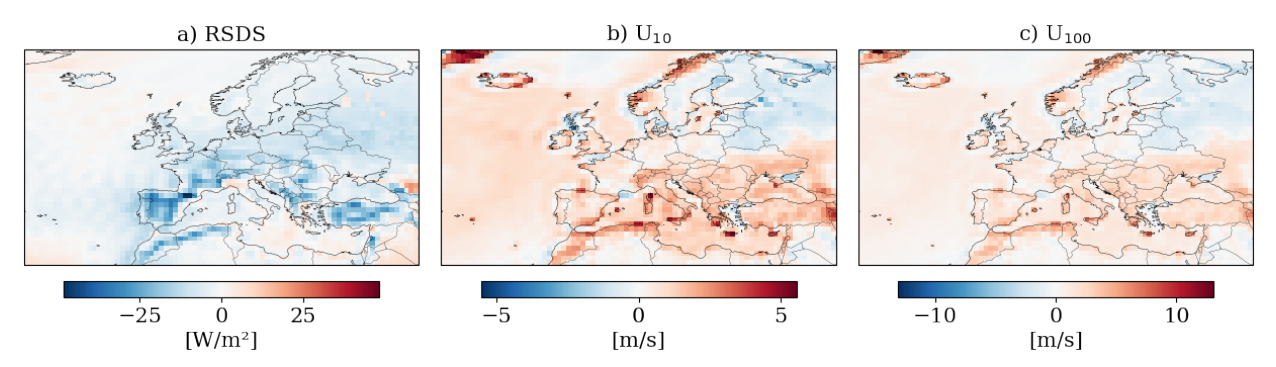


Figure 12: Mean Error (biases) for a) shortwave downward radiation at surface, b) wind speed at 10m height and c) wind speed at 100m height. The RMSE is computed only for the extended winters (NDJFM) 1990/91 to 2023/24; we use the ensemble mean of the GCFS hindcasts for the evaluation.

The root mean square errors (RMSE) for the shortwave downward radiation at surface field, the 10 m height wind field and the 100 m height extrapolated wind field are illustrated in Fig. 11. The RMSE is calculated over the analysis period, spanning November to March for each year from 1990/91 to 2023/24. For solar radiation, the highest errors are observed over inland regions of Southern Europe, with notable peaks over Turkey, the Balkans and the Iberian Peninsula. In contrast, surface wind fields exhibit larger deviations from ERA5 over oceanic areas — which lie outside the primary study region — while errors over land are generally lower. This may simply results by the fact that surface wind are higher over sea. Wind at hub height shows elevated RMSE values across much of the domain, with pronounced peaks over the Mediterranean islands and along the Norwegian coastline. When examining RMSE computed on anomaly fields (see Fig. 27.B), the spatial patterns closely resemble those seen in the RMSE of the full fields (Fig. 11). Overall, for all three variables, the RMSE magnitudes and spatial distributions are nearly identical between the total and anomaly fields. This consistency suggests that most of the model error arises from variability rather than biases in the mean state.

To evaluate the nature of these errors, the bias is also computed (Fig. 12 and Fig. 28.B). The mean error (ME) indicates that the model systematically underestimates solar radiation compared to the ERA5 reference, particularly inland. It slightly overestimates 10-meter wind speed (U_{10}), particularly over coastal regions of Southern Europe and along the Norwegian coastline. The U_{100} bias (Fig. 11 c) is very similar to U_{10} bias (Fig. 11 b), but the values range in a larger interval, $[-10 \, m/s; 10 \, m/s]$. Again, the results for the ME metric computed on the anomalies present very similar maps, both for the sign pattern and intensities.

The result reveals a spatially widespread negative bias for the shortwave downward radiation at surface and a positive bias for the wind speed at 10 m height in certain locations. The errors

for the wind speed at surface anomalies are translated onto the U_{100} field, too. We find that the extrapolation does not introduce new errors, but rather enhance the existing pattern for the wind speed at surface level. The biases described in this section influence the energy production indices defined in this thesis only to a limited extent, because the fields are weighted by terms accounting for the respective climatological means.

3.1.2 Energy production metrics

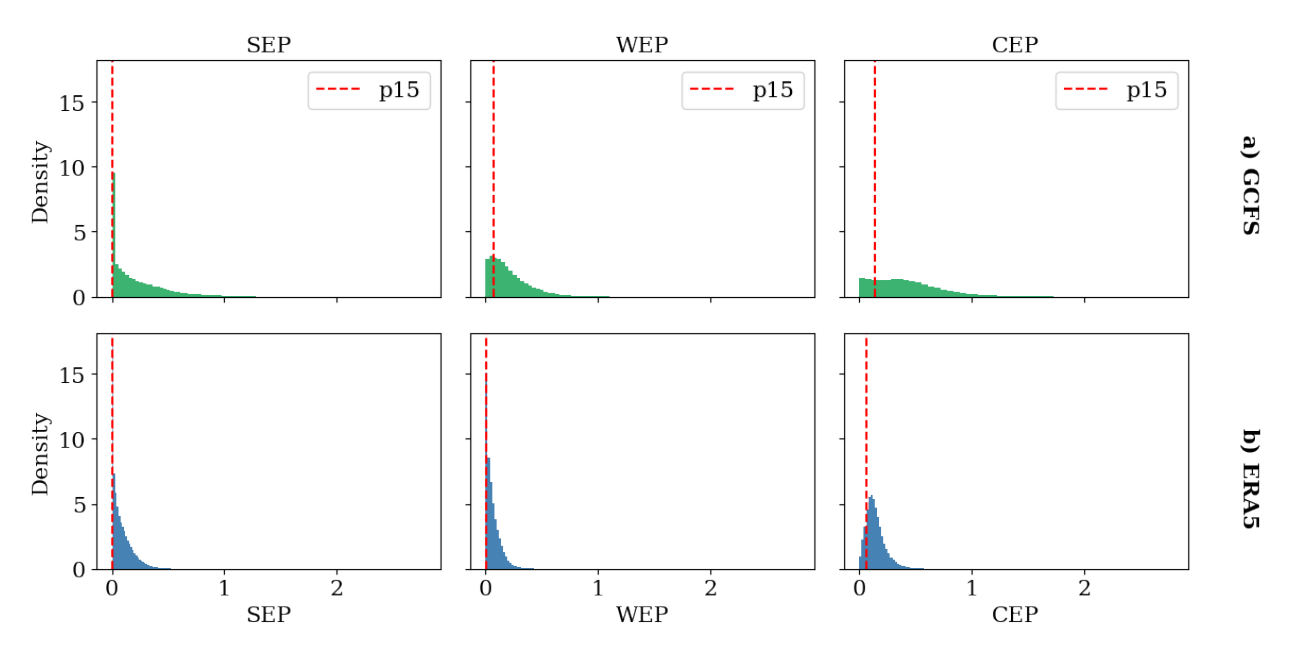


Figure 13: Density curves for the all grid points and all days (not zero) values of the SEP (first column), WEP (second column) and CEP (third column) indices. Values for a) all GCFS ensemble members and b) ERA5. The red lines identify the 15^{th} percentiles (computed on the ensemble mean for GCFS) which identify the extremes.

The solar, wind and compounded energy production indices biases are analysed through the distribution (Fig. 13) and again the error metrics RMSE and ME (Fig. 29.B and Fig. 30.B). The distributions present the *SEP*, *WEP*, *CEP* indices daily values from all ensemble members. The densities are derived from all grid points and days (excluding zero values) across the study period. The densities are expressed so that the integration of the curves returns 1. From the ensemble mean distribution (Fig. 31.B), the values of the 15th percentile are extracted to define the individual or compounded renewable energy droughts. For the solar and winter indices the curves in ERA5 are regular, shaped like a gamma distribution: positively skewed towards the left, lower tail and decreasing quite sharply towards the right tail. The model ensemble reproduce correctly the positive skew and overall shape for the *SEP* index, but it is less dense in the left, lower tail and

stretches towards higher values in the right, higher tail. The WEP density curve completely misses the skewness. The range extends to higher values, like for the solar, despite they do not influence the compounded drought definition which follows a thresholding method, it is still worth considering in sight of the physical interpretability of the following results. The SEP and WEP values range between 0 and 1, thus the CEP index ranges in the [0;2] interval. While ERA5 compounded index reaches 0.5 at maximum, the model values stretches over 1.0. This arises from the combined overestimation of both SEP and WEP individually. The combination of SEP and WEP also produces a bimodal distribution of CEP, differently from ERA5 whose curve reaches a single maximum. An overall strong positive bias is observed in the ME in Fig. 28.B, too. Although the ME calculated on the anomalies (Fig. 29.B) is small enough to be negligible; the error in representing the lower end of the distributions, especially for the wind index and thus also for the compounded, is relevant in the treatment of the extremes. Nonetheless, the left tail is still under-represented in the model, meaning neither the outliers reproduce those extremes.

3.2 VRE drought characterisation

Having evaluated the GCFS's representation of raw climatological fields and energy production metrics, the characterization of VRE drought events now follows. This analysis focuses on three key aspects: the mix of solar and wind energy during droughts, the persistence of these events and their spatial extent. Understanding these characteristics is essential for interpreting the model's prediction skill, which will be discussed in the following section.

3.2.1 Individual sources mix

The fraction of the *CEP* index derived from either *SEP* or *WEP*, indices is illustrated in Fig. 14. The maps depict which of the two components, *SEP* or *WEP*, dominates during compounded drought events for each month. The plot depicted here shows the results from ERA5 dataset, but the pattern from the GCFS ensemble mean are very similar (Fig. 32.B), thus the discussion will be unique. A clear meridional gradient is observed, with Northern Europe (i.e., Scandinavia, Iceland and the UK) predominantly relying on wind energy production (*WEP*), indicating a greater dependence on wind energy during compounded drought events. In contrast, Southern Europe (i.e., Italy, Greece and Turkey) tends to exhibit a mixed pattern, with a notable. shift towards solar energy production (*SEP*). Central Europe and the Iberian Peninsula, on the other hand, exhibit a seasonal variation in energy reliance. From November onwards, wind energy production (*WEP*) tends to dominate;

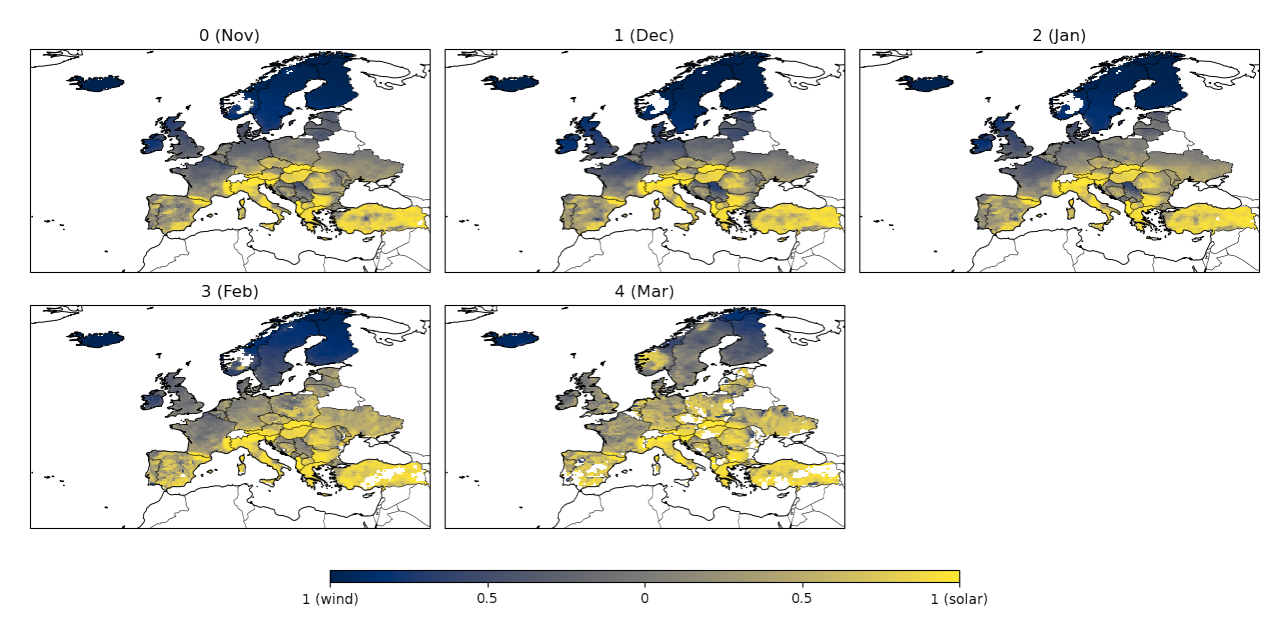


Figure 14: Dominance of energy source during VRE drought events. Each subplot refers to a lead time in [# months]. Dark blue (value = -1) indicates complete dominance of wind energy potential (WEP), while bright yellow (value = 1) indicates complete dominance of solar energy potential (SEP). Intermediate colours (i.e., grey) reflect mixed contributions from both sources. Values are computed from the ERA5 dataset.

by February, energy conditions become more balanced between wind and solar sources; lastly, in March, there is a marked shift towards a greater reliance on solar energy production (*SEP*). In Slovakia, Hungary and Albania the solar fraction noticeably dominates during all the months. It is worth noticing in these two countries the installed capacity for the wind energy is less then 0.1% of the combined solar and wind capacity, hence the results in Fig. 14 are explained. The opposite happens in Croatia and Kosovo, where the fraction is high for *WEP* for all 5 months, although in these countries the percentage of installed technologies is less unbalanced.

3.2.2 Persistence of VRE droughts

We analyse the distribution of drought events persistence for the two datasets, GCFS (left) and ERA5 (right) in Fig. 15. For each group of consecutive drought days (indicated as *drought event*), one value equivalent to the number of days in the event is considered. The density is highest at low persistence values, in both GCFS and ERA5, with a peak at 2 days length for the hindcasts and at 1 for the reanalysis. The densities rapidly decrease as persistence increases, indicating that most drought events are short-lived. The tail extending to higher persistence values is long and mostly unpopulated, suggesting that while rare, some drought events last above 5 days in both datasets.

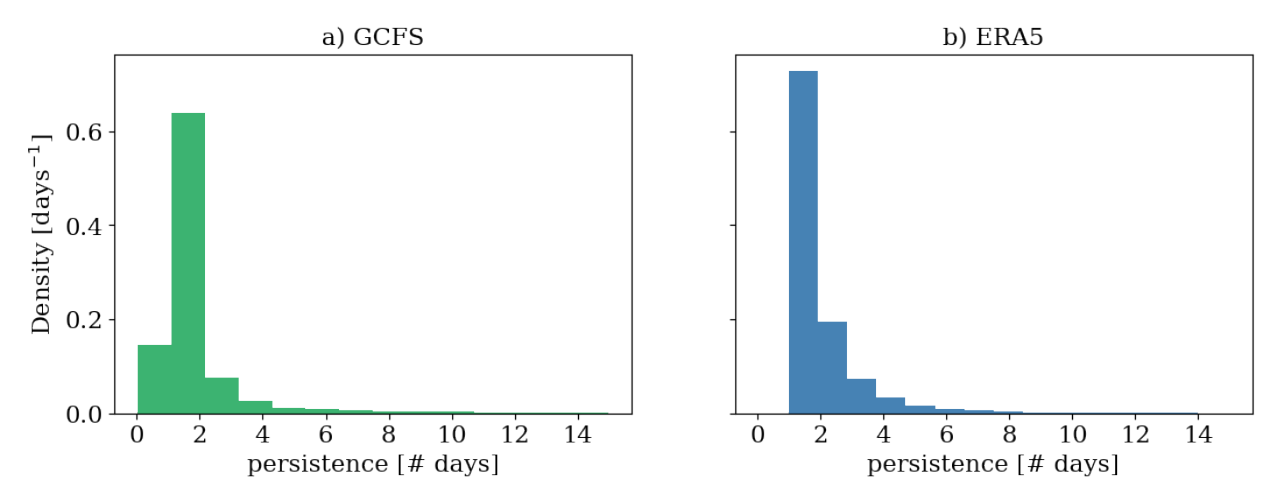


Figure 15: Density curves of the lengths in days of drought events in a) the GCFS model ensemble mean and b) ERA5. Bin width corresponds to 1 day.

3.2.3 Spatial extent of VRE droughts

The spatial extent of drought days — defined as the normalised count of grid points experiencing a VRE drought on a given day — is aggregated separately for Northern, Central and Southern Europe and for Europe in total. The ACC values are reported in Tab. 1. Correlation is high (except for the Northern Europe region) and always statistically significant. We find this result remarkable, consequently we explore the extent metric more in detail.

EU	NEU	CEU	SEU
0.55	0.15	0.59	0.65

Table 1: Anomaly correlation coefficients computed for the percentage of the region experiencing drought conditions, based on daily values from November to March (1990–2024). Columns show the coefficients for the entire domain (EU), Northern Europe (NEU), Central Europe (CEU) and Southern Europe (SEU). All values are statistically significant (p-value <0.05).

we investigate the difference between individual and compounded drought extents, in order to understand if they are ascribable to large-scale rather than local-scale weather conditions. The scores for ERA5 regional monthly mean extents in Fig. 16 show that the solar energy extreme lows are on average more vast than the compounded energy droughts, which, in turn, are vaster than the wind energy extreme lows for Northern Europe and all Europe. In the other regions, no event is registered below the *SEP* 15th percentile, so the extent is not illustrated. Nevertheless, the extent of the compound energy drought always overshoot the wind energy extreme lows extent, except in Southern Europe.

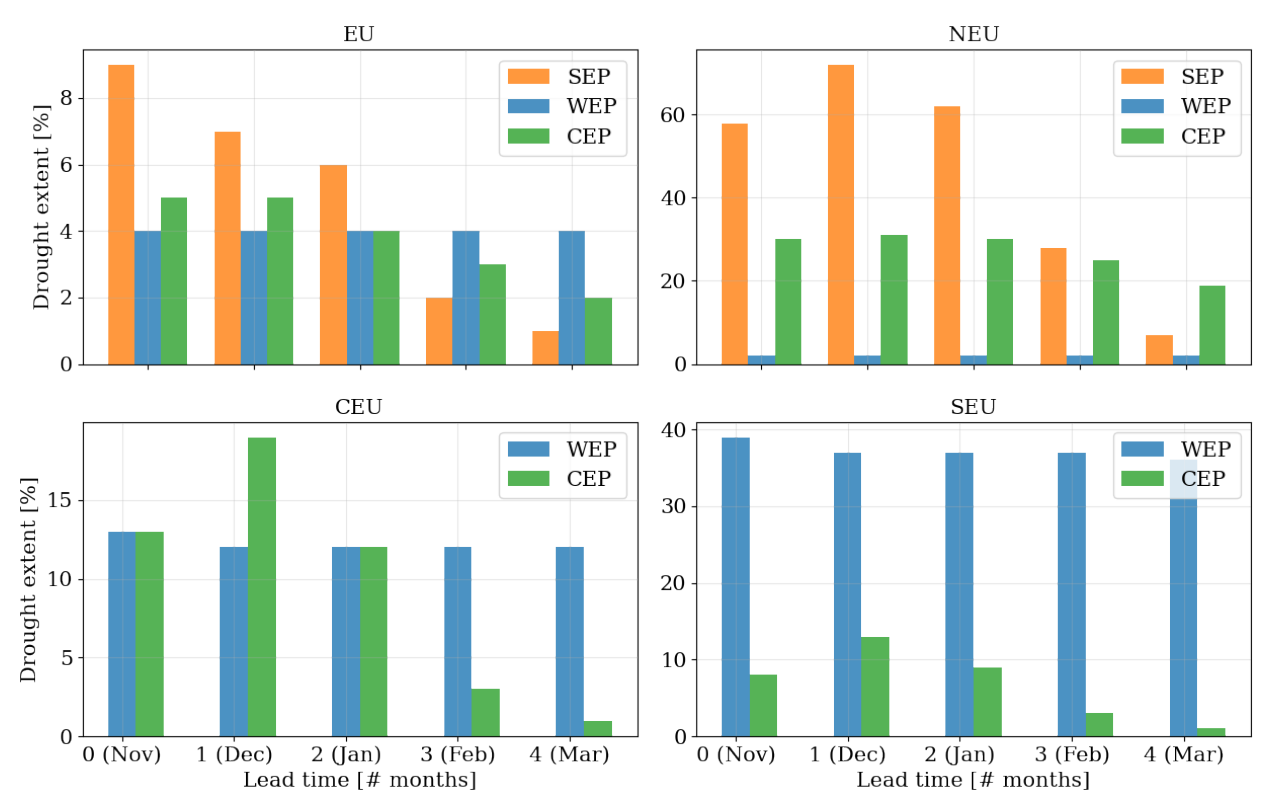


Figure 16: Average monthly drought extent among individual (SEP and WEP) and compounded (CEP) extreme lows. The data is grouped by region: all Europe and Northern (NEU), Central (CEU) and Southern (SEU) Europe. The x-axis representing the lead time. Calculated from ERA5

Then, we investigate the behaviour of the ensemble spread, instead of only adressing the ensemble mean. The series of scatter plots in Fig. 17 presents a comparative analysis of the GCFS ensemble distribution against ERA5 reanalysis data across the different regions and months. The data points are averaged by month, ranging from 0 to 4 months lead times, each colour refer to a specific month. For each ERA5 value the correspondent month-and-year values in the GCFS ensemble are depicted. To represent the ensemble spread a box is used: the whiskers stretch from the minimum to maximum values, the box contains the second and third quartiles values and a dot coincides with the ensemble mean. Moreover, a least-square linear regression is computed to provide a quantitative assessment of the correspondence in the plots. The regression metrics are shown in the top right corner, detailed version in Tab. 3.B. For all Europe, data points are densely clustered around the lower values of both axes, with a noticeable spread along the red dashed line (slope $\simeq 0.93$), but shifted, of about 7%. For Northern Europe (Fig. 17 b), the scatter is more dispersed compared to other regions, with data points spreading up to 25%. The distribution shows a significant overlap between different lead times suggesting low sub-seasonal variations, correctly predicted by the model. Conversely, GCFS ensemble mean reduces the inter-annual variability,

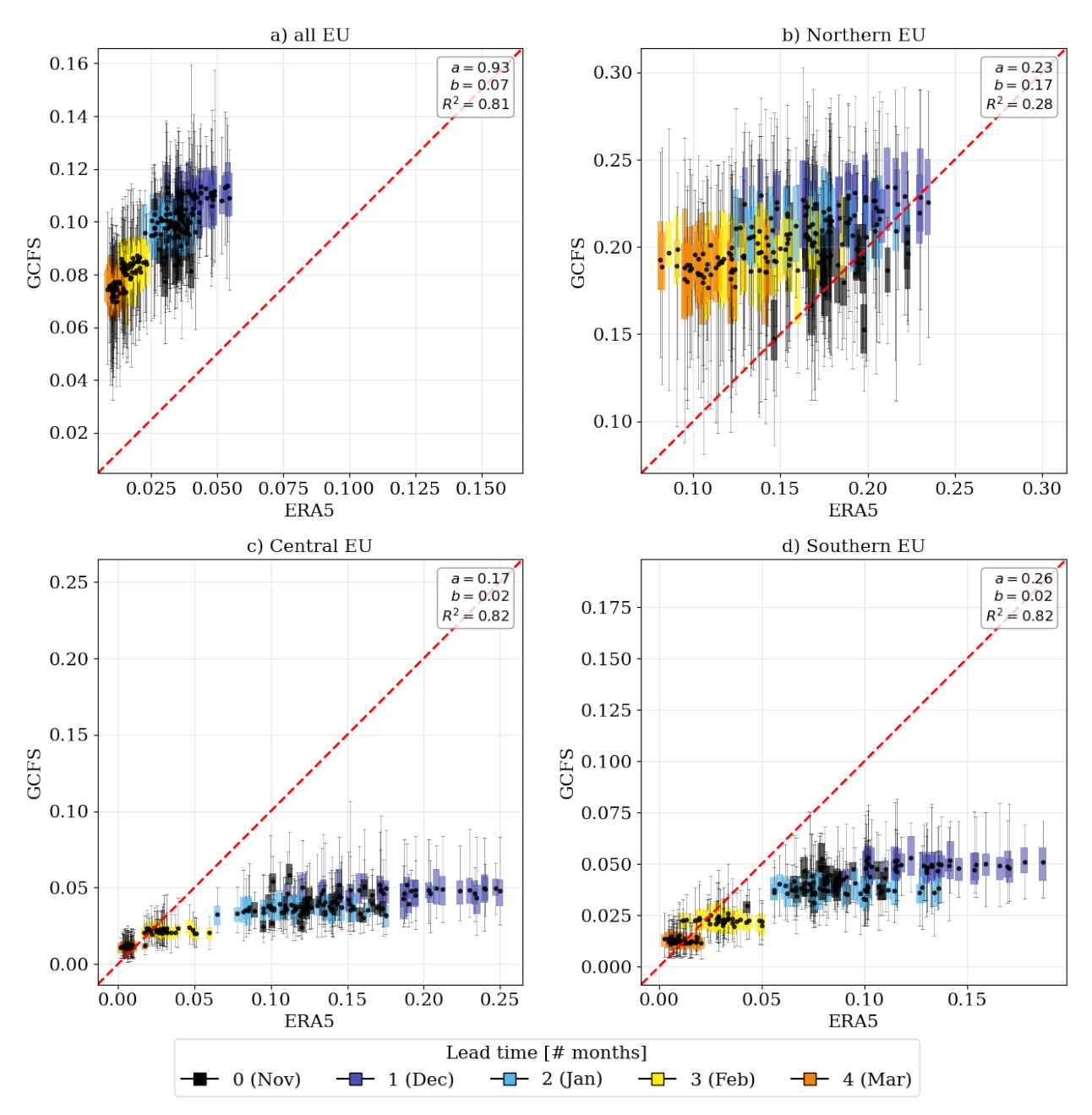


Figure 17: Scatter plots comparing GCFS ensemble distribution of monthly averaged drought extent (normalised) for distinct regional grouping: (a) all EU, (b) Northern EU, (c) Central EU and (d) Southern EU. The values are represented by boxes showing the ensemble minima and maxima (whiskers), first and third quartile (box) and mean (dot). Boxes are colour coded by lead time (in months). The red dashed line represent the 1:1 ideal correspondence. In the top right corner: slope (a), intercept (b), coefficient of determination (R^2) .

with the exception of the first hindcast month (0 month lead). Values, for Central Europe, range only between 0% and 7% with occasional members stretching up to 10%. While this low variability mostly coincides for the last two months in ERA5, the first lead month should range up to $\sim 15\%$ and $\sim 10\%$ the second. Lastly, Southern Europe has similar characteristics of Central Europe, with the same alignment along the red dashed line and inter-annual variability varying with the months. The first three hindcasts months have greater inter-annual variability than the last two, both in the GCFS and ERA5. It is worth noticing that $R^2 \simeq 0.8$ for the three regions: all, Central and Southern Europe; while it is very low for Northern Europe.

3.3 VRE droughts prediction skill

With a clear understanding of the spatial and temporal characteristics of VRE droughts, the GCFS's skill in predicting their frequency is now assessed. This section evaluates the anomaly correlation coefficients (ACC) for drought occurrences at the grid point level. The prediction of drought extent aggregated over larger regions is moderately reliable, as already mentioned in Section 3.2 (ACC measures in Tab. 1). We also examine the contributions of individual solar and wind indices to compounded drought predictability.

Due to the nature of the impact that VRE drought events have on the energy market and dis-

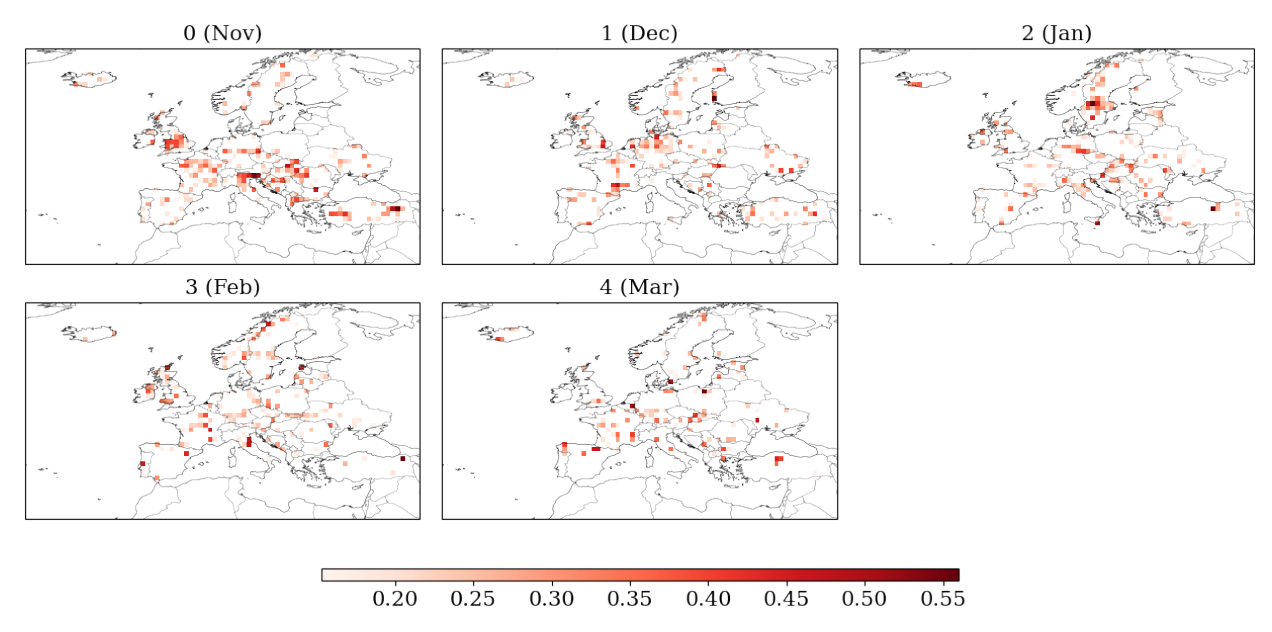


Figure 18: Correlation coefficients of anomalies for the monthly count of drought days are shown, displaying only statistically significant positive correlations (p-value <0.05). Each subplot refers to a lead time (in months). Maps illustrating the full correlation signal, including non-significant and negative values, are provided in Fig. 33.B.

tribution across Europe, the primary focus is on predicting the frequency of energy shortfalls, on a monthly or seasonal timescale. Therefore, the Anomaly Correlation Coefficient (ACC) is calculated for the monthly and wintertime frequency of VRE droughts to quantitatively assess the prediction skill of VRE drought occurrences. The total ACC scores are found in Tab. 4.B; the values are not significant (p-value >0.05) and in any case they never reach 0.1 or above. Instead, the maps in Fig. 18 show the significant (p-value <0.05) ACC along the time dimension only, grid point by grid point. Notably, regions with significant positive correlations are primarily concentrated in central and western Europe, with some variability in intensity and spatial extent as the lead time increases. At shorter lead times (0 and 1 month), the signal appears occasionally more coherent and intense. For example, in England, France and northern Italy, in November and northern France and northern Germany, in December. At longer lead times, the spatial coverage is highly heterogeneous and the correlation strength tends to diminish slightly. To explore the underlying reasons for the spatial incoherence observed in the ACC results for compounded energy drought occurrences, the same analysis is conducted separately for extreme low occurrences of the solar, wind and compounded energy indices. The statistically significant ACC maps for the monthly and November-to-March counts of days below the 15th percentile, without excluding droughts longer than 14 days are presented in Fig. 19. Again, as expected, the skill is the highest when the model is initialised in November and it gradually decreases with increasing lead time. The spatial patterns are heterogeneous, with areas of significant skill varying from month to month and across indices. For what concerns the solar energy extreme lows, the signal is not very informative, since the percentile threshold is never met in most of Europe. Events are recorded exclusively in Scandinavia, where any positive correlation may be influenced by the relatively lower inter-annual variability of the RSDS field during the winter months compared to other regions (Parding et al. 2014; Dommenget 2022). The wind, instead, shows widespread significant correlation, as does the compounded energy extremes, but the two also do not appear related, with the significant signal turning up consistently in different regions and with different intensity. For example, in December (1 month lead) pockets of significant correlation for the wind energy extremes appear over southern France, north-east Spain, Italy and western Germany, while for the compounded energy extremes they appear over northern France, England and Sweden.

In conclusion, the region average ACC (Tab. 4.B) suggests no prediction skill, however the maps indicate a few sparse location where the correlation is indeed relevant.

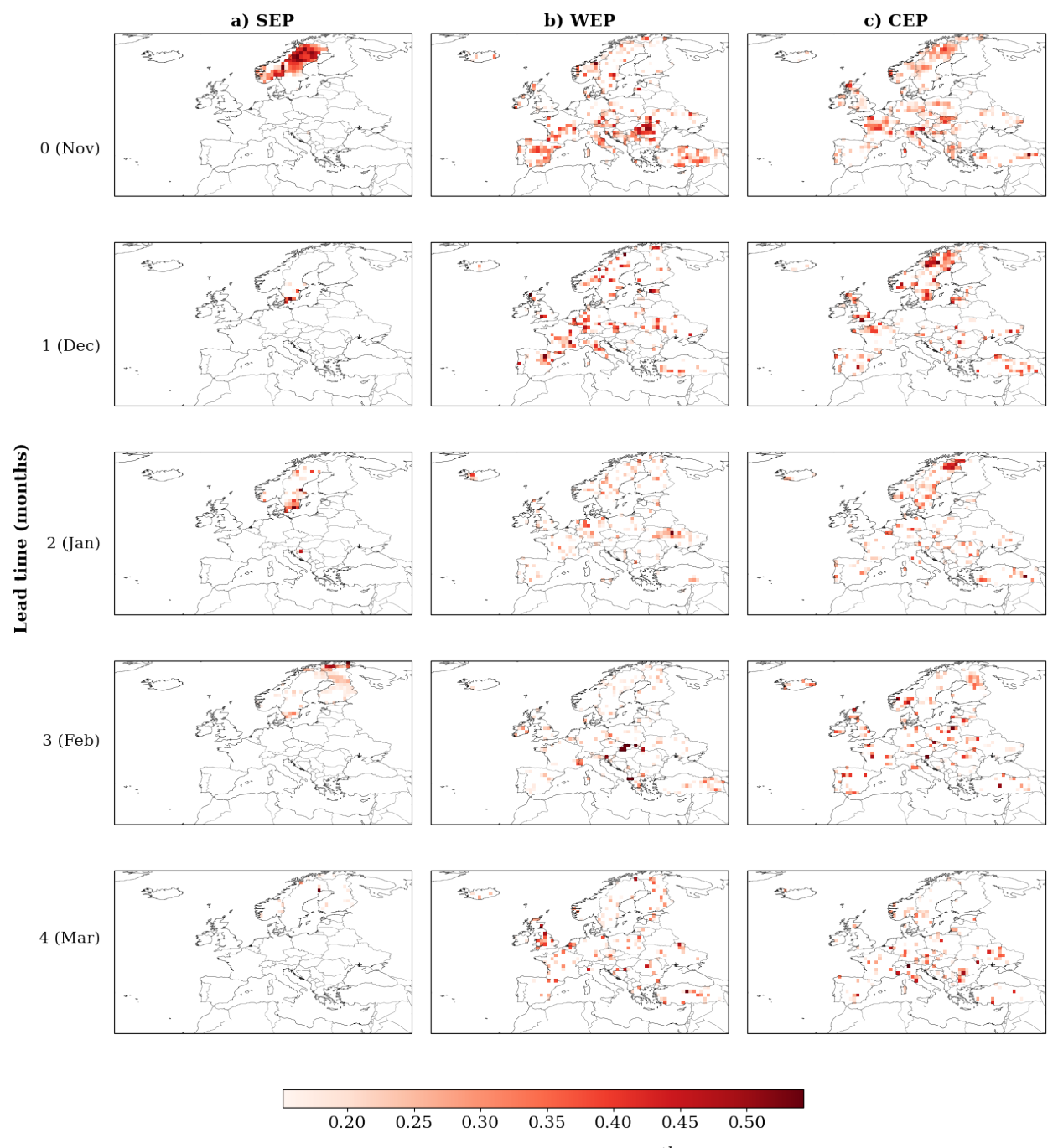


Figure 19: ACC for the monthly count of days below the 15^{th} percentile threshold are shown for the *SEP* index (first column), *WEP* index (second column) and *CEP* index (third column). Only statistically significant positive correlations (p-value <0.05) are displayed here. Maps showing the total correlation coefficients, including non-significant and negative values, are found in Fig. 34.B.

3.3.1 Individual drivers

To better assess the indices' behaviour, we evaluate the contributions of the individual solar and wind indices to the compounded VRE drought. For each *SEP* and *WEP* the monthly anomalies are calculated exclusively for the days classified as compounded drought days⁷.

To compare the values between the GCFS ensemble mean and the ERA5 reference, those anomalies are averaged monthly in order to obtain time series of the same length. The results are shown in Fig. 20. Here, similarly to the maps already examined (Fig.s 18 and 19), the signal of positive correlation is extremely scattered over Europe; even more, there are no clear clusters of coherent coefficients values. The locations marked in Fig. 18 by the skill in monthly count of drought days are repeated in Fig. 21 c, but masked to highlight the locations where the model shows skill in predicting neither SEP or WEP monthly mean anomalies for the drought days (grid points in Fig. 20 with no significant signal). It is evident that most of the relevant signal for the ACC of the compounded drought frequency occurs in locations where, instead, the model does not score a significant ACC in any of the two indices monthly mean anomalies for the drought days. Meaning that the GCFS performs well in simulating the monthly frequency of the compounded VRE drought days especially in regions where it does not perform well in simulating the variability during the drought days of neither individual sources energy potential index.

3.4 Validation of the compounded VRE drought definition

To test the robustness and interpretability of the compounded energy potential index and the consequent compounded VRE drought selection, the behaviour of the index, computed from ERA5 data, is compared against documented events reported in the literature. Although very few studies provide concrete examples of solar and wind compounded drought events with spatio-temporal detail, two cases are reported by Li et al. 2021, which we use here as benchmarks. The first occurred in Belgium, between the 15th and 17th and between the 22nd and 25th of January 2017 (evolution of the event in Fig. 37.B); the second in Germany, between the 16th and 26th of January 2017 (evolution of the event in Fig. 22). In both episodes, the index successfully detected the events (Fig. 36.B and 38.B), reproducing a significant spatial footprint. For Belgium, the index succesfully identifies the two temporal windows that characterised the event. However, where the event is extremely localised, the index is averaged over the entire Belgium, hence the index tends to be smoothed. These findings underscore the critical role of spatial resolution in the case of localised

⁷Events of 1 day to 14 days duration.

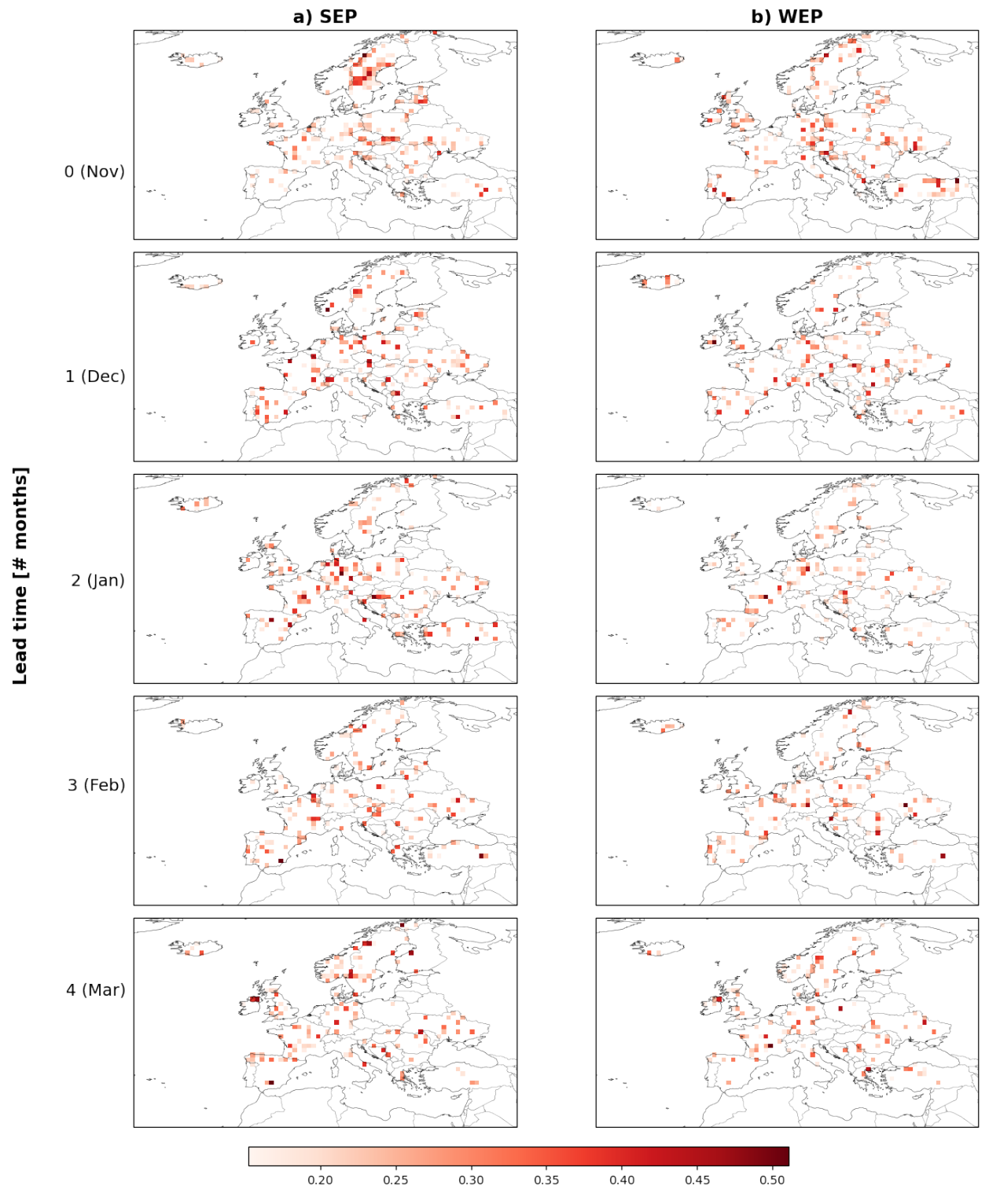


Figure 20: ACC of *SEP* and *WEP* monthly mean anomalies during drought days, computed between the GCFS ensemble mean and ERA5. Only the positive significant (p-value <0.05) signal is reproduced. Maps showing the total correlation coefficients, including non-significant and negative values, is found in Fig. 35.B.

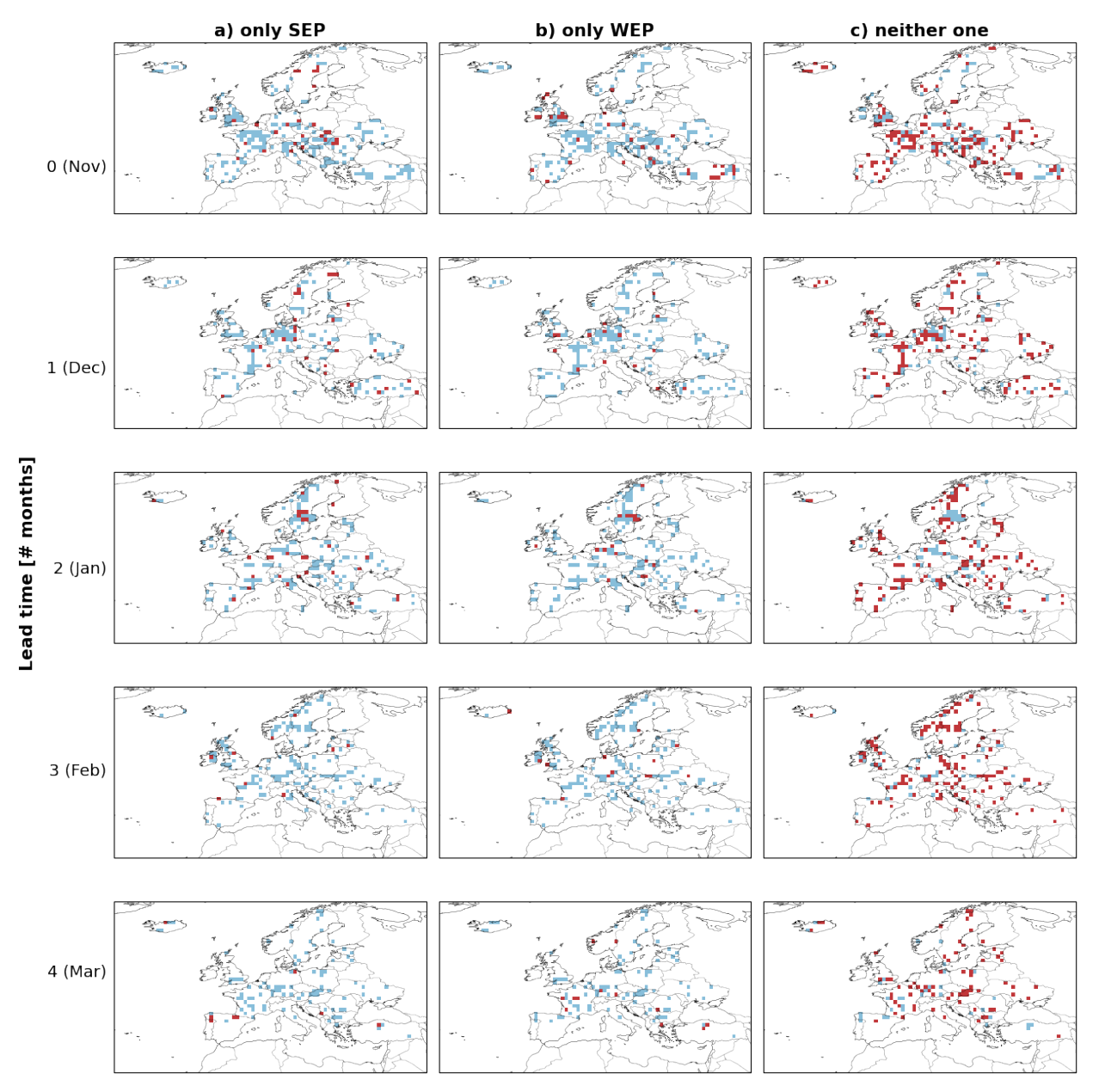


Figure 21: The highlighted locations are locations where ACC is positive and significant for the monthly count of drought day as in Fig. 18. In red, locations where the model shows skill in predicting: a) only SEP monthly mean anomalies for the drought days (in Fig. 20 a) b) only WEP monthly mean anomalies for the drought days (in Fig. 20 b); c) neither index. In blue otherwise.

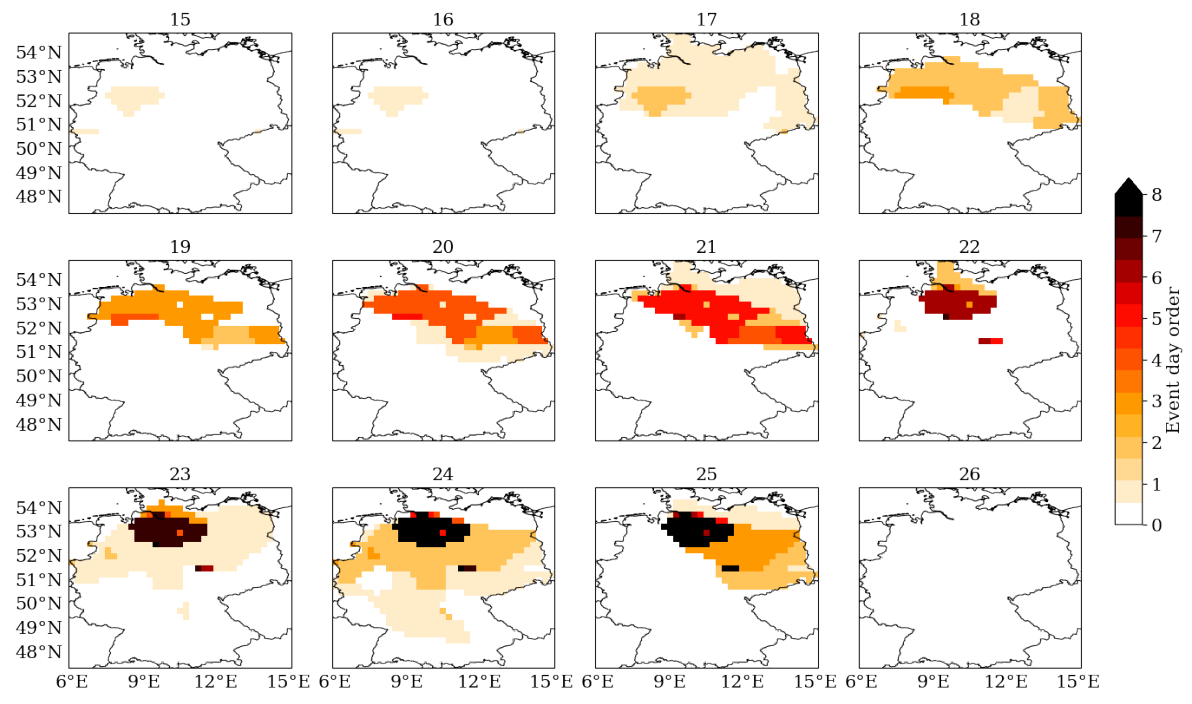


Figure 22: Map of Germany from the 15^{th} to the 26^{th} of January 2017, showing the ordinal day time series of the multiple-days drought event (for the definition of the index see Chapter 2).

extremes, the index can be significantly diluted when evaluated at coarser scales, such as the grid resolution of the GCFS model.

A further indirect validation is provided by Kittel et al. 2025, whose climatological study, based on model simulations, identified the winter of 1995/96 as the most critical period for the interconnected European grid. Consistent with this, the Europe-wide mean of the compounded index we use falls well below the drought threshold during that period, indicating a widespread reduction in renewable energy potential. However, this event cannot be analysed spatially within that study due to the large domain considered, the extent anomalies are instead depicted in Fig. 23. The study defined potential shortages without corroborating evidence from power system operations and, consequently, no further investigation is conducted.

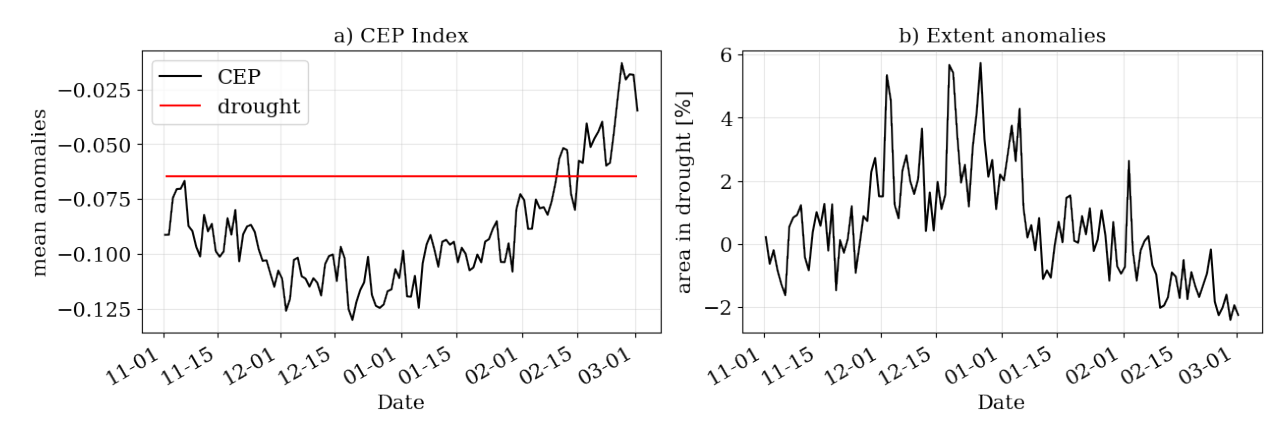


Figure 23: On the left, *CEP* index anomalies average over all Europe. On the right, the extent anomalies. The time frame is from the 1^{st} of November 1995 to the 1^{st} of March 1996.

Chapter 4

Dynamics and challenges of VRE availability

After we presented the results in Chapter 3, now we discuss their physical interpretation with the objective of assessing the GCFS 2.2 prediction skill of solar and wind compounded energy droughts in Europe. Based on the analysis presented in Fig. 18, in some locations the seasonal hindcasts can be reliable (i.e., Sweden and Finland for solar droughts, southern France and Spain for wind droughts, northern France and Scandinavia for compounded droughts), depending on the lead times. Interestingly, the skill does not appear to be clearly linked to neither solar nor wind indices, suggesting a non-additive behaviour, despite the definition of *CEP* index. As illustrated, the model exhibits limited skill in capturing the inter-annual variability of compounded VRE droughts, with forecast accuracy varying significantly across the spatial domain. Nonetheless, the index successfully identifies documented compounded energy drought events, such as the compounded drought in Belgium and Germany in January 2017. Although spatial resolution is critical for accurately detecting local extremes, aggregation over macro-areas increases the prediction skill. The model mostly fails to locate precisely the droughts at small-scales, but predicts large-scale conditions good enough to successfully produce a reliable measure of the drought extent across larger regions. In the following chapter we provide a more detailed discussion and interpretation of these findings.

4.1 Predictability of VRE droughts

The ACC are very low (\lesssim 0.2) and not statistically significant almost at all lead times for: individual solar and wind extremes, compounded extremes and compounded VRE droughts⁸ (Tab. 4.B). While this result is concerning, an analysis of the Anomaly Correlation Coefficient (ACC) over time reveals that certain localized regions exhibit forecast skill. This initial comparison between the Tab. 4.B and Fig. 18 suggests that, although the overall predictive skill across Europe is low, there are specific grid points where the monthly frequency of these events shows a statistically significant positive correlation with the ERA5 reference. Almost for all type of events analysed in this thesis (individual/compounded extremes, compounded droughts) we do not find clear regional

⁸Events of 1 day to 14 days duration, extremes count also drought events longer than 2 weeks.

clusters among these points, which is one of the most puzzling aspects of the results. Occasional coherent patterns appear, at shorter lead times, over France, Germany and UK.

Previous studies highlighted a link between compounded or even individual VRE droughts with large-scale circulation patterns in Europe, like the principal modes of variability and blocking regimes (Wiel et al. 2019a; Mockert et al. 2023). Therefore, assuming there is a relation between the occurrence of VRE droughts and large-scale atmospheric patterns, we expect seasonal forecasting models could perform moderately well. Global climate models knowingly perform better in predicting large-scale circulation patterns rather than small-scale dynamics. In the GCFS model — which features a horizontal resolution of approximately 100 Km — processes at scale lower than the grid resolution are not explicitly resolved, but rather parametrized (Randall et al. n.d.). Nevertheless, the results we present do not support this line of reasoning. A possible explanation is that while compounded VRE droughts are often driven by synoptic circulation regimes, their local manifestation depends on mesoscale processes (Wiel et al. 2019b), specifically cloud cover, the orography and local winds (i.e., sea breeze, mountain and valley breezes). For example, a Scandinavian blocking high may suppress both wind and solar energy across France (Wiel et al. 2019b), but local cloud cover or coastal wind effects could modulate the drought intensity quite differently between Paris and Nantes. The GCFS model may capture the large-scale circulation and its related radiation and wind speed anomalies, but it may fail to resolve the local intensities, leading to scattered skill even if the large-scale atmospheric flow is properly predicted. The fact that the individual SEP and WEP ACC scores are also spatially scattered in Fig. 20 suggests that the compounded signal inherits this fragmentation. Another element contributing to this reasoning comes from the compounded energy droughts persistences distribution in Fig. 15. We find that the GCFS tends to underestimate the frequency of one-day drought events, while overestimating those lasting two days. We believe that this discrepancy may be due to the fact that shorter events are often driven by local, small-scale extreme conditions, whereas longer-lasting events are more likely associated with large-scale atmospheric patterns. When local extreme conditions are not aligned with tendencies driven by the large-scale dynamics, the model probably fails to capture the event, which may explain the discrepancies between the GCFS and the ERA5 density curves in Fig. 15.

We investigate the causes of these occasional alignments by examining the individual indices and the characteristics of the drought events. Following a bottom-up approach (Wiel et al. 2019a), the aim is identifying potential common features among those scattered locations. However, we do not reveal any striking characteristic connecting those locations. As shown in Fig. 21 c, the majority of the points where the correlation is relevant does not have relevant correlation in the in-

dividual energy sources. Consequently, it remains unclear whether these episodic alignments occur randomly or are driven by underlying physical mechanisms.

4.1.1 Assessing the predictability of compounded and individual energy sources

Following the adoption of a bottom-up approach, we shift the analysis to a more granular level to decouple anomalies in solar and wind indices (Fig. 20) and to investigate their individual extremes (Fig. 19). We find that individual solar and wind extreme lows are not spatially correlated; on the other hand, certain regions are predominantly influenced by either the wind or the solar index (Fig. 14). Moreover, dynamical drivers of wind and radiation anomalies may act inversely on the two variables, meaning that a specific weather pattern may be positively correlated to the radiation anomalies, but causing negative wind anomalies. These types of relationships also vary significantly over a large area like Europe (Lledó et al. 2022). For example, in our analysis, in northern France — where VRE sources are relatively well balanced — the NAO index correlates positively with SEP anomalies and negatively with WEP anomalies. Therefore, during a strong positive NAO phase, it is likely that France will experience high positive solar energy potential anomalies and negative wind energy potential anomalies. Only in the regions where the wind anomalies are strong enough, or the cloud cover damps the intense radiation, or both, it is possible that a compounded drought will be recorded. The model must predict the large-scale atmospherical pattern (positive NAO), which would help correctly identifying the sign of the anomalies, but also the intensity must be correctly predicted to correctly represent the intersection of the sources and thus the compounded energy drought. As previously mentioned, the intensity is highly influenced by small-unresolved dynamics.

4.1.2 Role of model biases

First, the errors in the raw radiation (Fig. 11 and 28.B) suggest that the model tends to underestimate *RSDS*. In the MPI-ESM-HR model (used in the GCFS), the cloud water-to-rainwater conversion rate was reduced compared to the lower resolution MPI-ESM (Müller et al. 2018). The reason for that was successfully improving the variance of the Niño 3.4 index in the model. The conversion rate is the parameter representing the rate at which cloud water is converted to rainwater through collision and coalescence processes. A lower conversion rate results in more water being retained within the cloud, which dissipates more slowly or not at all, leading to increased cloud cover, liquid water path and water vapour path (Mauritsen et al. 2012) (Fig. 25). This primarily impacts tropical convec-

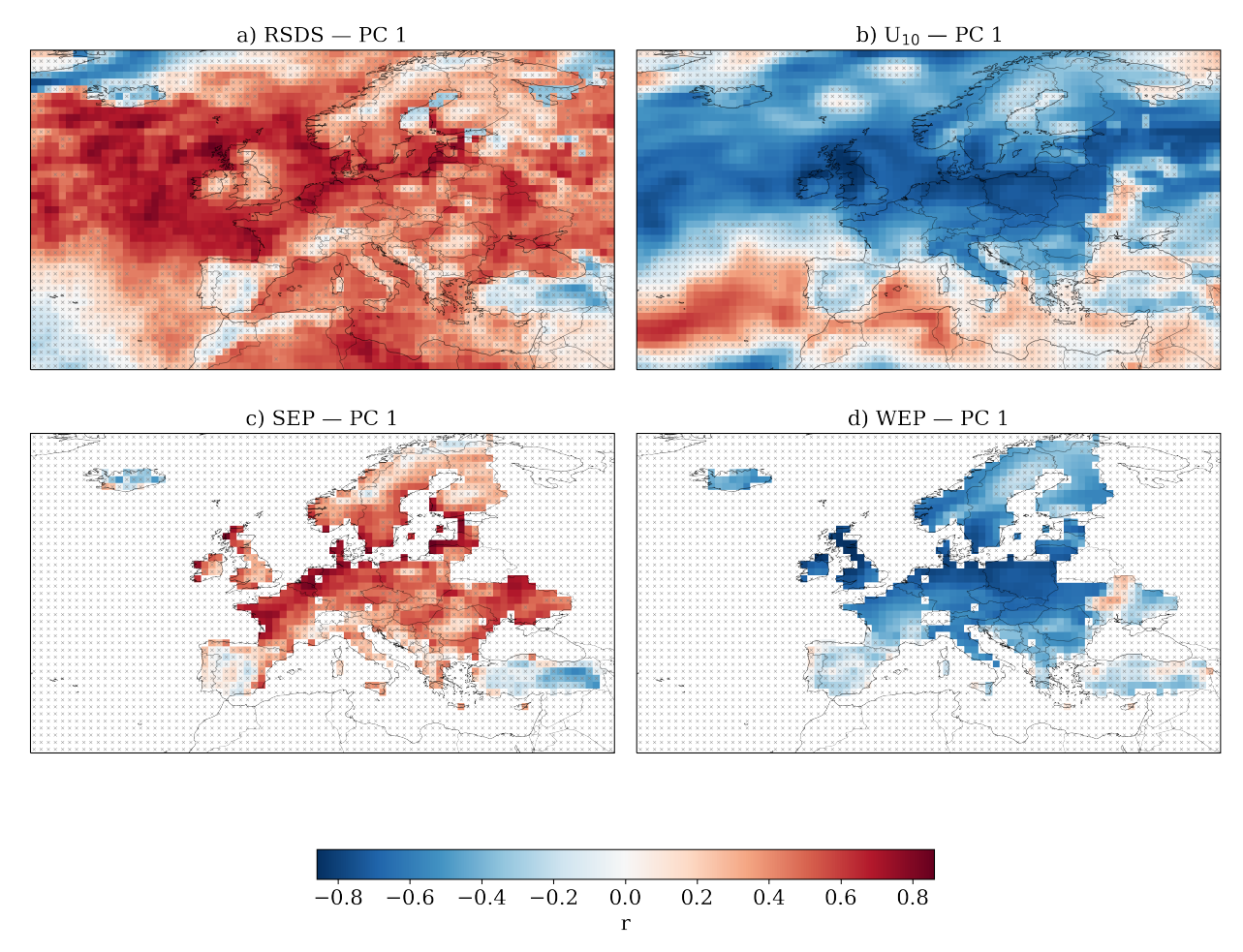


Figure 24: Correlations between the NAO index and ensemble mean anomalies of: a) surface shortwave radiation (RSDS), b) wind at 10 m height (U_{10}), c) SEP and d) WEP. Grey crosses indicate the non-significant coefficients. Only December to February (DJF) mean anomalies are used here. We provide more details of the computation in Appendix \mathbb{C} .

tion systems, since in winter time extratropical and sub-polar regions experience fewer convective clouds. They are instead dominated by stratus clouds, related to weather fronts (Wilcox et al. 2007). Anyway, we believe this parameter increases the persistence of clouds, especially convective systems (more frequent at lower latitudes where the strongest bias is located). This would explain the negative bias in shortwave downward radiation at surface found in this study, since *RSDS* is anti-correlated to the cloud cover and specifically to the cloud water content (Dutton et al. 2006; Stephens et al. 2010).

The distribution of *SEP* values (Fig. 13) differs notably, exhibiting a longer right tail compared to ERA5 values. Given the underestimation of the radiation field, we would expect the SEP index to also be underestimated, with a higher frequency of lower values. We attribute the difference to the operational definition of the index (Eq. 3), specifically the normalisation of *SEP*. To make an

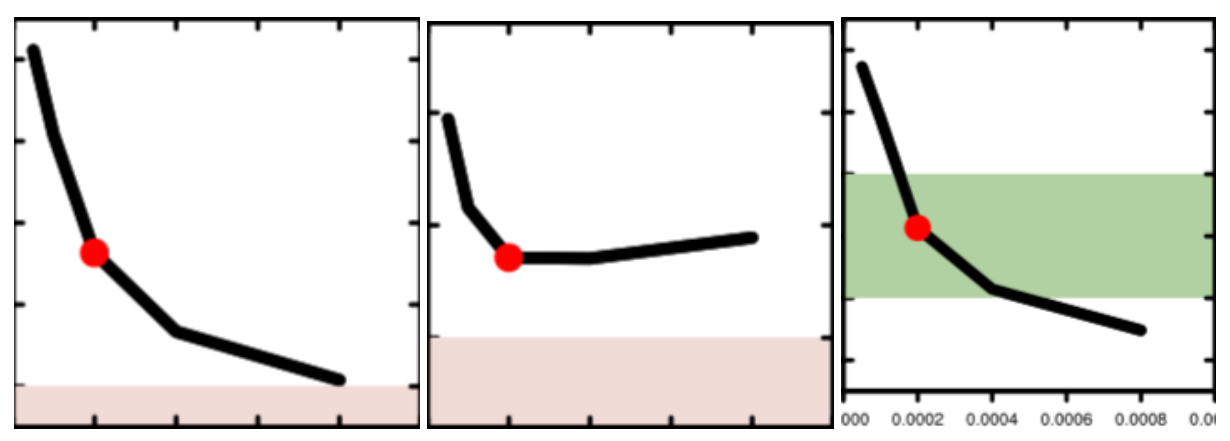


Figure 25: Overview of the influence of the conversion rate tuning parameter on various globally averaged model properties. In order: cloud cover (on the left), liquid water path (in the centre) and water vapour path (on the right) as function of the conversion rate. More details in Mauritsen et al., 2012, Fig. 3 (Mauritsen et al. 2012).

effective comparison, we scale the terms discussed here with respect to the correspondent ERA5 variables. Where the bias is unevenly spread, the *RSDS* ME scales as a factor of -10^{-1} , thus also SEP^* does, while the SEP^* country maxima scales, on average, as a factor of 1. Thus the ratio is greater for the GCFS; in other words, country maximum SEP^* is underestimated more than gridpoint SEP^* .

Considering the biases in the wind speed fields, orography may play a crucial role. The MPI-ESM-HR model did not apply a correction for orographic wave drag, as the winds were already adjusted in the Northern Hemisphere (Müller et al. 2018). Although Fig. 11 still shows slightly greater errors over mountainous regions such as the Alps and western Norway. In addition, the greatest deviations are registered near coastlines and especially over Mediterranean islands (i.e., Cyprus, Corsica, Greek islands). Because it is coarse, the model horizontal grid may not even consider as land the smaller islands, thus the high errors. As mentioned, the magnitude of the errors for U_{100} is almost double the errors for U_{10} . Nevertheless, both positive mean errors scale up to an average factor (over land) of the order of 10 times less the ERA5 U_{10} and U_{100} , since the wind speed at 100 m height is higher than closer to the surface. The WEP index distributions (Fig. 13) show an increment in the range of the values, which is in agreement with the detected bias, differently from the SEP case. The ensemble averaging is the cause of the major differences in shape with respect to ERA5, as highlighted by the difference with the distribution of Fig. 31.B. Conversely, we find that the model underestimates very low extreme values counts for both SEP and WEP. We believe those values represent short-lived droughts, spatially localised, like the 1-day events underestimated in the persistence distribution (Fig. 15).

Overall, for the WEP, and especially for the SEP cases, the final skill is determined by the alignment of local biases. Wherever these biases influence the multiple terms contributing to the index calculation in a way that balances out, those locations may exhibit skill. The spatial heterogeneity suggests that this alignment occurs not in regional clusters, but rather in a more random distribution.

4.1.3 VRE droughts extent and ensemble spread

Based on the preceding discussion, it is evident that accurately predicting VRE droughts depends on the reliable forecasting of a wide range of atmospheric conditions across multiple spatial and temporal scales. Alternatively, it depends on the coincidental cancellation of errors arising from the inaccurate prediction of several contributing variables. For example, highly underestimating *SEP* and moderately overestimating *WEP* would lead to correctly forecasting a drought even if the real-world case is mainly driven by weak *WEP*. Analysis of the extent and ensemble spread of solar, wind and compounded drought (Fig. 16) highlight the importance of highly localised conditions for extreme lows. The ACC scores with respect to the compounded energy drought extents are high and significant, showing that the model performance improves when evaluating metrics aggregated over larger regions. Thus we give particular attention to the ensemble spread of these variables (Fig. 17).

All the previous analysis focus on just the ensemble mean, but extreme events (like VRE droughts) are often driven by outliers in the ensemble distribution (Vavrus et al. 2015). In fact, the ensemble mean often smooths out extremes and also inter-annual variability. Recalling the link to NAO phases, Fröhlich et al. 2021 found a significant NAO prediction skill up to 0.4 for the GCFS 2.0, although raging between 0.1 and 0.62 among members. Looking at the ensemble spread is crucial, although in our case often not even the outliers predict the ERA5 drought extents (Fig.s 13 adn 17). The R^2 metrics (on the ensemble means-ERA5 linear regressions) are moderately high in the scatter plots shown in Fig. 17 for all Europe, Southern and Central Europe. High R^2 means some relation with the ERA5 values is detected in the linear regression, whilst for Northern Europe, where $R^2 \simeq 0.3$, we suppose non-linear discrepancies between ERA5 and model. Nevertheless, it is only in the scatter plot for Northern Europe, that the model ensemble consistently overspread the 1:1 correspondence line, with partially degrading scores at longer lead times. The observation that only the all-Europe extents exhibit a slope close to 1 reflects the influence of the thresholding method used. Specifically, droughts are defined using the 15^{th} percentile calculated over the entire domain. This approach was called *balancing effect* by Kittel et al. 2025, which differs from apply-

ing thresholds at the country level (called *portfolio effect*) or at individual grid points. The model ensemble overestimates the monthly mean extents only for the Northern Europe region, while it underestimates the extents in both of the other regions. Hence, we believe the model exaggerates the compounded extremes in very specific regions. As a consequence the threshold selects those extremes which result to be much more frequent in those specific regions, while in ERA5 the extremes are more homogeneously spread across Europe. We locate those regions in Scandinavia where, very likely because of the *SEP* (see Fig. 34.B), the model overestimates the extent of the droughts (Fig. 17 *b*), while it underestimates the extent of the droughts elsewhere (Fig. 17 *c* and *d*). Only over the all domain, within which the threshold is picked, the extent of the droughts is correctly simulated, aside from a clear bias.

An analysis focused on specific ensemble members could have helped in this case just over the region of Northern Europe. It is to be pointed out that working with ensemble means also lowers the inter-annual variability. Although in our case, as depicted in Fig. 17 for all, Central and Southern Europe, when the ensemble mean deviates consistently from ERA5 values, the majority of times, not even one member correctly predicts the extent. The only exception is seen for the months of February and especially March, notably during which the ERA5 data shows very little inter-annual variability (around 5% at maximum).

In conclusion, the model's performance improves when evaluating aggregated metrics over larger regions, as evidenced by high and significant ACC for compounded droughts. The skill highlighted here is not affected by the ensemble-mean smoothing-effect, in fact, even outliers often fail to predict the observed drought extents in ERA5. However, the NAO prediction skill in the GCFS ensemble ranges among members, with few scoring up to \sim 0.7. A more targeted analysis of individual ensemble members (i.e., ensemble subsampling) could provide further insights, improving NAO correlation. At the contrary, members-selection-methods would unlikely improve the drought extent inter-annual variability. This result is aligned with Bett et al. 2022, where they suggested the number of extreme events per season was unlikely linearly related to a climate driver.

In summary, the results obtained in this thesis can be explained by limitations in both the model and the study's methodology. They interact to account for the differences observed between the GCFS and ERA5 raw variables, the distribution of indices, and, ultimately, drought frequency and extent.

Starting with the first, a seasonal forecasting model like the GCFS provides daily quantities by aggregating hourly data. Solar energy production generally follows the same curve as radiation

intensity, showing a relatively regular increase in the morning and decrease later in the day. While wind energy features much greater daily variability. This is due not only to the inherent variability of wind itself but also to technical factors such as wind turbine cut-in and cut-off speeds (Wiel et al. 2019a). Studies are available on this subject (Lopez-Villalobos et al. 2022), but for the purposes of this investigation and considering the reliability of seasonal forecasts on such detailed time sampling, dealing with daily values is reasonable. Of course, a more detailed and rigorous daily analysis could be performed when analysing VRE droughts prediction skill of weather forecasts, focusing on shorter time ranges, but this goes beyond the scope of this thesis.

In addition to temporal resolution, spatial resolution is a key factor influencing the model's performance. Resolution was found critical for climate extreme detection (Brunner et al. 2025). Firstly, it influences the orography representation and thus the local, small-scale atmospherical circulations, like, for example, wind breezes. The GCFS model already implements a wind adjustment which was revealed to be beneficial in decreasing the surface wind velocities bias with respect to the MPI-ESM-LR model (Müller et al. 2018). On the contrary, higher spatial resolution did not show relevant improvements in the NAO predictability skill (Müller et al. 2018). As discussed, compounded VRE droughts were often found to be linked with large-scale circulation modes and blocking regimes (Wiel et al. 2019a; Wiel et al. 2019b; Jerez et al. 2013b; Lledó et al. 2022; Drücke et al. 2021; Mockert et al. 2023). The NAO is the most relevant of these patterns, showing a strong correlation with both wind speed and solar radiation. However, its predictive skill varies significantly among ensemble members, (Fröhlich et al. 2021). To make a comparison, the SEAS5 model (ECMWF's fifth generation seasonal forecast system), with a much higher grid point resolution of 36 Km, scores similarly between 0.12 and 0.67 for the NAO index correlation (Johnson et al. 2019). Instead, Scaife et al. 2014 found that NAO prediction skill rises slowly with the ensemble size in seasonal forecasting models. Specifically, around 50 members were considered ideal to capture the majority of the variability. In our case, the GCFS hindcasts run an ensemble size of only 30 members, while forecasts run with indeed 50 members. Despite some members had proven to reach high correlation coefficients (>0.5), the lower the ensemble size the lower the number of members with high skill. The ensemble mean smooth out those reliable results with less performative members and the final, averaged skill is worsened. Apart from NAO, also other regimes like the Scandinavian blocking and the East-Atlantic/Western Russia were related to the occurrence of compounded energy droughts (Wiel et al. 2019a; Mockert et al. 2023). Fröhlich et al. 2021 found a slight improvement from previous versions of the GCFS in the predictability of European blocking regimes for northern and western events, but not for south-eastern and central events. Differently

from the NAO variability, European blocking regimes predictability benefits from higher resolution (\sim 40 Km) (Jung et al. 2012).

The discrepancy between ensemble mean outputs and individual members. The ensemble averaging is a disadvantage also for the already weak inter-annual variability reproduced by some of the members, see Fig. 17. Given that few members are expected to show good correlation with the NAO index (Fröhlich et al. 2021; Scaife et al. 2014), the model flaws in forecasting larger interannual variability may be a result of the skill for the NAO index, rounded down in the ensemble mean. The winter NAO, when correctly predicted, showed low signal-to-noise ratio of the predictable signal, making it valuable for predictions of regional winter extremes (Scaife et al. 2014; Chiacchio et al. 2010; Zubiate et al. 2017). Despite the downsides linked to the ensemble mean and the evidence that revealed ensemble outliers to be crucial for extreme events detection (Vavrus et al. 2015); we show that the ensemble members in the first and fourth quartiles not always score close to the ERA5 reference (Fig. 17). Therefore, conducting an analysis on selected ensemble members could help identify common features that contribute to the skill in predicting compounded VRE droughts. However, such an analysis would still be affected by biases and non-linear discrepancies when compared to the ERA5 dataset.

A lack of bias correction is an apparent limitation to this study. The initial errors translate non-linearly to the indices and thus to the drought detection, which is moderately evident in the *RSDS* and subsequent *SEP* errors. The high ACC values for macro-regional extents, Tab. 1, highlight a strong potential, at least for aggregated variables, in detecting the anomalous extent of compounded VRE droughts. Thus, we believe that the biases do not significantly affect variability at larger spatial scales, but may influence the accuracy of small-scale localization. Therefore, we recommend that future studies implement a bias correction step before proceeding with the analysis.

A notable limitation of this study is the lack of a sensitivity test for the chosen 15^{th} percentile threshold. While the percentile-based approach ensures a consistent definition of extreme events across regions and time periods, the arbitrary selection of the 15^{th} percentile may influence the detected drought frequencies and spatial patterns. Previous work by Cannon (Cannon et al. 2015) demonstrated that wind energy extremes are highly sensitive to threshold selection, with skill varying non-linearly across regions. Given the added complexity of compounded solar-wind droughts, such sensitivity is likely amplified in our study. A systematic assessment of how different thresholds affect the frequency, extent and predictability of VRE droughts would strengthen the robustness of the results. This analysis is left for future research but we recognise it as a critical step to ensure the findings are not an artifact of the threshold choice.

Also related to the threshold, another limitation concern the selection method: the percentile of the all domain distribution. We suppose the GCFS selected 15% compounded extremes are denser in Northern Europe. We attribute this to model biases that lead to discontinuous GCFS-ERA5 differences in the droughts spatial distribution. Fig. 17 suggests that, when aggregating over all Europe, the peculiarities due to biases, noise and resulting percentile selection (which are likely spatially patchy) balance each other out, showing an encouraging results in the ACC scores (Tab. 1) and scatter plot with respect to ERA5 (Fig. 17). An alternative threshold selection method illustrated by Kittel et al. 2025 (portfolio effect), not explored in this study, may hold the benefits of cancelling out peaks of regional extremes that compromise the all droughts detection in the second case. Nevertheless, we find biases and non-linear departures from ERA5 are to be ascribed to mean state discrepancies and local specificities. In fact, day by day extent anomalies over large areas show moderately high skill (Tab. 1).

Despite the described limitations in the indices definitions and following droughts selection, we acknowledge that the index validated two cases cited in literature (i.e., Belgium and Germany, January 2017). This confirms that the definition based on compounded solar and wind energy potential can capture real low-production situations. One of the greatest advantages of the index we introduced is the combination of the two sources; the compounded index incorporated the individual sources energy potential allowing the definition of a unique threshold to define the compounded energy drought. Conversely, in literature, often two thresholds were used to identify individual sources energy droughts and then their coexistence analysed, a method not recommended in Kittel et al. 2025.

Chapter 5

Conclusions

In this thesis we have assessed the seasonal predictability of compounded variable renewable energy (VRE) droughts in Europe using the German Climate Forecast System (GCFS) version 2.2. The transition to renewable energy sources, specifically solar and wind, makes predicting periods of VRE availability critical. Reliable seasonal forecasts of VRE droughts, given their financial and societal impacts (Denholm et al. 2011), are pivotal to ensure grid stability and inform energy policy. Our findings reveal a complex picture: while predicting local drought occurrence remains challenging, the GCFS demonstrates significant and valuable skill in forecasting the large-scale spatial extent of these events.

5.1 Summary of methodology and key findings

To bridge a gap in the literature, we develop novel, generalizable indices for solar (SEP), wind (WEP) and compounded (CEP) energy production (Chapter 2). Unlike approaches reliant on specific turbines or PV models, these indices weight surface solar radiation and wind speed (all information that can be easily provided by forecasting systems) by national energy capacities. VRE droughts are defined using a threshold-based approach, with the 15^{th} percentile of the CEP distribution identifying extreme lows in energy production. Our method is applicable across diverse regions and energy systems. This offers a scalable framework for seasonal forecasting that is both meteorologically grounded and relevant to the energy sector.

The core finding (Chapter 3) is the GCFS significant prediction skill for the spatial extent of droughts when aggregated over macro-regions. The model achieves high and statistically significant ACC values for daily drought extents in Central Europe (0.59) and Southern Europe (0.65) (Tab. 1). We find limited skill in predicting the inter-annual variability of VRE drought frequency. ACC for local monthly occurrences are generally spatially heterogeneous (Fig. 18). Few regions — such as Scandinavia for solar droughts, southern France or Spain for wind droughts and northern France and Germany for compounded droughts — show significant positive correlations clusters (Fig. 19). This spatial heterogeneity aligns with findings from Bett et al. 2022, who observed

spatially scattered skill in seasonal forecasts of seasonal-mean wind speed and solar irradiance in Europe.

Interestingly, we found that the predictability of compounded droughts is not a simple function of the predictability of its individual solar or wind components (Fig. 21). This non-additive behaviour suggests that compounded droughts arise from complex, non-linear interactions between large-scale meteorological drivers (i.e., NAO and blocking regimes) and small-scale wind breezes and overcast conditions (driven by orography and coastal effects) (Wiel et al. 2019a; Mockert et al. 2023). Furthermore, we ascribe this complexity to the challenging role of major teleconnection patterns, primarily the NAO (Wiel et al. 2019a; Lledó et al. 2022). The influence of the NAO on compounded VRE availability is not straightforward; its correlation varies significantly in sign and intensity across European regions and between solar and wind resources (Fig. 24). This explains why the predictability of a compounded drought does not clearly align with that of its individual parts, which often exhibit complementary behaviours (Kaspar et al. 2019). For the GCFS to correctly predict a drought, it requires a precise alignment between a accurately forecasted large-scale circulation pattern and the resulting local weather conditions. The spatially scattered nature of the model's skill suggests that this alignment is not tied to consistent regional sources of predictability but occurs rather randomly.

5.2 Contribution to the seasonal predictability of VRE droughts

A primary contribution of this work is the development and validation of the compounded energy production index. This index provides a measure of energy system stress by integrating both solar and wind potential into a single metric. Its validation against documented drought events in Belgium and Germany in January 2017 confirms its ability to capture real-world VRE low-production situations (Sec. 3.4).

The spatial heterogeneity in prediction skill is itself an important finding. It reflects the inherent complexity of compounded VRE droughts, which are influenced by a combination of large-scale circulation patterns and local mesoscale processes. The GCFS, with its $\sim 100~Km$ horizontal resolution, is able to simulate the large-scale dynamics (Fröhlich et al. 2021) that create widespread drought conditions, as evidenced by the high skill in extent forecasting. However, it does not resolve the finer-scale processes that determine the precise location and intensity of droughts, leading to the scattered grid-point skill. Nevertheless, a key implication of our research is the demonstrated feasibility of using seasonal forecasting systems, like the GCFS, for predicting VRE drought extents at coarser scales. This skill, while limited locally, is precisely what is needed to satisfy the require-

ments of strategic energy planning and large-scale grid management, especially for coordinating resources across interconnected national systems.

5.3 Limitations and future research outlook

This study is sensitive to certain methodological choices, which also point toward potential avenues for future research and improvements. The use of a fixed 15^{th} percentile threshold, while statistically consistent, may influence the detected drought spatial patterns. Future work should include a sensitivity analysis across different thresholds (i.e., 10^{th} , 20^{th} percentiles). They should also implement a bias-correction step to mitigate model systematic errors, which likely contribute to regional imbalances in drought extent estimation (Northern Europe Fig. 17).

The established link between VRE availability and large-scale teleconnection patterns, coupled with the model's variable skill in predicting them (Fröhlich et al. 2021 assessed GCFS NAO prediction skill ~0.40), suggests several strategies to enhance forecasts. Firstly, statistical or machine learning models could leverage bridging methods to enhance forecast skill. Tools more advanced than linear or multi-linear regressors could use teleconnection indices as predictors and better capture non-linear interactions (Bett et al. 2022; Lledó et al. 2022). Secondly, rather than relying on the ensemble mean, which smooths out extremes, selecting members that best represent key teleconnection patterns could extract more skillful predictions from the existing ensemble. This method, referred to as ensemble subsampling (Dobrynin et al. 2018; Dobrynin et al. 2022), was employed in literature, specifically for climate extreme detection (Paolini et al. 2025), so it represents a promising application in this case, too. Thirdly, employing high-resolution models, such as Regional Climate Models (RCMs), can better resolve mesoscale processes (Müller et al. 2018). RCMs could test the hypothesis that while large-scale patterns modulate the occurrence of drought-prone conditions, mesoscale processes control their local intensity and precise manifestation.

In conclusion, we demonstrated that while the direct prediction of local VRE drought frequency using the GCFS remains a challenge, the model shows promising and operationally valuable skill in forecasting the large-scale spatial extent of compounded droughts. This capability to provide advance warning of widespread *Dunkelflaute* (dark-and-dull) conditions is crucial for energy system operators, enabling optimized deployment of backup generation and storage. By leveraging generalized meteorological metrics, we have provided a foundational and scalable framework for the seasonal forecasting of compounded VRE droughts. We advised future improvements should

consider bias correction, threshold sensitivity test, bridging methods, ensemble subsampling and higher-resolution modelling. As Europe's energy transition accelerates, such predictions will be indispensable for building a resilient and reliable renewable-powered grid.

Appendix A

Data and methodology

In this appendix, we provide detailed technical specifications and supplementary analyses to support the data and methodology described in Chapter 2. The focus is on two key aspects: the GCFS configuration and VRE droughts persistence bound.

German Climate Forecast System (GCFS) 2.2: Appendix A.1 outlines the model configuration, including its coupled components, resolution, initialization and boundary conditions. These details are essential for understanding the GCFS's capabilities and limitations in simulating the meteorological fields used to derive the solar (SEP), wind (WEP) and compounded (CEP) energy production indices.

VRE Droughts persistence bound: Appendix A.2 addresses the treatment of extremely long drought events (lasting over 14 days). These events, while rare, are excluded from the main analysis to focus on short-to-medium duration droughts (1–14 days), which are more operationally relevant for energy system planning.

Together, these sections provide the technical foundation for the data processing and methodological choices that underpin our results.

A.1 German Climate Forecast System 2.2

Tab. 2.A summarizes the key technical specifications of the German Climate Forecast System (GCFS) version 2.2, including its coupled model components, resolution, initialization data and boundary conditions. The GCFS is based on the MPI-ESM-HR model and provides hindcasts we employ for the historical period 1990–2024. The system's configuration influences its ability to resolve large-scale climate patterns while parametrizing smaller-scale processes. These details are critical for interpreting the model's performance in predicting variable renewable energy (VRE) droughts, particularly in regions where local dynamics (i.e., orography or coastal effects) play a significant role.

Model	Coupled model: ECHAM 6.3.05 (atmosphere), JSBACH 3.20p1 (land), MPIOM 1.6.3 (ocean)
Coupling frequency	1 hour
Horizontal resolution and grid	T127 (\sim 100 Km) on regular Gaussian grid
Atmosphere hindcast initialisation	ERA5
Ocean hindcast initialisation	Ensemble Kalman Filter, adapted to MPIOM for 3D Temperature and Salinity using EN4 data
Sea-ice hindcast initialisation	Ensemble Kalman Filter using OSISAF
Land hindcast initialisation	Indirect via atmosphere initialisation
Hindcast ensemble size	30
Hindcast set	Static
Boundary conditions	Ozone, vulcanic aerosol and greenhouse gases forcings are provided by CMIP6.
	Tropospheric aerosols by MACv2.

Table 2.A: GCFS specifics (Penabad 2025).

A.2 VRE droughts persistence bound

The spatial distribution of compounded VRE droughts lasting longer than 14 days, Figure 26.A, which were excluded from the main analysis. Such prolonged events are rare and often climatologically justified (i.e., persistent low solar radiation in Scandinavia during winter). Masking these events ensures the study focuses on short-to-medium duration droughts (1–14 days), which are more relevant for operational energy system planning. The map highlights regions where long-lasting droughts occur.

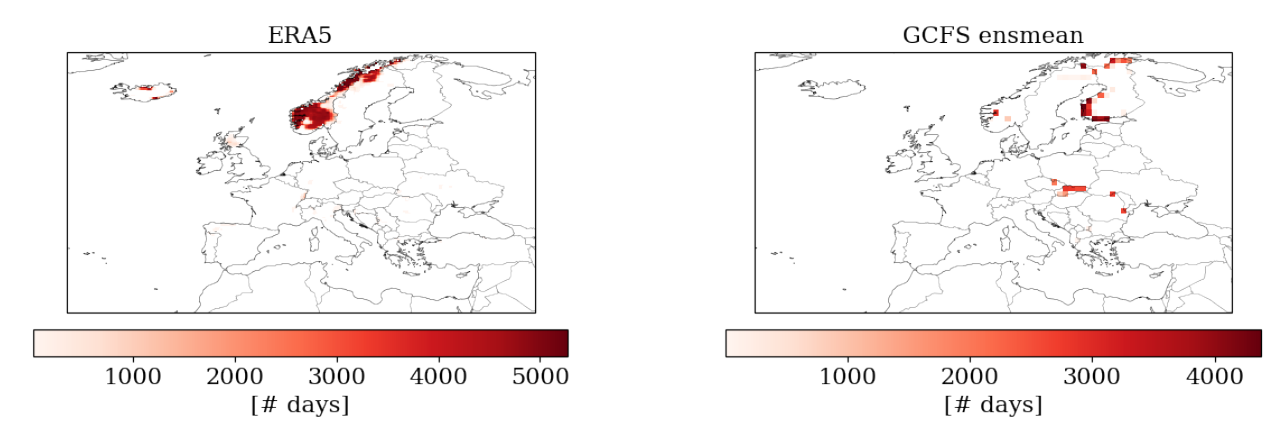


Figure 26.A: Count of the compounded VRE droughts with extremely long persistence (over 14 days long) which are masked out in our analysis of droughts occurrences. ERA5 (left) and GCFS ensemble mean (right).

Appendix B

Results

This Appendix complements Chapter 3 by presenting additional results and diagnostics that deepen the understanding of the GCFS's performance in predicting VRE droughts. The appendix is organized into four sections.

Primary Field Biases (B.1): this section examines the error metrics (RMSE and ME) for the primary meteorological fields—surface shortwave radiation and wind speed at $10\ m$ and $100\ m$ heights. We distinguish between errors in the raw fields and their anomalies, revealing whether discrepancies arise from systematic biases or inter-annual variability. These diagnostics are critical for interpreting the model's skill in simulating the physical drivers of VRE droughts.

Droughts Characterisation (B.2): the spatial and temporal characteristics of VRE droughts, including the dominance of solar versus wind energy during drought events, are further explored. The maps and figures illustrate how the GCFS reproduces or deviates from observed patterns in the ERA5 reanalysis.

VRE Drought Predictability (B.3): detailed spatial maps and tables of ACC for the frequency of VRE droughts and individual solar and wind extremes are provided. These results highlight the spatial heterogeneity of the model's skill, with pockets of significant predictability among broader areas of low correlation. We underscore the challenges of forecasting compounded events, which depend on complex interactions between solar and wind drivers as explained in Chapter 4.

Validation (B.4): the last section validates the *CEP* index against documented drought events in Belgium and Germany (January 2017). Linear regression diagnostics and spatial maps demonstrate the index's ability to detect these events, albeit with some smoothing of local extremes. This validation reinforces the robustness of the index for regional-scale applications while acknowledging limitations in resolving fine-scale variability.

Overall, Appendix B provides comprehensive supporting evidence for the findings discussed in Chapter 3, offering deeper insights into the model's strengths, weaknesses and the physical dynamics underlying VRE drought predictability.

B.1 Primary field biases

Maps in Fig.s 27.B to 30.B display the error metrics of: surface shortwave downward radiation, 10 m wind speed and 100 m wind speed, calculated over extended winters (NDJFM) from 1990/91 to 2023/24. Comparing the total signal RMSE in Fig. 11 and the anomalies RMSE in Fig. 27.B, for example, reveals whether errors arise from mean state biases or inter-annual variability. The spatial patterns are nearly identical, indicating that most model errors stem from variability rather than systematic offsets. Notably, wind speed errors are amplified at 100 m due to extrapolation, but no new biases are introduced. The model underestimates solar radiation (negative bias in Fig.

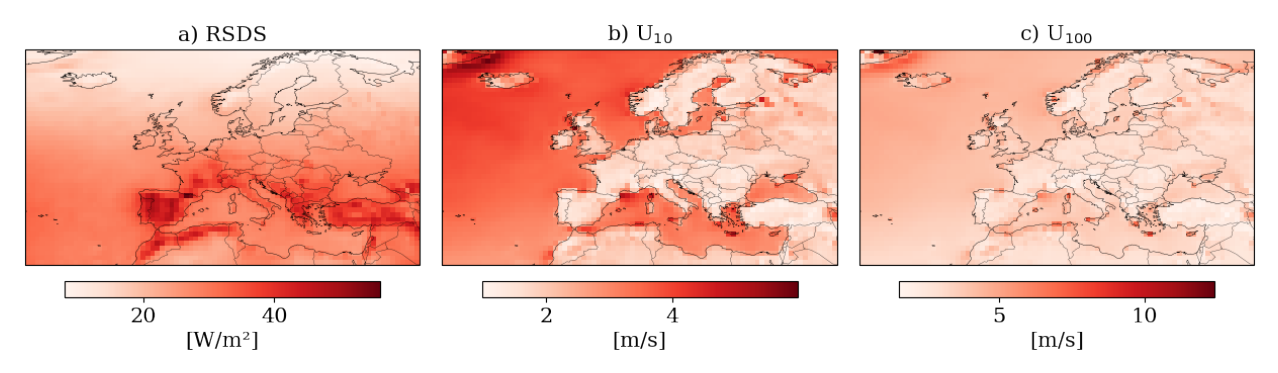


Figure 27.B: Root mean square error for the field anomalies of a) the shortwave downward radiation at surface, b) the wind speed at $10 \ m$ height and c) the wind speed at $100 \ m$ height. The RMSE is computed only for the extended winters (NDJFM) 1990/91 to 2023/24; the GCFS model data is averaged on the ensemble.

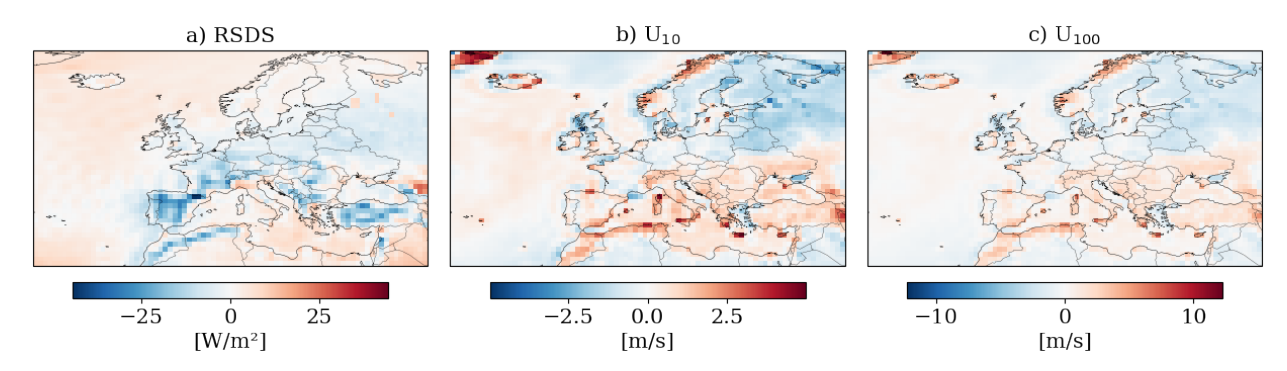


Figure 28.B: Mean error for a) the shortwave downward radiation at surface anomalies, b) the wind speed at $10 \ m$ height anomalies and c) the wind speed at $100 \ m$ height anomalies. The ME is computed only for the extended winters (NDJFM) 1990/91 to 2023/24; the GCFS model data is averaged on the ensemble.

28.B) across most of Europe, likely due to overestimated cloud cover, while overestimating wind speeds, particularly along coastal and mountainous regions.

The ME for anomalies (rather than raw fields) isolates biases in the model's inter-annual variability. The patterns closely resemble those in Fig. 27.B, confirming that errors in anomalies are consistent with errors in the mean state. These biases propagate into the energy production indices (SEP, WEP, CEP) but are mitigated or enhanced by the climatological weighting in the index definitions. The comparison between ensemble mean and ERA5 distribution of all days, all grid points, indices is instead illustrated by Fig. 31.B. These biases suggest that the GCFS struggles to capture both the magnitude and temporal evolution of key meteorological drivers for VRE droughts and that translates into VRE indices, too.

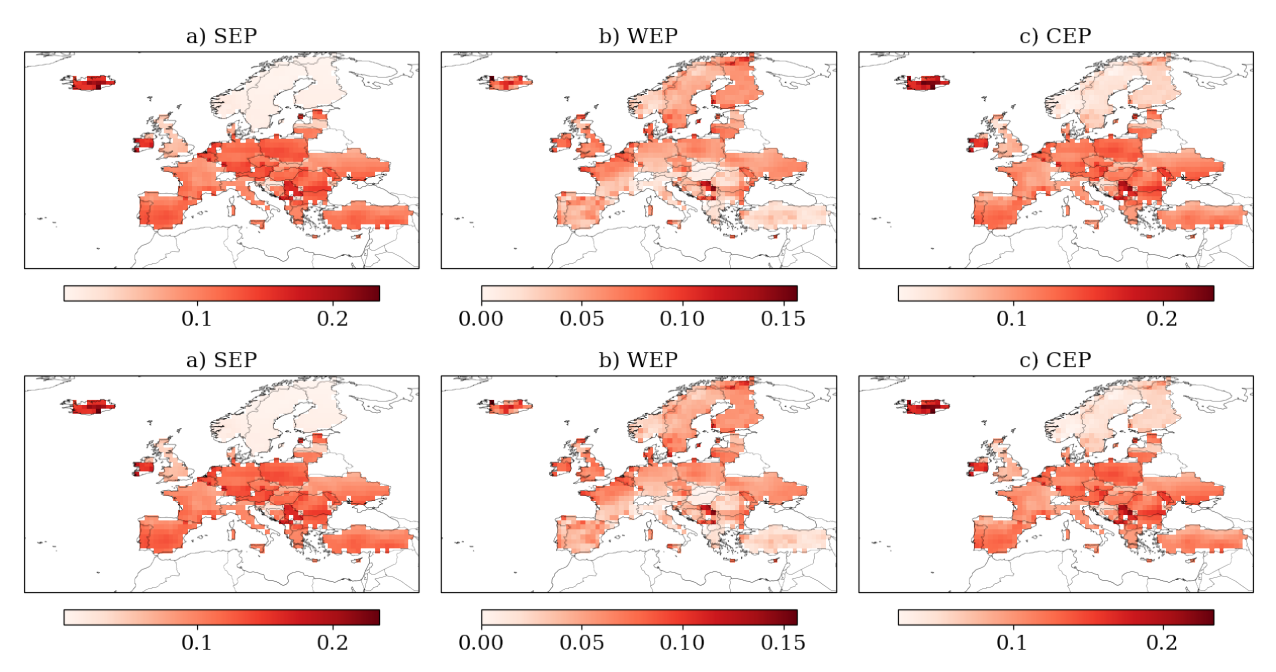


Figure 29.B: Root mean square error for energy production indices (above) and their anomalies (below). The RMSE is computed only for the extended winters (NDJFM) 1990/91 to 2023/24; the GCFS model data is averaged on the ensemble.

B.2 VRE droughts characterisation

Fig. 32.B mirrors Fig. 14 but uses the GCFS ensemble mean to show which energy source (solar or wind) dominates during compounded droughts. The meridional gradient—wind dominance in the north, solar in the south—is reproduced, though the model's biases (i.e., overestimated WEP in Scandinavia) may exaggerate certain patterns. The similarity to ERA5 (Fig. 16) validates the model's ability to capture broad spatial trends, if not exact magnitudes. Tab. 3.B quantifies the relationship between ERA5 reanalysis and GCFS ensemble mean for drought extent across Europe. The high R^2 values (\sim 0.8) for all Europe, Central and Southern Europe indicate strong agreement

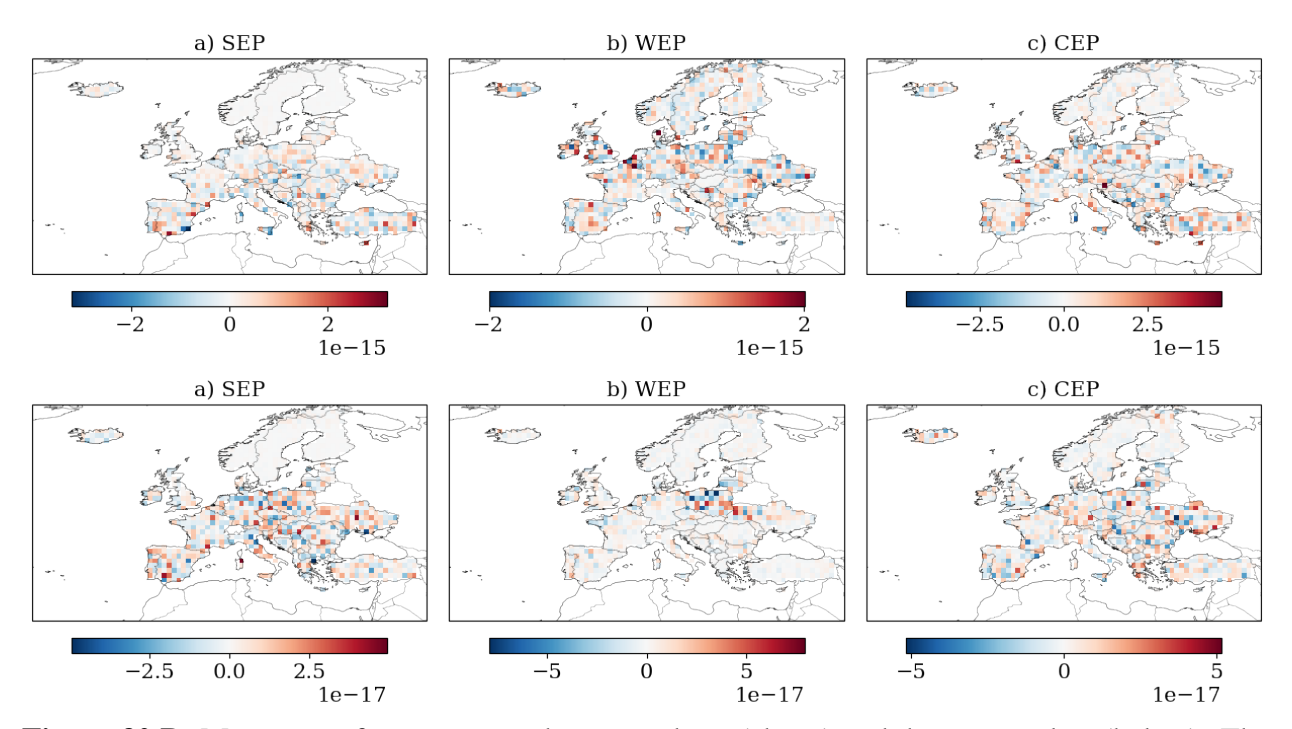


Figure 30.B: Mean error for energy production indices (above) and their anomalies (below). The RMSE is computed only for the extended winters (NDJFM) 1990/91 to 2023/24; the GCFS model data is averaged on the ensemble.

	EU	NEU	CEU	SEU
p-value	2.36e-62	6.57e-14	8.95e-64	1.71e-63
Standard error	0.035	0.028	0.006	0.010

Table 3.B: Linear regression diagnostics between ERA5 reanalysis (x) and the GCM ensemble mean (y) across: all Europe (EU), Northern (NEU), Central (CEU) and Southern (SEU) Europe, on the columns. Include the p-value, statistical significance, (first row) and standard error of the slope (second row).

at aggregated scales. The slope and intercept metrics reveal systematic biases, such as the model's tendency to overestimate drought extent in the north. The p-values confirm the robustness of these results.

B.3 VRE droughts prediction skill

Tab. 4.B provides ACC scores for the monthly and winter (NDJFM) counts of compounded VRE droughts and solar, wind and compounded extremes. *CEP* extremes differ from compounded drought because of the duration filter applied in the definition of drought: events longer than 2 weeks are not considered in the drought count, but they are in the extremes count. The lack of

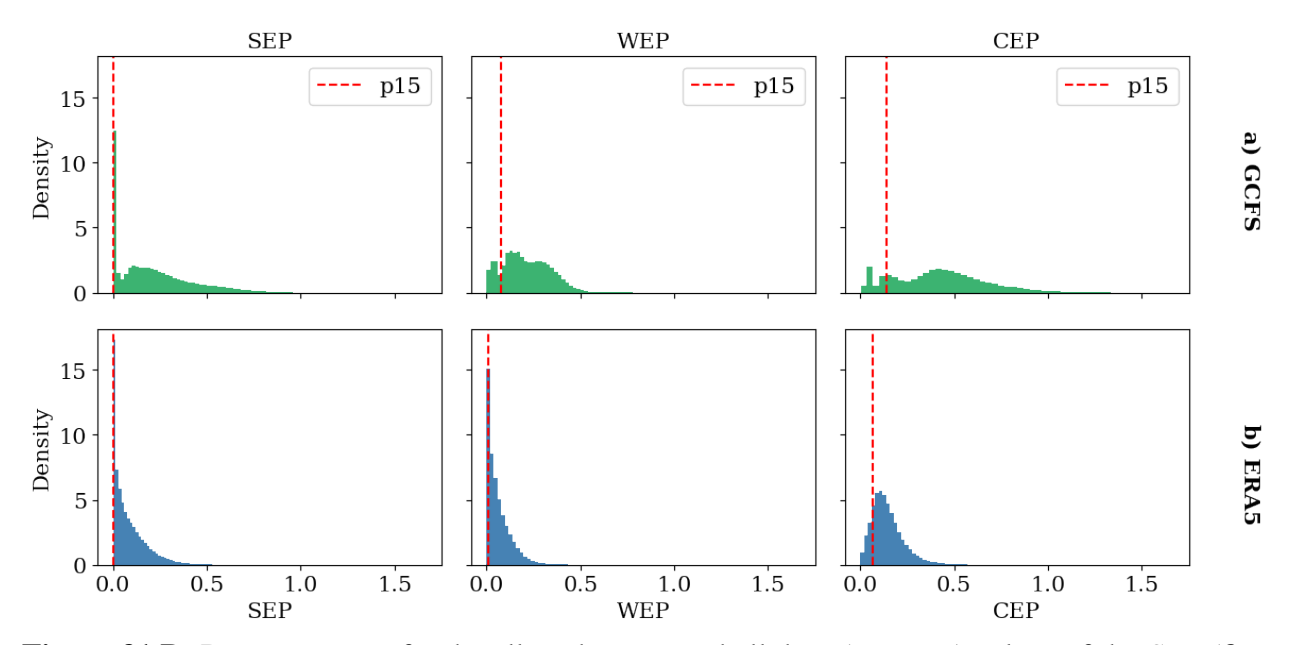


Figure 31.B: Density curves for the all grid points and all days (not zero) values of the *SEP* (first column), *WEP* (second column) and *CEP* (third column) indices. Values for a) GCFS ensemble mean and b) ERA5.

statistically significant values (p-value >0.05) underscores the model's limited skill in predicting inter-annual variability at the grid scale. However, the occasional significant correlation (underlined) hint at localized predictability, explored further in the spatial maps (Fig.s 34.B, 33.B). The following maps show the full ACC signal (including non-significant and negative values) for compounded VRE drought frequencies (Fig. 33.B). While most of Europe exhibits low or insignificant correlations, pockets of positive skill are found. The spatial heterogeneity reflects the model's struggle to resolve local-scale processes. Similarly, Fig. 34.B extends the analysis to individual solar (SEP), wind (WEP) and compounded (CEP) extremes. The scattered significant correlations suggest that prediction skill is not uniformly tied to either solar or wind drivers but depends on complex interactions between the two. The lack of coherent regional clusters emphasizes the challenge of forecasting compounded events.

Lastly, adding to Fig. 20, we illustrate the full signal of the ACC maps for the SEP and WEP monthly mean anomalies during drought days.

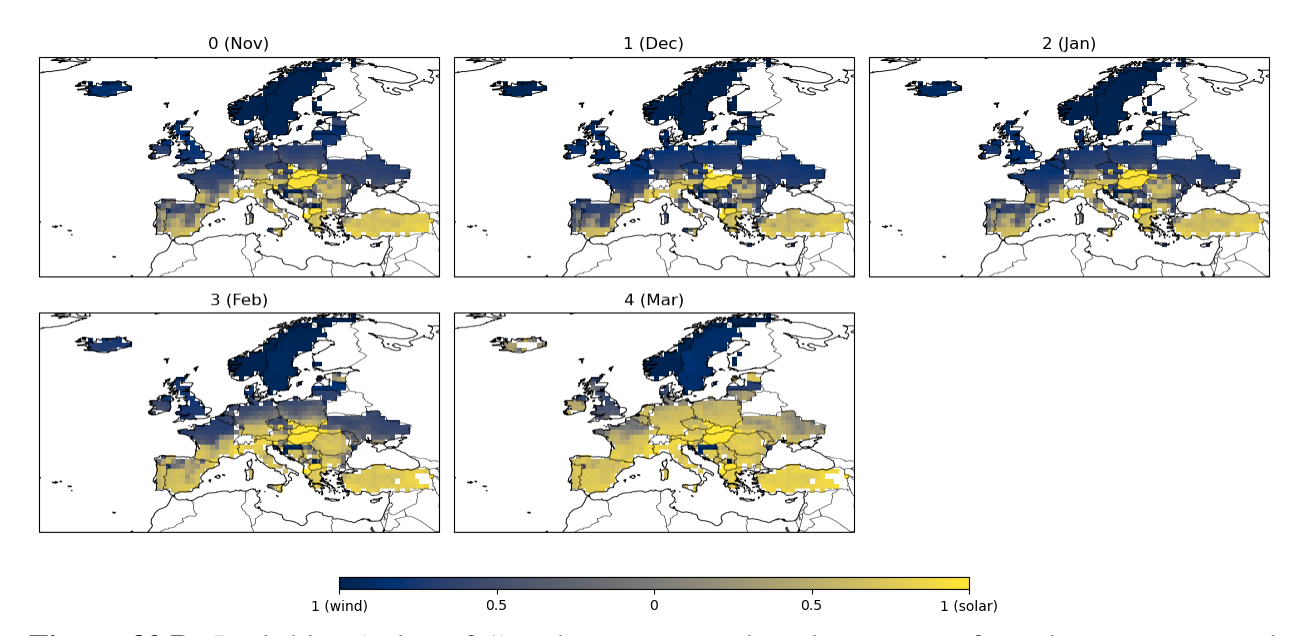


Figure 32.B: Dark blue (value of 1) indicates a complete dominance of wind energy potential (*WEP*), while bright yellow (value of 1) signifies a complete dominance of solar energy potential (*SEP*). Intermediate colours (i.e., grey) represent varying degrees of contribution from both sources. Each subplot refers to a different lead time (in months). Values computed from the GCFS ensemble mean.

	0 month lead	1 month lead	2 month lead	3 month lead	4 month lead	wintry count
comp. drought	0.038	0.027	-0.012	0.018	0.010	0.057
SEP	0.053	0.085	0.009	0.228	0.049	0.142
WEP	-0.026	-0.013	-0.028	0.133	0.019	0.063
СЕР	0.047	-0.002	-0.012	0.128	0.065	0.107

Table 4.B: Anomalies correlation coefficients computed along all dimensions (time, longitude, latitude) for the monthly count and total NDJFM count of compounded energy drought days (first row) and of days in which the index falls below the 15^{th} percentile threshold (second to fourth row). The coefficients that score a p-value <0.05 are underlined.

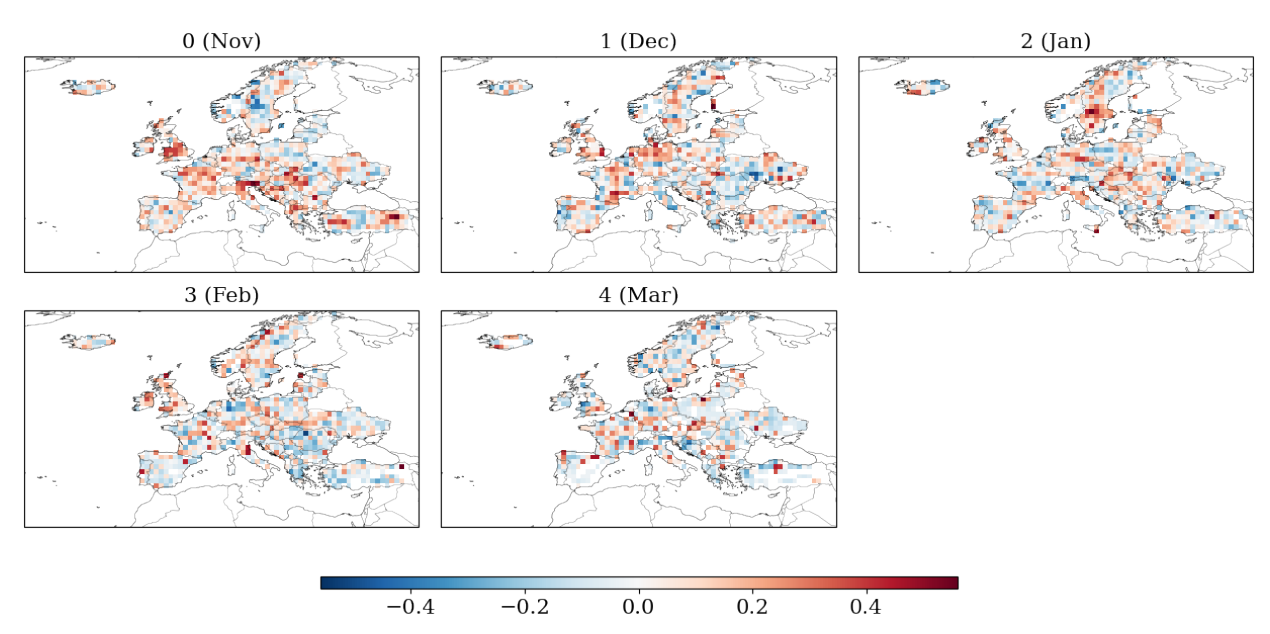


Figure 33.B: ACC for the monthly count of drought days. Each subplot refers to a lead time (in months). Computed on the GCFS ensemble mean and ERA5 (NDJFM 1990/91-2023/24).

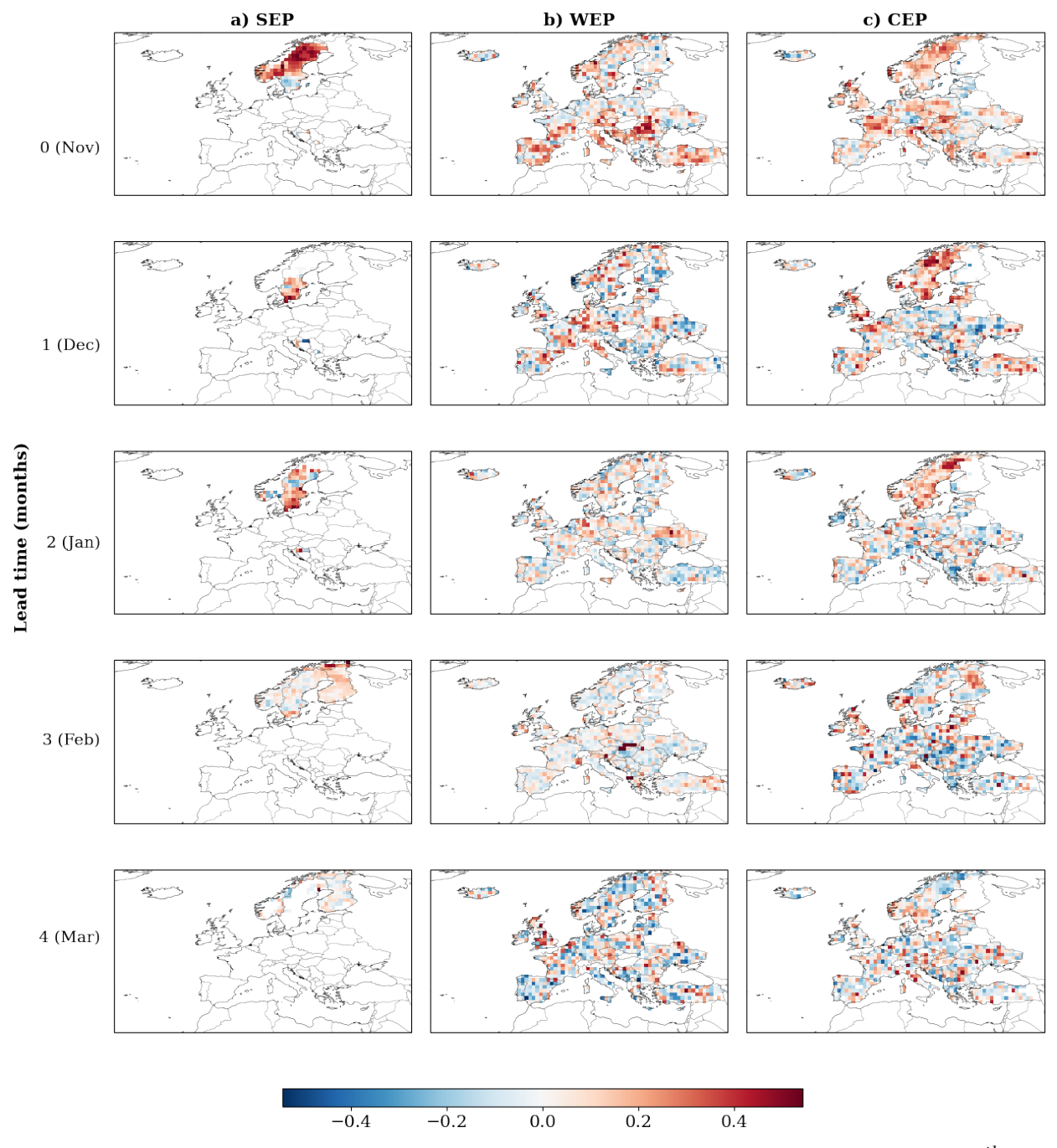


Figure 34.B: Anomalies correlation coefficients for the monthly count of days below the 15^{th} percentile threshold for the a) SEP index, b) WEP index and c) CEP index. Computed on the GCFS ensemble mean and ERA5 (NDJFM 1990/91-2023/24).

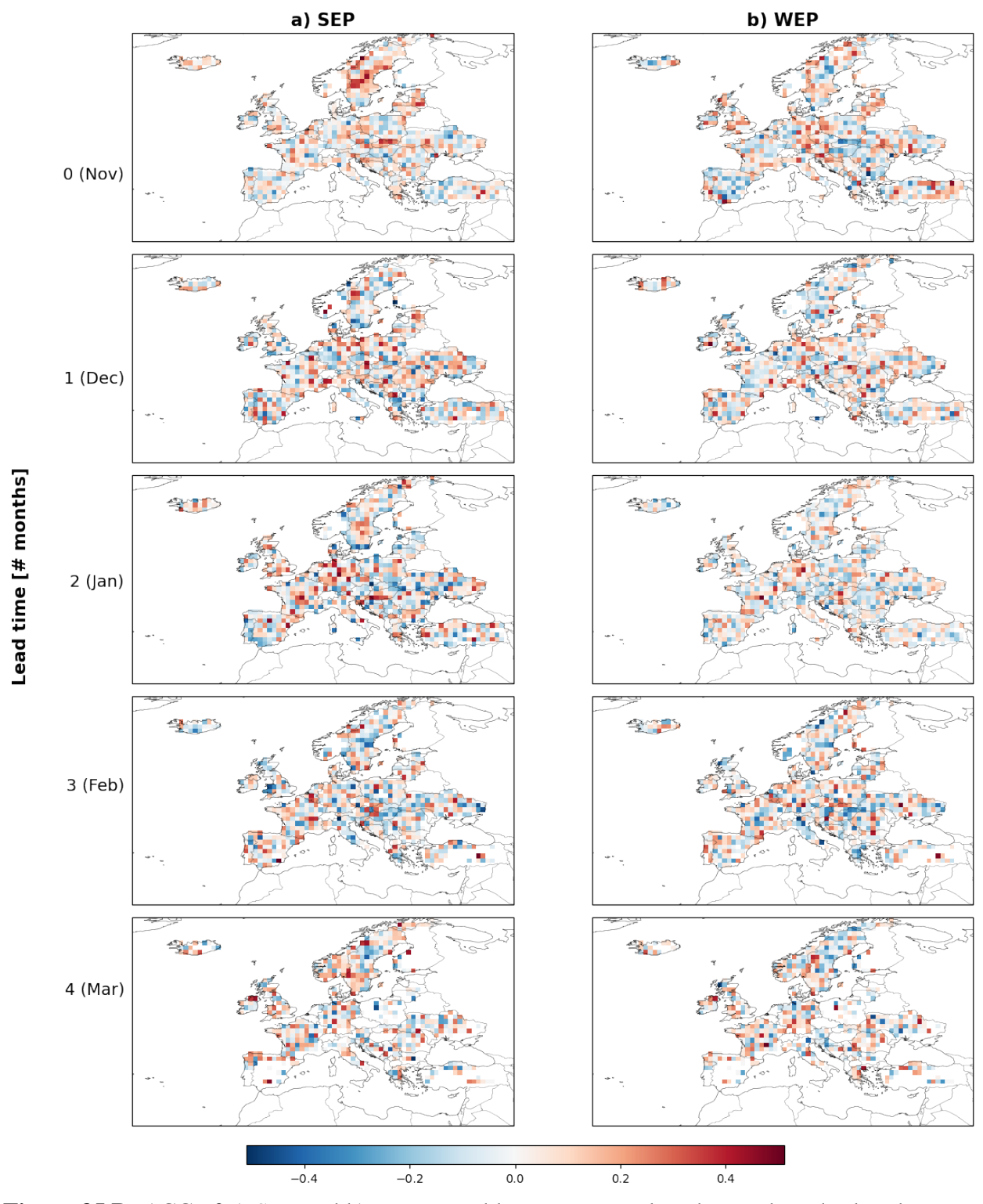


Figure 35.B: ACC of a) *SEP* and b) *WEP* monthly mean anomalies during drought days between GCFS ensemble mean and ERA5.

B.4 Validation of VRE droughts metrics

CEP index anomalies and persistence for Belgium (January 2017) validates the compounded index against the documented drought event (Li et al. 2020). The index successfully detects the event, though spatial averaging dilutes the signal. The persistence map confirms the temporal evolution of the drought, aligning fairly well with reported dates $(15^{th}-17^{th})$ and $22^{nd}-25^{th}$ (Li et al. 2020). In addition, the maps (Fig. 37.B) tracks the progression of the event, using the ordinal day index (Section 2.3). The GCFS captures the event's spatial footprint, though with reduced intensity compared to ERA5. This highlights the model's utility for large-scale detection but limited resolution for local extremes. For the second case study in Germany, January 2017, the drought reportedly reduced German VRE share to 10% of the total energy mix (Walker 2017). In this case, the signal is clearer and the *CEP* index for is validated for the German drought event (Fig. 38.B). The anomalies and persistence align with observed data, though the model smooths out peak intensities. The case study demonstrates the index's robustness for regional-scale applications.

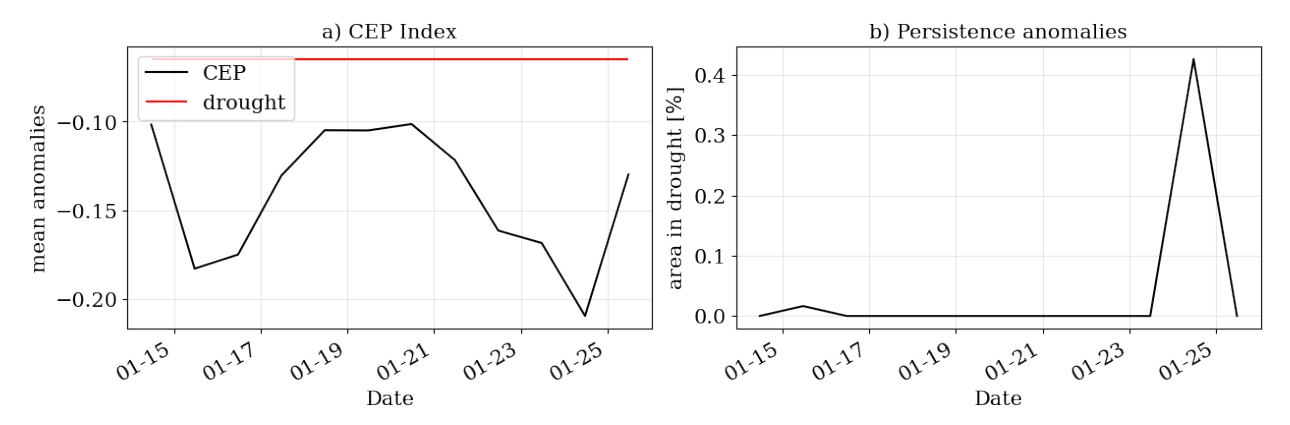


Figure 36.B: On the left, *CEP* index anomalies average over Belgium. On the right, the persistence index defined in Section 2.3 also averaged over Belgium. The time frame is from the 14^{th} to the 25^{th} of January 2017.

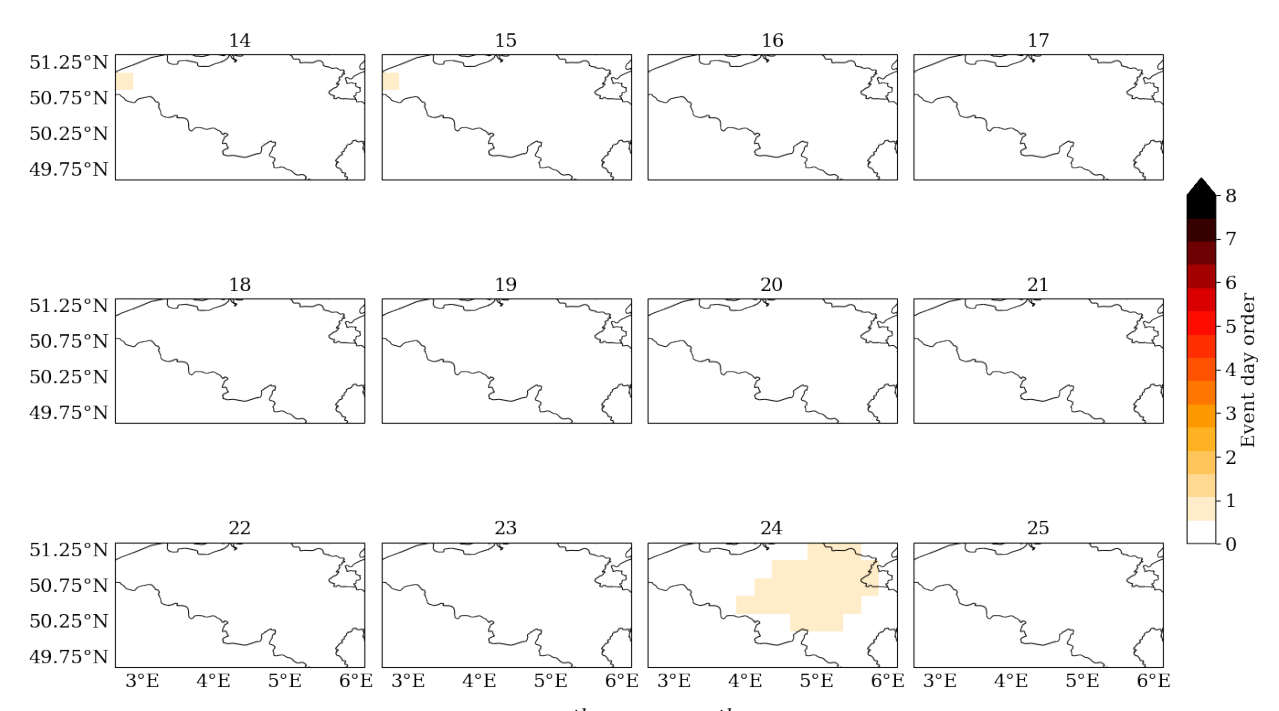


Figure 37.B: Map of Belgium from the 14^{th} to the 25^{th} of January 2017, showing the he ordinal day time series of the multiple-days drought event (for the definition see Section 2.3).

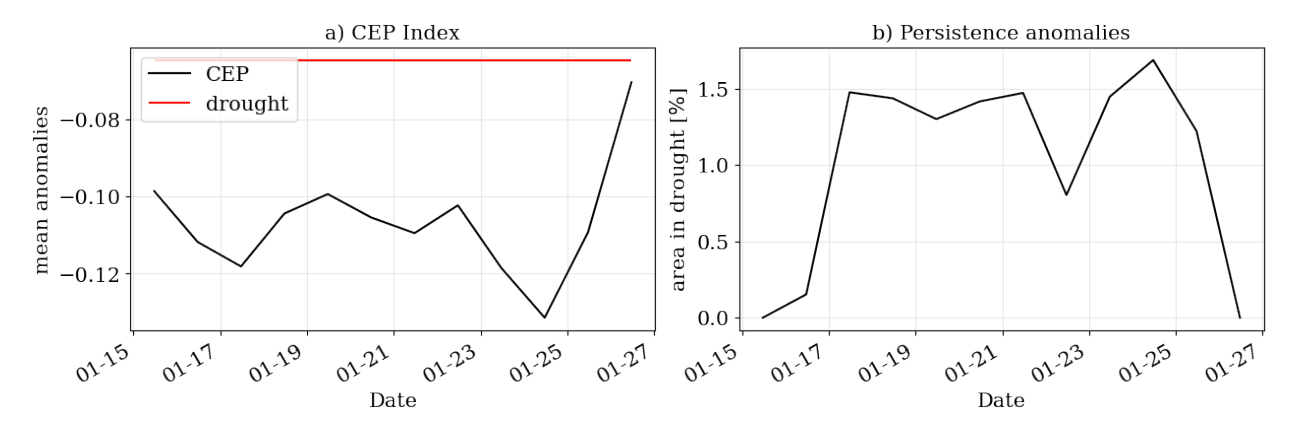


Figure 38.B: On the left, *CEP* index anomalies average over Germany. On the right, the persistence index defined in Section 2.3 also averaged over Germany. The time frame is from the 15^{th} to the 26^{th} of January 2017.

Appendix C

GCFS large-scale circulation patterns

We identified the leading modes of winter (December–February, DJF) climate variability over Europe by performing an Empirical Orthogonal Function (EOF) decomposition on seasonal mean anomalies of the $500 \ hPa$ geopotential height field. The first four EOF patterns, shown in Fig. 39.C, correspond to the major large-scale circulation patterns influencing European climate, with EOF1 representing the North Atlantic Oscillation (NAO). The associated indices for each mode were computed as the Principal Components (PCs), which are the projections of the geopotential height field onto the orthogonal EOF bases. This analysis was applied to the model ensemble mean over the 1990–2024 historical period. To quantify the relationship between these circulation modes

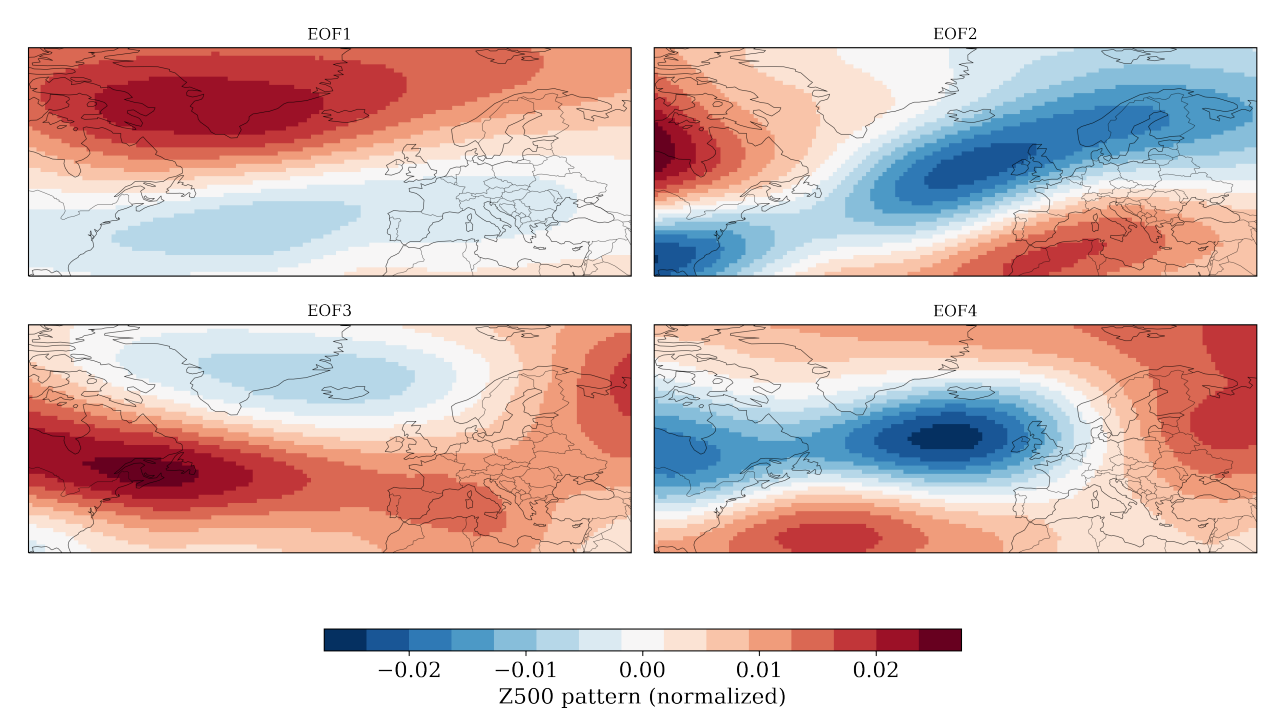


Figure 39.C: The first four EOFs of DJF 500 hPa geopotential height anomalies, representing the dominant modes of atmospheric variability over Europe. EOF1 corresponds to the NAO pattern.

and key energy variables, we computed the Pearson correlation coefficient between each PC and the DJF anomalies of surface solar radiation (RSDS), 10 m wind speed (U_{10}) and the solar (SEP) and

wind (*WEP*) energy production indices. The results for the NAO (PC1) are discussed in the main text (Fig. 24). We further assessed the direct link to VRE droughts by correlating each PC with the DJF count of compounded drought events (Fig. 40.C). The most robust significant correlations were found over Scandinavia. Other regions exhibited more sporadic significant signals: positive correlations in Scotland and parts of Eastern Europe for PC1 (NAO), negative in central France for PC2, negative in southern England for PC3 and positive in the Balkans for PC4. A comparison with

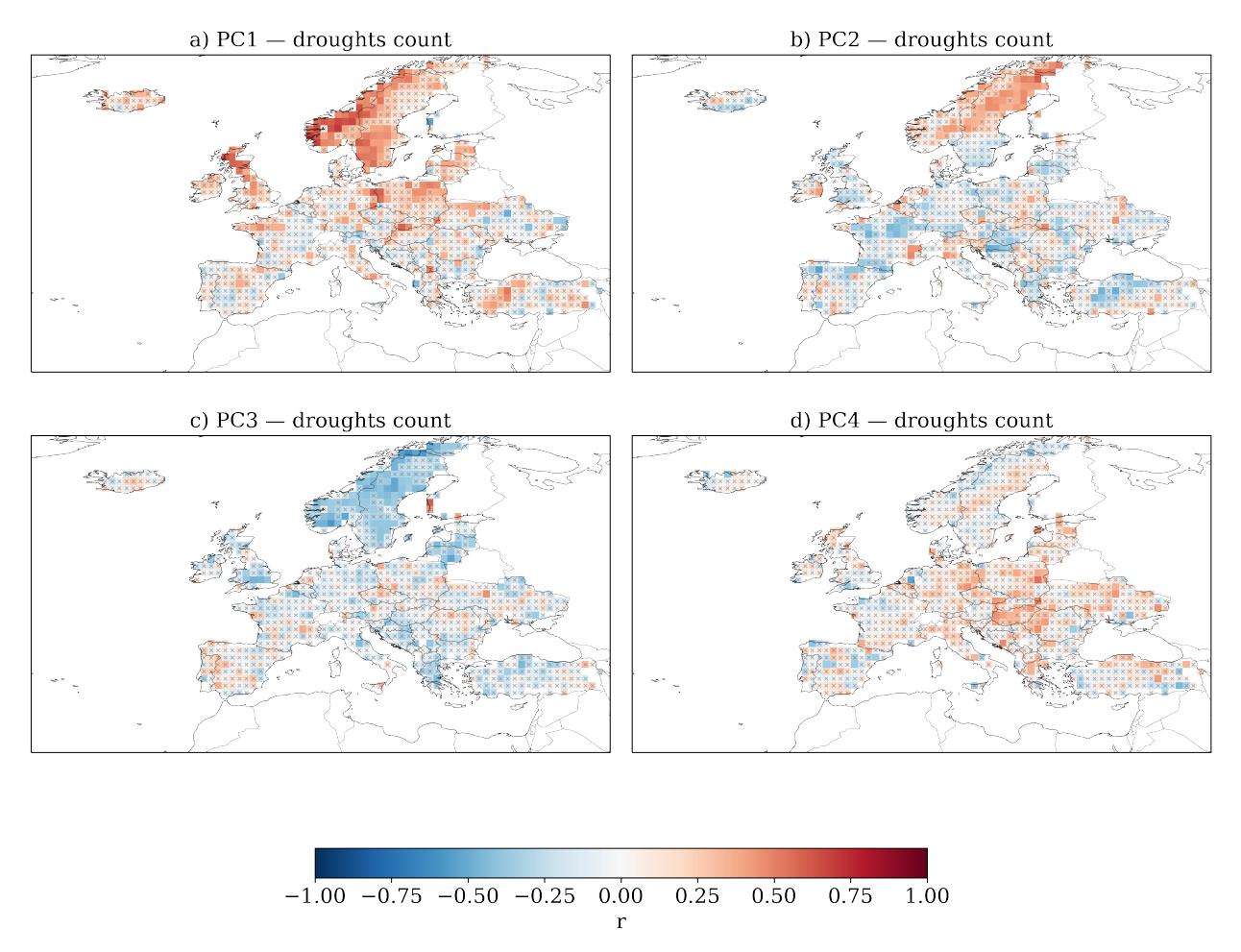


Figure 40.C: Correlations between the PC indices 1 to 4 and ensemble mean DJF count of compounded droughts. Grey crosses indicate the non-significant coefficients.

existing studies (Lledó et al. 2022; Bett et al. 2022) reveals notable differences in these correlation patterns (Fig. 2). Such metrics are highly sensitive to the calculation methodology, data source and analysed period. Consequently, the results presented here, based on the ensemble mean of the GCFS, are not intended as a comprehensive review but rather to provide an initial insight into the links between large-scale circulation and VRE variables within the specific GCFS forecasting system.

Acknowledgments

This thesis was built upon the wisdom and kindness of many people. First, I must acknowledge Dr. Sebastian Brune for his help in providing the datasets. My sincere gratitude goes to my supervisor, Dr. Salvatore Pascale, whose insights always pushed me to improve and to be critical of my findings.

My time at Universität Hamburg was incredibly formative, and I was warmly welcomed by Dr. Leonard Borchert and Dr. Marlene Klockmann. From the start, I was surrounded by people who found value in my work, listened to my findings, and supported me when I faced challenges. Leonard's unwavering enthusiasm was a constant source of encouragement, and Marlene's acute insights continuously helped me refine the details of this work. Thank you all for your guidance and patience; I consider myself fortunate to have worked with you and I will always treasure the months spent in Hamburg.

Bibliography

- Albert, Michael J. (2022). "The global politics of the renewable energy transition and the non-substitutability hypothesis: towards a 'great transformation'?" In: *Review of International Political Economy* 29 (5), pp. 1766–1781. ISSN: 14664526. DOI: 10.1080/09692290.2021.1980418.
- Araújo, Nícolas M.F.T.S. et al. (Aug. 2024). "Variability and Sensitivity of Models Used to Estimate Photovoltaic Production". In: *Energies* 17 (16). <bs/>
 sENSITIVITY

 Accurate estimations are pivotal not only for

 feasibility analyses but also for gauging economic and socio-environmental impacts. ISSN: 19961073. DOI: 10.3390/en17164177.
- Bett, Philip E. et al. (Apr. 2013). "European wind variability over 140 yr". In: *Advances in Science and Research* 10 (1), pp. 51–58. DOI: 10.5194/asr-10-51-2013.
- Bett, Philip E. et al. (Aug. 2022). "A simplified seasonal forecasting strategy, applied to wind and solar power in Europe". In: *Climate Services* 27. this is cool and from troccoli, p. 100318. ISSN: 24058807. DOI: 10.1016/j.cliser.2022.100318. URL: https://linkinghub.elsevier.com/retrieve/pii/S240588072200036X.
- Brunner, Lukas et al. (July 2025). "A global perspective on the spatial representation of climate extremes from km-scale models". In: *Environmental Research Letters* 20 (7). ISSN: 17489326. DOI: 10.1088/1748-9326/ade1ef.
- Cannon, D. J. et al. (2015). "Using reanalysis data to quantify extreme wind power generation statistics: A 33 year case study in Great Britain". In: *Renewable Energy* 75. Nice plots for wind extremes, reproduce for EU., pp. 767–778. ISSN: 18790682. DOI: 10.1016/j.renene.2014.10.024.
- Capellán-Pérez, Iñigo et al. (2020). "MEDEAS: a new modeling framework integrating global biophysical and so-cioeconomic constraints". In: *Energy & Environmental Science* 13 (3), pp. 986–1017. ISSN: 1754-5692. DOI: 10.1039/C9EE02627D.
- Charney, J. G. (1966). "The feasibility of a global observation and analysis experiment". In: *Bull. Amer. Meteor. Soc.* 47, pp. 200–230. URL: https://cir.nii.ac.jp/crid/1573105973931712256.bib?lang=en.
- Chiacchio, Marc et al. (2010). "Influence of NAO and clouds on long-term seasonal variations of surface solar radiation in Europe". In: *Journal of Geophysical Research Atmospheres* 115 (10). ISSN: 01480227. DOI: 10.1029/2009.JD012182.
- Ciucci, Matteo (Mar. 2024). Renewable energy.
- Commission, European (Apr. 2025). Electricity production capacities for renewables and wastes. DOI: 10.2908/nrg_inf_epcrw. URL: https://ec.europa.eu/eurostat/databrowser/view/nrg_inf_epcrw/default/table?lang=en&category=nrg.nrg_quant.nrg_quanta.nrg_inf.
- Denholm, Paul et al. (Mar. 2011). "Grid flexibility and storage required to achieve very high penetration of variable renewable electricity". In: *Energy Policy* 39 (3), pp. 1817–1830. ISSN: 03014215. DOI: 10.1016/j.enpol.2011.01.019.
- Dobrynin, Mikhail et al. (Apr. 2018). "Improved Teleconnection-Based Dynamical Seasonal Predictions of Boreal Winter". In: *Geophysical Research Letters* 45 (8), pp. 3605–3614. ISSN: 0094-8276. DOI: 10.1002/2018GL077209.

- Dobrynin, Mikhail et al. (Oct. 2022). "Hidden Potential in Predicting Wintertime Temperature Anomalies in the Northern Hemisphere". In: *Geophysical Research Letters* 49 (20). ISSN: 0094-8276. DOI: 10.1029/2021GL095063.
- Dommenget, Dietmar (May 2022). An Introduction to Climate Dynamics, pp. 397–397.
- Drücke, Jaqueline et al. (Feb. 2021). "Climatological analysis of solar and wind energy in Germany using the Gross-wetterlagen classification". In: *Renewable Energy* 164. read until sec 3, pp. 1254–1266. ISSN: 18790682. DOI: 10.1016/j.renene.2020.10.102.
- Dutton, Ellsworth G. et al. (Oct. 2006). "Decadal variations in surface solar irradiance as observed in a globally remote network". In: *Journal of Geophysical Research Atmospheres* 111 (19). ISSN: 01480227. DOI: 10.1029/2005JD006901.
- Eurostat, European Commission. (2025). Shedding light on energy in Europe. Publications Office.
- François, B. et al. (Mar. 2016). "Increasing climate-related-energy penetration by integrating run-of-the river hydropower to wind/solar mix". In: *Renewable Energy* 87, pp. 686–696. ISSN: 18790682. DOI: 10.1016/j.renene. 2015.10.064.
- Fröhlich, Kristina et al. (Feb. 2021). "The German Climate Forecast System: GCFS". In: *Journal of Advances in Modeling Earth Systems* 13 (2). ISSN: 19422466. DOI: 10.1029/2020MS002101.
- Gualtieri, Giovanni (Mar. 2019). "A comprehensive review on wind resource extrapolation models applied in wind energy". In: *Renewable and Sustainable Energy Reviews* 102, pp. 215–233. ISSN: 13640321. DOI: 10.1016/j.rser.2018.12.015.
- Gunderson, I. et al. (Feb. 2015). "Climate and land-use change impacts on potential solar photovoltaic power generation in the Black Sea region". In: *Environmental Science & Policy* 46, pp. 70–81. ISSN: 14629011. DOI: 10.1016/j.envsci.2014.04.013. URL: https://linkinghub.elsevier.com/retrieve/pii/S1462901114000859.
- Hassan, Qusay et al. (2024). A comprehensive review of international renewable energy growth. DOI: 10.1016/j.enbenv.2023.12.002.
- Hersbach, H. et al. (Apr. 2017). Complete ERA5 from 1940: Fifth generation of ECMWF atmospheric reanalyses of the global climate.
- IPCC (June 2023a). "Europe". In: Climate Change 2022 Impacts, Adaptation and Vulnerability. Bednar-Friedl, B., R. Biesbroek, D.N. Schmidt, P. Alexander, K.Y. Børsheim, J. Carnicer, E. Georgopoulou, M. Haasnoot, G. Le Cozannet, P. Lionello, O. Lipka, C. Möllmann, V. Muccione, T. Mustonen, D. Piepenburg, and L. Whitmarsh, 2022: Europe. In: <i>Climate Change 2022: Impacts, Adaptation and Vulnerability. </i>Contribution of Working Group II to the Sixth Assessment Report of the Intergovernmental Panel on Climate Change [H.-O. Pörtner, D.C. Roberts, M. Tignor, E.S. Poloczanska, K. Mintenbeck, A. Alegría, M. Craig, S. Langsdorf, S. Löschke, V. Möller, A. Okem, B. Rama (eds.)]. Cambridge University Press, Cambridge, UK and New York, NY, USA, pp. 1817–1927, doi:10.1017/9781009325844.015. Cambridge University Press, pp. 1817–1928. Doi: 10.1017/9781009325844.015. URL: https://www.cambridge.org/core/product/identifier/9781009325844%23c13/type/book_part.
- (Aug. 2023b). "Mitigation Pathways Compatible with Long-term Goals". In: *Climate Change* 2022 *Mitigation of Climate Change*. Cambridge University Press, pp. 295–408. DOI: 10.1017/9781009157926.005.
- Jerez, S. et al. (2013a). "The impact of the north atlantic oscillation on renewable energy resources in Southwestern Europe". In: *Journal of Applied Meteorology and Climatology* 52 (10), pp. 2204–2225. ISSN: 15588424. DOI: 10.1175/JAMC-D-12-0257.1.

- Jerez, Sonia et al. (2013b). "Time-scale and extent at which large-scale circulation modes determine the wind and solar potential in the Iberian Peninsula". In: *Environmental Research Letters* 8 (4). ISSN: 17489326. DOI: 10.1088/1748-9326/8/4/044035.
- Jerez, Sonia et al. (Dec. 2015). "The impact of climate change on photovoltaic power generation in Europe". In: *Nature Communications* 6. ISSN: 20411723. DOI: 10.1038/ncomms10014.
- Johnson, Stephanie J. et al. (Mar. 2019). "SEAS5: The new ECMWF seasonal forecast system". In: *Geoscientific Model Development* 12 (3), pp. 1087–1117. ISSN: 19919603. DOI: 10.5194/gmd-12-1087-2019.
- Jung, T. et al. (May 2012). "High-Resolution Global Climate Simulations with the ECMWF Model in Project Athena: Experimental Design, Model Climate, and Seasonal Forecast Skill". In: *Journal of Climate* 25 (9), pp. 3155–3172. ISSN: 0894-8755. DOI: 10.1175/JCLI-D-11-00265.1.
- Kaspar, Frank et al. (July 2019). "A climatological assessment of balancing effects and shortfall risks of photovoltaics and wind energy in Germany and Europe". In: *Advances in Science and Research*. Vol. 16. Copernicus Publications, pp. 119–128. DOI: 10.5194/asr-16-119-2019.
- Kittel, Martin et al. (Sept. 2024). "Measuring the Dunkelflaute: how (not) to analyze variable renewable energy shortage". In: *Environmental Research: Energy* 1 (3), p. 035007. ISSN: 2753-3751. DOI: 10.1088/2753-3751/ad6dfc. URL: https://iopscience.iop.org/article/10.1088/2753-3751/ad6dfc.
- (July 2025). "Quantifying the Dunkelflaute: An analysis of variable renewable energy droughts in Europe". In: URL: http://arxiv.org/abs/2410.00244.
- Kubik, M L et al. (May 2011). "Using meteorological wind data to estimate turbine generation output: a sensitivity analysis". In: *Worl Renewable Energy Congress* 2011 Sweden.

 Sensitivity to wind profile
 Applications, pp. 4074–4081.
- Li (2025). "Dunkelflaute events: characterization, prediction and future projection". PhD thesis. Technische Universiteit Delft. DOI: 10.4233/uuid:74c8540f-470b-4e0c-a895-e2dccd9c62da. URL: https://doi.org/10.4233/uuid:74c8540f-470b-4e0c-a895-e2dccd9c62da.
- Li, Bowen et al. (Sept. 2020). "Quantifying the Predictability of a 'Dunkelflaute' Event by Utilizing a Mesoscale Model". In: *Journal of Physics: Conference Series*. Vol. 1618. PREDICTABILITY
br/>case study april 30 2018 netherlands. IOP Publishing Ltd. DOI: 10.1088/1742-6596/1618/6/062042.
- (Jan. 2021). "Mesoscale modeling of a "Dunkelflaute" event". In: *Wind Energy* 24 (1). not read yet, pp. 5–23. ISSN: 10991824. DOI: 10.1002/we.2554.
- Lledó, Llorenç et al. (Mar. 2022). "Seasonal prediction of renewable energy generation in Europe based on four teleconnection indices". In: *Renewable Energy* 186, pp. 420–430. ISSN: 18790682. DOI: 10.1016/j.renene.2021. 12.130.
- Lopez-Villalobos, C. A. et al. (Nov. 2022). "Analysis of the influence of the wind speed profile on wind power production". In: *Energy Reports* 8. <bs/>
 sensitivity on wind intrepolation choice

 or chosing wind speed extrapolation method, pp. 8079–8092. ISSN: 23524847. DOI: 10.1016/j.egyr.2022.06.046.
- Lorenz, Edward N. (Mar. 1963). "Deterministic Nonperiodic Flow". In: *Journal of the Atmospheric Sciences* 20 (2), pp. 130–141. ISSN: 0022-4928. DOI: 10.1175/1520-0469(1963)020<0130:DNF>2.0.CO; 2.
- MacLachlan, C. et al. (Apr. 2015). "Global Seasonal forecast system version 5 (GloSea5): a high-resolution seasonal forecast system". In: *Quarterly Journal of the Royal Meteorological Society* 141 (689), pp. 1072–1084. ISSN: 0035-9009. DOI: 10.1002/qj.2396.

- Mauritsen, Thorste et al. (Sept. 2012). "Tuning the climate of a global model". In: *Journal of Advances in Modeling Earth Systems* 4 (8). ISSN: 19422466. DOI: 10.1029/2012MS000154.
- Mavromatakis, F. et al. (July 2010). "Modeling the photovoltaic potential of a site". In: *Renewable Energy* 35 (7), pp. 1387–1390. ISSN: 09601481. DOI: 10.1016/j.renene.2009.11.010.
- Merryfield, William J. et al. (June 2020). "Current and emerging developments in subseasonal to decadal prediction". In: *Bulletin of the American Meteorological Society* 101 (6), E869–E896. ISSN: 00030007. DOI: 10.1175/BAMS-D-19-0037.1.
- Mockert, Fabian et al. (July 2023). "Meteorological conditions during periods of low wind speed and insolation in Germany: The role of weather regimes". In: *Meteorological Applications* 30 (4). ISSN: 14698080. DOI: 10.1002/met.2141.
- Müller, W. A. et al. (July 2018). "A Higher-resolution Version of the Max Planck Institute Earth System Model (MPI-ESM1.2-HR)". In: *Journal of Advances in Modeling Earth Systems* 10 (7), pp. 1383–1413. ISSN: 19422466. DOI: 10.1029/2017MS001217.
- Paolini, Luca Famooss et al. (Jan. 2025). "Hybrid statistical–dynamical seasonal prediction of summer extreme temperatures in Europe". In: *Quarterly Journal of the Royal Meteorological Society* 151 (766). ISSN: 1477870X. DOI: 10.1002/qj.4900.
- Parding, Kajsa et al. (2014). "Decadal variability of clouds, solar radiation and temperature at a high-latitude coastal site in Norway". In: *Tellus, Series B: Chemical and Physical Meteorology* 66 (1). ISSN: 16000889. DOI: 10.3402/tellusb.v66.25897.
- Penabad, Eduardo (Feb. 2025). Description of GCFS2.2-v20231101 C3S contribution.
- Peterson, Ernest W et al. (1978). "On the Use of Power Laws for Estimates of Wind Power Potential". In: *Journal of Applied Meteorology and Climatology* 17 (3), pp. 390 –394. DOI: 10.1175/1520-0450(1978)017<0390: 0TUOPL>2.0.CO; 2. URL: https://journals.ametsoc.org/view/journals/apme/17/3/1520-0450_1978_017_0390_otuopl_2_0_co_2.xml.
- Pierro, Marco et al. (Apr. 2022). "Progress in regional PV power forecasting: A sensitivity analysis on the Italian case study". In: *Renewable Energy* 189, pp. 983–996. ISSN: 18790682. DOI: 10.1016/j.renene.2022.03.041.
- Randall, David A et al. (n.d.). Measurements, Models, and Hypotheses in the Atmospheric Sciences. Tech. rep.
- Scaife, A. A. et al. (Apr. 2014). "Skillful long-range prediction of European and North American winters". In: *Geophysical Research Letters* 41 (7), pp. 2514–2519. ISSN: 19448007. DOI: 10.1002/2014GL059637.
- Schulzweida, Uwe (Oct. 2023). *CDO User Guide*. Version 2.3.0. DOI: 10.5281/zenodo.10020800. URL: https://doi.org/10.5281/zenodo.10020800.
- Soci, Cornel et al. (Oct. 2024). "The ERA5 global reanalysis from 1940 to 2022". In: *Quarterly Journal of the Royal Meteorological Society* 150 (764), pp. 4014–4048. ISSN: 1477870X. DOI: 10.1002/qj.4803.
- Stephens, Graeme L. et al. (2010). "Dreary state of precipitation in global models". In: *Journal of Geophysical Research Atmospheres* 115 (24). ISSN: 01480227. DOI: 10.1029/2010JD014532.
- Susskind, Lawrence et al. (June 2022). "Sources of opposition to renewable energy projects in the United States". In: *Energy Policy* 165. ISSN: 03014215. DOI: 10.1016/j.enpol.2022.112922.
- Vavrus, Stephen J. et al. (2015). "Interpreting climate model projections of extreme weather events". In: *Weather and Climate Extremes* 10, pp. 10–28. ISSN: 22120947. DOI: 10.1016/j.wace.2015.10.005.
- Walker, Tamsin (Aug. 2017). "Dark season for renewables". In: Deutsche Welle.

- Wang, Lin et al. (2021). "Teleconnection along the Asian jet stream and its association with the Asian summer monsoon". In: *Indian Summer Monsoon Variability*. Elsevier, pp. 287–298. DOI: 10.1016/B978-0-12-822402-1.00009-0.
- White, Christopher J. et al. (July 2017). "Potential applications of subseasonal-to-seasonal (<scp>S2S</scp>) predictions". In: *Meteorological Applications* 24 (3). cite for subseasonal approximative pifcture, pp. 315–325. ISSN: 1350-4827. DOI: 10.1002/met.1654.
- Wiel, K. van der et al. (Sept. 2019a). "Meteorological conditions leading to extreme low variable renewable energy production and extreme high energy shortfall". In: *Renewable and Sustainable Energy Reviews* 111, pp. 261–275. ISSN: 18790690. DOI: 10.1016/j.rser.2019.04.065.
- Wiel, Karin Van Der et al. (Sept. 2019b). "The influence of weather regimes on European renewable energy production and demand". In: *Environmental Research Letters* 14 (9). ISSN: 17489326. DOI: 10.1088/1748-9326/ab38d3.
- Wilcox, Eric M. et al. (Jan. 2007). "The frequency of extreme rain events in satellite rain-rate estimates and an atmospheric general circulation model". In: *Journal of Climate* 20 (1), pp. 53–69. ISSN: 08948755. DOI: 10.1175/JCLI3987.1.
- Yuan, Xiaojun et al. (Aug. 2018). *The interconnected global climate system-a review of tropical-polar teleconnections*. DOI: 10.1175/JCLI-D-16-0637.1.
- Zubiate, Laura et al. (Jan. 2017). "Spatial variability in winter NAO—wind speed relationships in western Europe linked to concomitant states of the East Atlantic and Scandinavian patterns". In: *Quarterly Journal of the Royal Meteo-rological Society* 143 (702), pp. 552–562. ISSN: 1477870X. DOI: 10.1002/qj.2943.

In the codes developed for this thesis, the Climate Data Operators (CDO) software was extensively used: Schulzweida 2023.

During the preparation of this thesis, I made use of generative artificial intelligence tools, specifically Le Chat, developed by Mistral AI. This tool was primarily employed between May 2025 and October 2025, with the aim of code debugging and supporting the creation of graphs useful for result analysis. The use particularly concerned the sections on VRE droughts predictability and index validation (Chapter 3) and Results (Appendix B and C).